Department of Meteorology

University of Reading

Dual-Wavelength Radar Studies of Clouds

Robin James Hogan

A thesis submitted for the degree of Doctor of Philosophy

August 1998

Abstract

The importance of clouds in the earth's radiation budget has long been recognised, but a lack of knowledge of their properties and behaviour means that their representation is one of the major uncertainties in current climate models. There is therefore an urgent need for observations on both a case-study and global basis to get a better understanding of cloud processes and to obtain a global climatology of cloud parameters, particularly water content and effective radius.

In this thesis the potential of millimetre-wave radar to make these essential remote measurements is explored, with particular emphasis on dual-wavelength radar. In stratocumulus it is shown using aircraft data that, by differential attenuation, coincident 35 and 94 GHz radars should be able to measure liquid water content to within 0.05 g m^{-3}, and this is compared with a second technique which uses Doppler spectra and should be able to measure liquid water content to within 10–30% in radiatively significant clouds.

Next, the important issue of cirrus crystal density is addressed, for which a new expression is derived as a function of diameter. This is then used in the interpretation of measurements taken during an intercomparison flight of the UK Meteorological Office (UKMO) aircraft over Chilbolton. It is shown that reflectivity calculated from the in situ measurements agrees well with that measured by the radar.

The feasibility of using spaceborne dual-wavelength radar to measure crystal size in cirrus, and therefore ice water content more accurately than with a single radar, is explored using aircraft data. It is shown that the combination of 79 and 215 GHz radars is best, being able to measure ice water content and size to 15–30%, provided the reflectivity is at least 15 dB greater than the minimum detectable. The technique is demonstrated using observations by the 35 and 94 GHz radars at Chilbolton, and the derived parameters are compared with the analyses of the UKMO Unified Model.

Acknowledgements

I am greatly indebted to my supervisor **Anthony Illingworth** for his guidance, enthusiasm and generosity during the last three years. It has been a pleasure working with him and hope this thesis is at least a partial realisation of the flurry of ideas that he bombarded me with when I first arrived at Reading.

Secondly, a big thank-you to **Phil Brown** of the UK Meteorological Office for providing the aircraft data which has been such a fundamental part of this thesis, and for answering all my many questions on how to interpret it. Thanks also to **Peter Francis** for useful discussions on the density of ice crystals which led to the writing of Chapter 4, and to **Doug Johnson** for helpful insights into the ASTEX data used in Chapter 3.

I very much appreciate the hard work done by those at RAL and Chilbolton to keep the radars going, and particularly wish to thank **Jon Eastment**, **Darcy Ladd** and **John Goddard**.

I am grateful to all the members of the Radar Group at Reading for their support; to **Chunlei Liu** for valuable discussions regarding the scattering properties of ice crystals, to **Mark Blackman** for providing me with loads of impenetrable code and for generally fixing things, to **Tim Smyth** for being a great mate, to **Andrew Openshaw** for managing all the data and to **Danny Chapman** for welcome interludes of croquet, as well as more than a few top computing tips. Thanks also to **Richard Allan** for temporarily putting aside his preference for clear skies to answer my questions on the radiative properties of clouds.

Cheers to all the good friends I've made at the department for all the fun, curry and entertaining coffee-room conversations I've enjoyed over the last three years. A special mention must go to the crowd in Room 1U08 whose capacity for distraction is astonishing—what would I have done without those marathon lunchtime tetris sessions or being told the latest tennis, cricket and football scores simultaneously every ten seconds?

Most of all I thank my parents, **Martin** and **Lorna Hogan** for their unfailing love and support, and thank them and my brothers and sister for providing a happy haven of chaos to which I could retreat and relax on those rare occasions when I needed a break from Radar Meteorology. Lastly I would like to express my gratitude to my grandparents **Ken** and **Joyce Wood** for their generous financial support throughout my time at university.

Contents

CHAPTER ONE

Introduction

1.1 Importance of clouds for climate and radiation

Much concern has been expressed in recent years about the possibility that the climate may be changing in response to human activities, and particularly in the news media attention has focussed on the theory that anthropogenic emissions of greenhouse gases, such as carbon dioxide, are causing an increase in global mean surface temperatures. The theoretical basis behind the contention that these gases, by their absorption of thermal radiation, have a warming effect on the surface is very strong, but it is difficult to infer an exact change in surface temperature in response to an increase in their concentration because of our poor understanding of the myriad of feedback processes which act in the real ocean-atmosphere system. Such feedbacks include changes in the amount of water vapour in the atmosphere (the most important greenhouse gas), changes in snow and ice cover and therefore the earth's albedo, changes in ocean circulation or in its uptake of carbon dioxide, and changes in cloud distribution or cloud properties. Clouds represent a major uncertainty.

To even the most casual of observers the importance of clouds in determining surface temperature is obvious, due to their ability to both obscure the sun during the day, and to trap thermal radiation near the ground at night. This is no less true on a global scale, where clouds represent the most important variable in determining how much solar energy (hereafter 'shortwave') is absorbed by the climate system and how much thermal infrared energy (hereafter 'longwave') is radiated back to space. In the shortwave, clouds have a cooling effect on climate because they increase the global albedo. The main contribution is from low stratus and stratocumulus, but optically thick cirrus associated with mid-latitude cyclones and tropical convection also plays a part. In the longwave on the other hand clouds have a warming effect which increases with cloud-top altitude; high clouds re-emit the thermal radiation they absorb from the surface at a much lower blackbody temperature. These two effects are large but opposing, and the net effect is a cooling; in one of the first attempts to model the climate system, Manabe and Strickler (1964) estimated that without clouds the global mean surface temperature would be 13°C higher.

The response of surface temperatures to a forcing such as increased carbon dioxide depends crucially on how cloud properties and distribution would change, and this is very uncertain. Mitchell et al. (1989) found with a single General Circulation Model (GCM) that the change in mean surface temperature associated with a doubling of carbon dioxide varied between 1.9°C and 5.2°C depending on how clouds were represented in the model. Similarly, in a comparison of 19 climate GCMs with predicted rather than fixed clouds, Cess et al. (1990) showed that the sensitivity of surface temperature to an externally induced perturbation of the climate system varied by more than a factor of three, and that this disparity was primarily due to differences in the representation of clouds. Arking (1991) removed the effects of other climate feedbacks from these results to extract those of clouds alone, and found that 7 of the models had a negative feedback, so even the *sign* of the surface temperature tendency due to clouds in an alternative climate scenario is in doubt. A more recent comparison by Cess et al. (1996) showed less disagreement, although this belied the fact that there were still large differences in the short- and longwave responses of the various models. It is not surprising that the representation of clouds is regarded as the 'Achilles Heel' of climate models.

The greenhouse gas mechanism is far from the only means by which the climate might change. It is clear that the climate system has undergone huge fluctuations in the past, and one of the big questions is whether these were forced by some change in the energy budget, or are simply a manifestation of the natural long-timescale variability that non-linear systems can exhibit.

In this thesis we consider the potential of cloud radar to remotely measure cloud water content and particle size in the most two most common cloud types (and the most important for climate), stratocumulus and cirrus. The scope of the thesis is limited to developing algorithms by which these parameters can be measured, and the purpose of this chapter is to put such techniques in context by reviewing the current state of climate modelling and determining the accuracy and sensitivity that such observations should achieve.

1.2 Climate modelling

Much is known about the microphysical processes which occur in clouds, such as the growth mechanisms of individual droplets, but the challenge for climate modelling is to bridge the divide between this and the radiative and dynamical behaviour of clouds on the large scale. The inevitable limitation is computer power. In order to include all the necessary processes and yet run in a reasonable time, current GCMs operating in climate mode can afford a resolution of around 100 km at best, and the effects of clouds, which are forced by atmospheric motions on a much smaller scale, must be parameterised in the most rudimentary fashion.

Typically clouds are represented as a grid-box average of liquid or ice water content which is either diagnosed every timestep as a function of humidity and temperature, or in more advanced schemes is a prognostic variable (Smith 1990, Tiedtke 1993). This is then related to the radiative properties of the cloud via parameterisations for effective radius (r_e), single scatter albedo (ω) and asymmetry parameter (g) as a function of the wavelength of the radiation. Liquid droplets are close enough to spherical that Mie theory can be applied and so r_e is the only variable about which there is much doubt, but for ice crystals things are far more complicated because all three of these parameters are a function of crystal type, orientation, density and size, which are generally unknown. Of course to correctly calculate the radiative effects of a model grid-box containing either liquid or ice-phase cloud requires the water content to be known accurately, and another substantial problem is how to parameterise cloud cover and the effects of inhomogeneous cloud fields.

It has been shown that small differences in the most basic assumptions which it is necessary to make in climate modelling can have a strong effect on the resulting cloud water content; for example, slight differences in assumed ice crystal terminal velocity in cirrus clouds were found to have a significant effect on the ice water content (IWC) of tropical cirrus (Tiedtke et al. 1993). Some potentially important effects are not even included in climate models, such as possible increases in the concentration of the aerosols which act as cloud condensation nuclei (for example by fossil fuel or biomass burning), which would reduce the effective radius of liquid water clouds and therefore increase their albedo (Twomey 1974).

Some simplifications that it is necessary to make in climate models can produce unavoidable inconsistencies which cannot be removed by 'tuning' the available parameters. For instance most current models use the plane-parallel approximation for boundary-layer clouds in which horizontal inhomogeneities are neglected, which makes radiative transfer calculations far more tractable. However real clouds, which vary greatly in the horizontal, have an intrinsically lower albedo for a given liquid water path (LWP). Current models are tuned so that their albedos match those measured by satellites, and therefore they must underestimate LWP; it was shown by Barker (1996) that the magnitude of the discrepancy is likely to often exceed 20%, and in very inhomogeneous cloud fields could theoretically be as much as an order of magnitude. Hence cloud absorption is likely to be considerably underestimated. In a similar vein it was reported by Browning (1994) that simple cloud schemes based on relative humidity tend to be tuned to give the correct radiative heating, but this inevitably results in them having the wrong latent heating.

1.3 Measuring requirements for constraints on models

It is clear from the above discussion that there is a need to validate the representation of clouds in climate models if any confidence is to be ascribed to their predictions. Three roles for observing systems can be identified for this purpose:

1. To get a better physical understanding of the important processes that are occurring in clouds and to suggest ways that these might be represented in models;

2. Comparison of observations with model analyses and forecasts on a case study basis, to verify not only that models are able to simulate real clouds accurately, but also that the existing observational network and assimilation procedures (which provide the initial state from which forecast models are run) are good in their diagnosis of clouds;

3. To produce a global climatology of cloud location, type, water content and effective radius with which climate models can be compared.

For the usefulness of observing techniques to be objectively assessed, the accuracy and sensitivity they can achieve should be compared with that required to provide a useful constraint on climate models. Unfortunately to assess how accurate observations need to be is unavoidably subjective, and one should therefore be somewhat wary of such assessments presented in the literature which are then immediately used to justify the use of a particular technique, despite its inherent inaccuracies.

Few assessments of 'user requirements' have been presented in the literature. Browning (1994) described the results of a survey in which the directors of 20 climate modelling groups had described what they regarded as the priority issues on which to concentrate in parameterising the large-scale effects of clouds and cloud-related processes. The responses highlighted a multitude of areas in which the physical basis behind model parameterisations was poor and needed to be improved. Concern was expressed about the lack of good observations of liquid and ice water content, as well as of droplet size distributions, but no quantitative estimate of the required accuracy was given.

The Hadley Centre for Climate Prediction and Research has published a specification of climate data requirements (Hadley Centre 1994). Their cloud-related requirements can be separated into two. Firstly they identified a need for observations to provide a better understanding of cloud processes in order that the water cycle can be better represented in models. This would involve 'process study experiments' in which measurements would be taken of (i) cloud top and base, (ii) cloud liquid water profile and ice water content, and (iii) cloud particle phase and size distribution. Once the parameterisation of such variables is adequate then the following would be required on a continuous and global basis at a resolution of 250 km:

- Cloud cover to a precision of better than 10%, with 2-3% long-term stability;
- Cloud liquid and ice content with column content to an accuracy of 10%;
- Cloud top, base and vertical distribution with a 1 km vertical resolution;
- Cloud phase and particle size to an accuracy 1 μm.

Radiation budgets are required to within 5 W m^{-2}, and the report stressed that these should be regarded as 'first estimates' of the requirements.

More rigorous estimates of the required accuracy and sensitivity can be formulated. Brown et al. (1995) explicitly determined a cirrus cloud to be 'radiatively significant' if it changed the outgoing longwave radiation (OLR) or flux divergence within the cloud layer by 10 W m^{-2}, or changed the downwelling longwave flux at the surface by 5 W m^{-2}. It turns out that the requirement on OLR is the most stringent. Note that the typical accuracy of a surface or aircraft pyrgeometer is around 10 W m^{-2} (e.g. Grant and Hignett 1998), and infrared radiances can be measured from space to an accuracy of around 5 W m^{-2} (Barkstrom et al. 1989). From these criteria, Brown et al. showed that a radiatively significant cirrus cloud has a longwave absorption optical depth ($\tau_{\rm ir}$) of at least 0.07 in the mid-latitudes and at least 0.04 in the tropics. From this ice water path (IWP) can be estimated using the following expression, which is valid provided the crystals are much larger than the wavelength of the radiation (Stephens et al. 1990, Francis et al. 1994):

$$\tau_{\rm ir} = \frac{3}{4}\frac{\rm IWP}{\rho_{\rm i} r_{\rm e}}, \qquad (1.1)$$

where ρ_i is the density of solid ice. Hence for a 1 km thick cloud with a typical r_e of 37 µm (Foot 1988), this translates into a requirement for instruments to be able to detect clouds with an IWC of down to 0.0032 g m^{-3} in the mid-latitudes and 0.0018 g m^{-3} in the tropics. In thin cirrus r_e is likely to be less than the mean value of 37 µm; Brown et al. (1995) considered a value of 10 µm for which the corresponding IWCs become 0.0009 and 0.0005 g m^{-3} respectively.

Brown et al. (1995) also showed that the required accuracy of a measurement of optical depth, which results in the longwave fluxes and flux divergence being within the same defined limits, was approximately a factor of two for mid-latitude cirrus and a factor of 1.4 for tropical cirrus. Similar accuracies should therefore be achievable for measurements of IWC and r_e.

We can apply a similar argument to estimate the requirements for the accuracy and sensitivity of stratocumulus measurements. For low clouds it is the shortwave albedo effect rather than the longwave effect which is of most climatological importance, so we shall define a radiatively significant cloud as one which increases the reflected shortwave radiation by 10 W m^{-2} or more. Assuming a clear-sky albedo of 0.15 (Hartmann 1993), a solar zenith angle of 45° and a downwelling shortwave flux at cloud top of 700 W m^{-2}, the minimum reflectance of such a cloud is 0.02 (where its absorption has been neglected). From Table 6.2 of Liou (1980) we estimate that this corresponds to an visible extinction optical depth τ_{vis} of 0.13. Using the relationship of Slingo (1990):

$$\tau_{vis} = \frac{3}{2}\frac{LWP}{\rho_l r_e}, \tag{1.2}$$

where ρ_l is the density of liquid water, we find that for a typical r_e of 10 µm, this corresponds to an LWP of 0.9 g m^{-2}. In an adiabatic cloud, liquid water content (LWC) increases with height at a rate of approximately 1 g m^{-3}/km (Nicholls 1984), for which this LWP would correspond to a 45 m thick cloud with a mean LWC of around 0.02 g m^{-3}. Often stratocumulus clouds are sub-adiabatic however; for an increase with height of 0.25 g m^{-3}/km, say, this LWP corresponds to a 90 m thick cloud with a mean LWC of 0.01 g m^{-3}.

The required accuracy has been estimated using the parameterisation for reflectance of Liou and Wittman (1979) which is applicable to thicker, absorbing clouds. Again using the condition that the reflected shortwave radiation should be known to within 10 W m^{-2}, we find that up to an LWP of 200 g m^{-2}, measurements of LWP (and therefore LWC and r_e) should be accurate to around 10%. The required accuracy decreases for even thicker clouds because the rate of increase in albedo with LWP is smaller.

Cirrus	Mid-latitude	Tropical
τ_{ir} sensitivity	0.07	0.04
Accuracy of τ_{ir}, LWP, LWC and r_e	$+100\%$, -50%	$+40\%$, -30%
IWP sensitivity ($r_e = 37\,\mu$m)	$3.2\ \mathrm{g\,m^{-2}}$	$1.8\ \mathrm{g\,m^{-2}}$
IWP sensitivity ($r_e = 10\,\mu$m)	$0.9\ \mathrm{g\,m^{-2}}$	$0.5\ \mathrm{g\,m^{-2}}$
IWC sensitivity ($r_e = 37\,\mu$m,1 km layer)	$0.0032\ \mathrm{g\,m^{-3}}$	$0.0018\ \mathrm{g\,m^{-3}}$
Stratocumulus	All latitudes	
τ_{vis} sensitivity	0.13	
Accuracy of τ_{vis}, LWP, LWC and r_e	$\pm10\%$	
LWP sensitivity ($r_e = 10\,\mu$m)	$0.9\ \mathrm{g\,m^{-2}}$	
LWC sensitivity ($r_e = 10\,\mu$m, adiabatic cloud)	$0.02\ \mathrm{g\,m^{-3}}$ (45 m layer)	
LWC sensitivity ($r_e = 10\,\mu$m, sub-adiabatic cloud)	$0.01\ \mathrm{g\,m^{-3}}$ (90 m layer)	

Table 1.1: Approximate requirements for the accuracy and sensitivity of cloud measurements, in order for the radiation budget to be constrained to within 10 W m^{-2}. Note that an adiabatic stratocumulus cloud is taken to be one for which LWC increases with height at a rate 1 g m^{-3}/km (Nicholls 1984), and a sub-adiabatic cloud is taken to be one for which this is 0.25 g m^{-3}/km.

These targets are summarised in Table 1.1, and represent those required to constrain the radiation budget to within 10 W m^{-2}. Such procedures are very useful for getting an approximate estimate of the requirements for retrieval algorithms, but should not be regarded as 'set in stone' because typical values for parameters such as r_e and cloud depth had to be specified subjectively. Also the blunt assessment of whether a cloud is 'radiatively significant' is a little misleading because it is perfectly conceivable that, for example, cirrus clouds with lower optical depths than this arbitrary threshold could exist in vast but undetected expanses in the upper troposphere and hence have a cumulative effect equalling the less frequent occurrences of thicker cloud.

Note also that our requirements are somewhat less stringent than those suggested by the Hadley Centre (1994), partially because they specified radiation budgets to be to accurate to 5 W m^{-2} rather than 10 W m^{-2} (although it is straightforward to modify our estimates accordingly), but the main difference is that they grouped stratocumulus and cirrus together in their requirements for r_e and water content, despite the fact that the radiation budget is somewhat less sensitive to changes in cirrus. Hence the specification that size (i.e. r_e) should be measured to within 1 µm represents an accuracy of around 10% for stratocumulus (which is the same as our assessment), but around 3% for cirrus, which should be regarded as excessively stringent.

Given that there are virtually no existing techniques to systematically make vertically-resolved measurements of cloud properties, it is likely that good use could be made of most measurements, even if they do not quite attain the user requirements presented here. It is interesting to note that the satellite method for retrieving LWP in stratocumulus presented by Greenwald et al. (1993) is accurate to only 16 g m^{-2} in near-cloudless regions, rising to around 20 g m^{-2} in cloudy regions, and despite the fact that according to our criterion a radiatively significant stratocumulus cloud can have an LWP of only 0.9 g m^{-2}, these measurements are regarded as very valuable and are widely used.

1.4 Cloud-measuring instrumentation

1.4.1 Passive instruments in space

Passive radiometric measurements of the earth from space have been available for a number of decades and have greatly improved our understanding of the energy balance of the earth. Before they were available, estimation of the effects of clouds on surface temperature was based on very limited ground-based observations of albedo and cloud cover, such as those presented by London (1957). The most extensive attempt to measure the global properties of clouds from space was the International Satellite Cloud Climatology Project (Rossow and Schiffer 1991), in which all the visible and infrared information from the various polar orbiting and geostationary satellites was used to provide cloud amount and cloud top height for each of four basic cloud types. The radiative effect of clouds could be directly determined by comparing the fluxes from adjacent cloudy and cloud-free regions, but for model validation the observations were of limited value since if the modelled and observed outgoing fluxes did not agree then it was far from clear where the cloud representation in the model was likely to be at fault. Obscuration was also a problem in the presence of multiple cloud layers.

Satellite measurements have improved considerably in the last few years, with microwave radiometry providing LWP routinely over oceans free from sea-ice (Greenwald et al. 1993), and multispectral measurements being used to estimate particle size at the top of stratocumulus (Han et al. 1994) and in cirrus (Baran et al. 1998), although validation is required. However there is as yet no method for measuring ice water path from space, and the problems of obscuration and poor vertical resolution still remain.

1.4.2 Lidar

We now consider active instruments which, by sending out a pulse of radiation and timing its return, are able to much more accurately measure distances and therefore the vertical distribution of clouds. Since the major effect of clouds in the earth's radiation budget is in the visible and the thermal infrared, these would perhaps seem to be the most obvious choices for the wavelengths of an active system. Both visible and infrared lidars have been built, and they generally exhibit excellent sensitivity and range resolution. For visible lidars the geometric optics approximation is generally valid in all clouds (since wavelength is much smaller than diameter) which means that the backscatter is roughly proportional to the second moment of the size distribution. This is precisely the parameter required by radiation schemes, but a several problems present themselves. First and foremost is the fact that, just like atmospheric radiation, lidar wavelengths are noticeably attenuated in clouds with an optical depth greater than around 0.1, which includes all liquid water clouds and the thicker cirrus. This makes quantitative interpretation of the returned signal difficult, and can cause a complete loss of signal after only a few hundred metres of penetration into stratocumulus. However it is possible for attenuation to be used to retrieve the optical depth of semi-transparent clouds, by comparing the molecular backscatter directly below cloud base and above cloud top with a nearby cloudless profile. This is much easier at short wavelengths because of the much stronger Rayleigh scattering by the oxygen and nitrogen molecules, but care must be taken to account for the presence of aerosols (Young 1995).

Lidar backscatter is very sensitive to the exact structure of individual ice crystals, which is a major headache for quantitatively interpreting observations of cirrus since crystal habits and orientations are generally unknown. Extra parameters are available from lidars that have depolarisation or multiple-wavelength capability and these should enable cirrus measurements to be interpreted more quantitatively.

During the Lidar In-space Technology Experiment (LITE), a nadir-pointing multiple-wavelength lidar was operated from the space shuttle for a period of over two weeks (Winker et al. 1996), producing impressive images of clouds and aerosols. However this experiment highlighted the further problem for spaceborne lidar of multiple scattering, whereby in thick clouds the returned signal can be the result of more than one scattering event, and therefore appear to originate from a greater range. As well as the possibility of making quantitative deductions from the data becoming even more remote, multiple scattering can even have the effect of smearing out cloud boundaries beyond recognition.

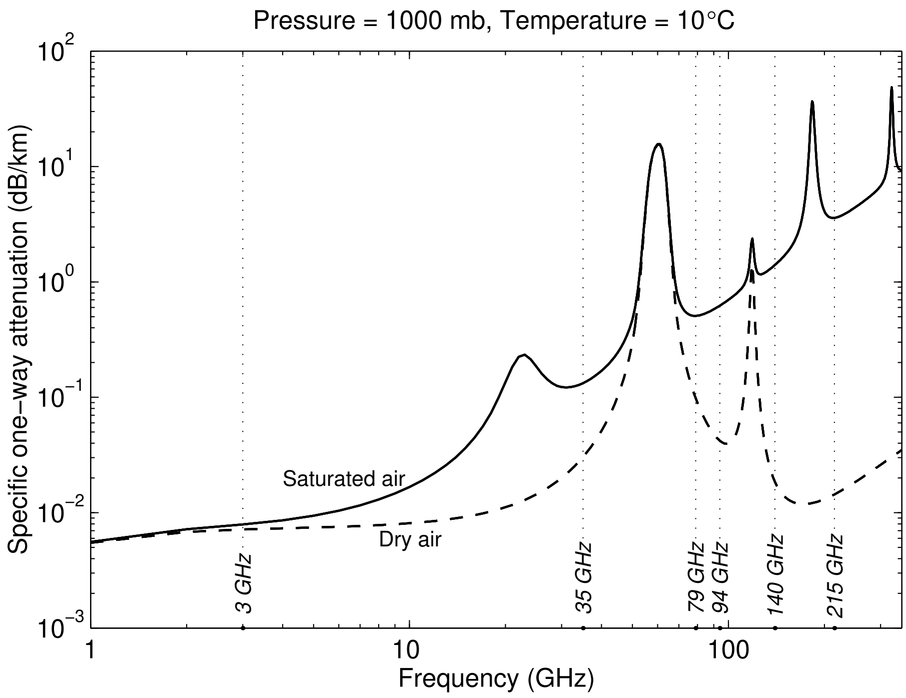

Figure 1.1: One-way attenuation due to atmospheric gases as a function of frequency, for dry and saturated air at 1000 mb and 10°C. Superimposed are dotted lines indicating the six frequencies considered in this thesis.

1.4.3 Radar

The only other region of the electromagnetic spectrum for which clear-air attenuation is small enough that active instruments can be considered is the microwave region. The fraction of microwave power that is scattered by atmospheric particulates is far less than in the visible, making attenuation very small and multiple scattering negligible, but conversely resulting in a generally lower sensitivity. Scattering occurs predominantly in the Rayleigh regime (where wavelength is much larger than diameter), for which backscattered power is proportional to the fourth power of frequency and the sixth power of diameter. Rain radars typically have wavelengths of centimetres so that attenuation is negligible. For sensitivity to the much smaller particles in clouds, millimetre-wave radars are most suitable, although attenuation by atmospheric gases (predominantly water vapour and molecular oxygen) becomes important, and so wavelengths are chosen to lie in the minima between the strong absorption lines. Figure 1.1 shows gaseous attenuation as a function of frequency for both dry and saturated air at a pressure of 1000 mb and a temperature of 10°C, calculated using the line-by-line model of Liebe (1985). Superimposed are dotted lines corresponding to the six frequencies considered in this thesis. Observations will be presented from the three radars located at Chilbolton, Hampshire: the Chilbolton Advanced Meteorological Radar (CAMRa) at 3 GHz (Goddard et al. 1994a), the 35 GHz Rabelais radar (on loan from the University of Toulouse), and the recently-acquired 94 GHz Galileo radar (funded by ESTEC). The remaining three frequencies are considered in the context of a spaceborne radar in Chapter 5. The technology required to construct radars at frequencies of 79 GHz and higher at a reasonable cost has only been available for a decade or so (Lhermitte 1987, Clothiaux et al. 1995, Mead et al. 1989), and there is still much work to be done to fully exploit their potential for cloud research.

Because of the dependence of the returned signal on the sixth power of diameter, it is convenient to express cloud and precipitation measurements in terms of the radar reflectivity factor (Z), given simply by

$$Z = \int_0^\infty D^6 n(D) dD \qquad \mathrm{mm^6 m^{-3}} \tag{1.3}$$

where D is diameter and $n(D)dD$ is the number concentration of drops with diameters in the range D to $D + dD$. However this expression is valid only for liquid water drops in the Rayleigh scattering regime. In order to account for the effects of Mie scattering (which occurs when diameter and wavelength are of the same order) and ice (which backscatters a smaller fraction of the incident radiation), this is generalised to

$$Z = \int_0^\infty \frac{|K|^2}{0.93} D^6 \gamma(D) n(D) dD \qquad \mathrm{mm^6 m^{-3}} \tag{1.4}$$

where γ is the ratio of Mie to Rayleigh backscattered power, and $|K|^2$ is the dielectric parameter which depends on the dielectric constant of the particles, and has the value 0.93 for liquid water at centimetre wavelengths. D is defined here as the diameter of a sphere with the same volume as the particle. Z as defined in (1.4) is sometimes referred to as the effective reflectivity factor, and the reader should be aware that it is the habit of radar meteorologists (including myself) to refer to it simply as 'reflectivity'. Since Z varies over many orders of magnitude it is common to express it in the logarithmic unit dBZ:

$$Z[\mathrm{dBZ}] = 10 \log_{10}(Z[\mathrm{mm^6 m^{-3}}]) \tag{1.5}$$

Clearly the power of six means that Z is not directly related to any cloud parameter we wish to measure, so the challenge is to use it in combination with other remotely measurable parameters to estimate r_e and water content. A sizable body of literature exists on ways to tackle this problem, but rather than reviewing it all here the relevant papers are discussed in the introductions to each chapter. In this thesis the primary source of additional information is provided by using two radars at different frequencies; in stratocumulus the difference in liquid water attenuation is exploited to measure LWC and in cirrus the difference in Z due to Mie scattering is used to estimate crystal size and therefore IWC more accurately than would be possible with a single radar. Use is also made of Doppler and polarimetric information.

1.4.4 Aircraft

No summary of cloud-measuring instrumentation would be complete without mention of the crucial role played by aircraft to provide in situ measurements of size spectra. Such measurements are expensive and cannot be taken on an operational basis, but they can provide valuable insights into the physical processes occurring in clouds, and are vital to the validation of remote retrieval techniques. Indeed, two chapters of this thesis are based entirely on such data, predominantly from the UKMO C-130 Hercules aircraft.

1.4.5 Active instruments in space

The greatest advance in measuring the global effect of clouds on climate in the next decade is likely to be from the launch of a spaceborne radar and/or lidar, a proposal currently being considered by the European Space Agency (the 'Earth Radiation Mission'). This would enable a global climatology of vertically-resolved cloud properties to be retrieved over a period of several years. Many of the techniques used by ground-based active instruments would not be possible from space because of (among other things) reduced sensitivity, resolution and dwell time, so much work remains to be done to determine the most effective combination of instruments for measuring cloud properties from space. In Chapter 5 the potential of spaceborne dual-wavelength radar for measuring the ice water content of cirrus clouds is examined.

1.5 Unanswered questions

Several controversial issues in the field of clouds and climate have received much interest recently which, if verified, would necessitate a major rethink of the cloud processes that should be regarded important for climate. One such issue is that of so-called anomalous absorption, whereby synchronous measurements of solar radiation above and below stratiform cloud suggest that either clouds or water vapour absorb significantly more solar radiation than previously thought (Cess et al. 1995). Some estimates of the deficit are as much as 50 W m^{-2}, averaged globally (Evans et al. 1995). Many possible explanations have been suggested, such as oversimplified radiation models (particularly with regard to the treatment of inhomogeneous cloud fields), aerosol absorption, poor model reproduction of water vapour continuum absorption, and even measurement error. However it is far from agreed that anomalous absorption really exists; detailed aircraft measurements and radiative transfer calculations by Hayasaka et al. (1995) and Taylor et al. (1996) were found to be entirely consistent, suggesting that the effect may be illusory.

Another such issue is that of the possible role of the sun in the large natural variability that the climate system has exhibited in the past; if this could be established it would throw a completely new light on our understanding of climate change. The case for the link rests on apparent correlations between solar activity, principally but not exclusively the 11-year sunspot cycle, and meteorological parameters such as temperature and rainfall (comprehensively reviewed by Hoyt and Schatten 1997). This is treated with scepticism by most climate scientists because the actual change in solar irradiance is tiny and so according to current theory could never induce a temperature change large enough to measure. The most popular mechanism being pursued relates to the flux of galactic cosmic rays at the tropopause, which has a distinct decadal cycle because of the interaction with the solar wind, in addition to a well defined diurnal cycle. Through a chain of rather speculative mechanisms this is alleged to influence weather systems, for example via the scenario suggested by Tinsley and Deen (1991): cosmic rays determine tropospheric ion production, the consequent charging of supercooled droplets at the tops of clouds increases the rate of ice nucleation, which in turn increases the flux of ice crystals and leads to a larger release of latent heat which can intensify convection and cyclones.

If either of these two hypotheses were substantiated then the validity of radar retrievals would not be affected, although radar-measured cloud parameters would certainly be interpreted differently. Radar measurements alone are unlikely to provide evidence for or against these effects.

Unanswered questions do exist however for which radar techniques could potentially provide some answers. A good example is the problem of mixed-phase clouds, about which very little is known. Commonly in GCMs the ice/liquid water fraction is parameterised as a simple function of temperature between 0°C and around -15°C, and in the UKMO Unified Model, a small change in this function was found to reduce the IWC in the mid-latitude storm tracks by up to a factor of four (Gregory and Morris 1996). Such schemes are very simplistic and unphysical and could undoubtedly be improved upon with remote measurements of ice/liquid water ratio. A possible approach using Doppler spectra measured at two wavelengths is outlined in Section 3.4.

1.6 This thesis

In this chapter the importance of clouds in the climate system and the difficulty in representing them in models has been discussed. The approximate requirements for the accuracy and sensitivity of observations to provide a useful constraint on climate models have been set out.

In Chapter 2 the theoretical basis behind the accuracy and sensitivity of radar measurements is reviewed and extended. The main issue for a cloud radar is its sensitivity, and much care must be taken to ensure that as much of the signal as possible is extracted from the noise.

The potential of two active ground-based techniques to measure liquid water content in stratocumulus is explored in Chapter 3, using aircraft microphysical data from ASTEX. The first uses dual-wavelength radar at 35 and 94 GHz and the second uses a single radar which has the capability to measure Doppler spectra.

The remainder of the thesis is devoted to cirrus clouds. In Chapter 4, it is found from reanalysis of work presented in the literature that a commonly-used expression for crystal density is likely to be an underestimate, and a new expression is presented. This is then used in the interpretation of observations from an intercomparison flight of the UKMO C-130 aircraft and the Chilbolton radars.

In Chapter 5 we explore the potential of spaceborne dual-wavelength radar to make global measurements of crystal size in cirrus, and therefore retrieve ice water content more accurately than would be possible with a single radar. Aircraft data is analysed in detail to determine the accuracy achievable for six different frequency combinations. The technique is tested in Chapter 6, where results are presented from a case study in which the 35 and 94 GHz radars at Chilbolton were used to measure crystal size and ice water content in a thick cirrus cloud. The findings of Chapter 4 are used to also calculate effective radius and optical depth. The observations are compared with the analyses of the UKMO Unified Model.

Finally in Chapter 7, the results of the thesis are summarised and the accuracy of the various techniques are compared with the requirements outlined in this chapter.

CHAPTER TWO

Analysis of cloud radar data

2.1 Introduction

Meteorological research with traditional centimetre-wave 'weather' radar has tended to be primarily concerned with the regions of highest reflectivity—the severe storms, the hail shafts and the flood-producing downpours. The emphasis is quite different for cloud radar where the interest in clouds stems from their effect on the earth's radiation budget rather than from their role in severe weather. It is therefore crucial to ensure that instrument sensitivity is maximised, since large expanses of thin diffuse cloud can be as radiatively important as less frequent occurrences of thicker cloud.

This chapter is concerned with ways to improve the sensitivity and accuracy of cloud radar data, focussing on the procedures to be implemented after the measurements have been taken, rather than on hardware modifications. Firstly the theoretical factors which determine the accuracy of radar measurements are described, and the existing theory is extended to be applicable to the measurements proposed in this thesis. In particular we derive an expression for the precision of radar reflectivity in the presence of noise and when not all pulses are independent. Then the practical problems faced in the processing of real data are discussed, including the correction of various systematic errors due to deficiencies in the hardware. Finally the considerations for the processing of dual-wavelength radar data are outlined briefly.

2.2 Theoretical accuracy of reflectivity measurements

2.2.1 Fundamentals

The signal measured by a radar after sending out a single pulse consists of

1. Backscatter from hydrometeors;
2. Backscatter from non-meteorological targets in the atmosphere (birds and insects);
3. ‘Bragg scatter’ from refractive index inhomogeneities on the scale of half the wavelength of the radiation (which is negligible at millimetre wavelengths);
4. Backscattered radiation from surface targets (ground clutter);
5. Thermal emission by the atmosphere;
6. Receiver noise.

The sensitivity of radar to backscatter from hydrometeors is governed by the magnitude of the contribution from other sources; in most of the depth of the atmosphere this will be thermal emission and receiver noise, but clutter from birds, insects and the ground can dominate near the surface.

At each range-gate the echo returned from a single pulse can be considered to be a complex voltage $V = I + iQ$, where I and Q are the in-phase and quadrature components. Where clutter is significant, it is usually impossible to extract the meteorological contribution and the data must be rejected. We shall therefore consider the case when only hydrometeors (the ‘signal’) and noise are present, in which case I and Q consist of the sum of the contributions from these two sources ($I = I_S + I_N$ and $Q = Q_S + Q_N$, with the suffixes S and N denoting signal and noise respectively). If the radar does not have Doppler capability then only the power P, given by

$$P = VV^* = I^2 + Q^2 \tag{2.1}$$

is measured. Unlike the return from a single target, the return from distributed targets fluctuates with time as the individual particles rearrange themselves with respect to each other a distance comparable to the wavelength of the radiation, and the individual backscattered waves constructively and destructively interfere. Noise also fluctuates in this way. It is necessary to take the mean over many pulses in order to reduce this fluctuation and increase the accuracy of the measured reflectivity. The mean power is the sum of the mean signal and mean noise components:

$$\bar{P} = \bar{S} + \bar{N}, \tag{2.2}$$

and the estimated reflectivity factor is then simply the signal estimate after range correction and calibration

$$\hat{Z} = C\hat{S}r^2 = C(\bar{P} - \hat{N})r^2 \tag{2.3}$$

where C is some calibration coefficient and r is the range.

Systematic error in $\hat{Z}$ depends on the calibration and is dealt with in Section 2.3.2, but in the remainder of this section we are concerned with the error in our estimate of signal power, $\hat{S}$, which determines the *random* error in $\hat{Z}$.

2.2.2 Accuracy of a single pulse

Since I and Q for a single pulse consist of the sum of a large number of random, independent variables, it follows from the Central Limit Theorem that they will have a (zero-mean) Gaussian probability distribution:

$$p(I) = \frac{1}{\sqrt{2\pi}\,\sigma_{I,Q}} \exp\left(-\frac{I^2}{2\sigma_{I,Q}^2}\right) \tag{2.4}$$

and similarly for Q. The probability distribution for P is therefore a simple exponential distribution:

$$p(P) = \frac{1}{\sigma_P} \exp\left(-\frac{P}{\sigma_P}\right). \tag{2.5}$$

The standard deviation of this distribution is equal to the mean, and is given by

$$\sigma_P = \bar{P} = 2\sigma_{I,Q}^2. \tag{2.6}$$

In logarithmic units the standard deviation is 5.6 dB (Doviak and Zrnić 1993).

The same equations also apply separately to the signal and noise components of the power.

2.2.3 Number of independent pulses

Suppose the average power $\bar{P}$ is calculated from M samples, a time τ_s apart. The standard error in $\bar{P}$ is then given by

$$\Delta P = \frac{\sigma_P}{\sqrt{M_I}} = \frac{\bar{P}}{\sqrt{M_I}} \tag{2.7}$$

where M_I is the *equivalent* number of independent pulses. If the noise is much larger than the signal then every pulse will be independent, and $M_I = M$. However, if the signal is much larger than the noise, then M_{I} is equal to $M_{\mathrm{I},S}$, the number of independent pulses for the signal only, which depends on the time it takes for the individual particles to move relative to one another such that the signal is essentially uncorrelated (the 'time to independence'). In between these two extremes, M_{I} will be some kind of weighted average between M and $M_{\mathrm{I},S}$.

It was shown by Papoulis (1965) that

$$\frac{1}{M_{\mathrm{I}}} = \sum_{m=-(M-1)}^{M-1} \frac{M-|m|}{M^2} \rho_{\mathrm{r}}(m\tau_{\mathrm{s}}), \tag{2.8}$$

where $\rho_{\mathrm{r}}(m\tau_{\mathrm{s}})$ is the normalised autocorrelation between the receivers output samples a time $m\tau_{\mathrm{s}}$ apart. For a square-law detector (i.e. one which determines $\bar{P}$ by averaging estimates of the power rather than the amplitude or the logarithm of the power) such as that at Chilbolton, $\rho_{\mathrm{r}} = \rho_P^2$ (Papoulis 1965), where ρ_P is the normalised autocorrelation function of I or Q.

According to Doviak and Zrnić (1993), the *unnormalised* autocorrelation at lag $m\tau_{\mathrm{s}}$ is given by

$$R(m\tau_{\mathrm{s}}) = \bar{P}\rho_P(m\tau_{\mathrm{s}}) = \bar{S}\rho_S(m\tau_{\mathrm{s}}) + \bar{N}\rho_N(m\tau_{\mathrm{s}}), \tag{2.9}$$

where ρ_S and ρ_N designate the normalised autocorrelation of the I or Q components of the noise and signal respectively. Since the noise is uncorrelated from one pulse to the next, $\rho_N(m\tau_{\mathrm{s}})$ is equal to the delta function δ_m where δ_m is 1 for $m = 0$ and zero otherwise. Hence

$$\begin{aligned} \rho_r(m\tau_{\mathrm{s}}) = \rho_P^2(m\tau_{\mathrm{s}}) &= \left(\frac{\bar{S}}{\bar{P}}\rho_S(m\tau_{\mathrm{s}}) + \frac{\bar{N}}{\bar{P}}\delta_m\right)^2 \\ &= \frac{\bar{S}^2}{\bar{P}^2}\rho_S^2(m\tau_{\mathrm{s}}) + \frac{\bar{N}^2 + 2\bar{S}\bar{N}}{\bar{P}^2}\delta_m. \end{aligned} \tag{2.10}$$

It can be seen from (2.8) and (2.10) that the correct weighting between M and $M_{\mathrm{I},S}$ to determine M_{I} is given by

$$\frac{1}{M_{\mathrm{I}}} = \frac{\bar{S}^2}{\bar{P}^2}\frac{1}{M_{\mathrm{I},S}} + \frac{\bar{N}^2 + 2\bar{S}\bar{N}}{\bar{P}^2}\frac{1}{M}. \tag{2.11}$$

Finally this is substituted into (2.7) to get

$$\Delta P = \left(\frac{\bar{S}^2}{M_{\mathrm{I},S}} + \frac{\bar{N}^2 + 2\bar{S}\bar{N}}{M}\right)^{\frac{1}{2}} \tag{2.12}$$

We now derive an expression for $M_{\mathrm{I},S}$. Assuming the Doppler velocity spectrum is Gaussian with a standard deviation σ_w, the normalised autocorrelation function for I or Q of the signal is given by (Doviak and Zrnić 1993):

$$\rho_S(m\tau_\mathrm{s}) = \exp\left[-8\left(\frac{\pi\sigma_w m\tau_\mathrm{s}}{\lambda}\right)^2\right]. \tag{2.13}$$

Inserting $\rho_S^2(m\tau_\mathrm{s})$ into (2.8) we get

$$\frac{1}{M_{\mathrm{I},S}} = \sum_{m=-(M-1)}^{M-1} \frac{M-|m|}{M^2} \exp\left[-\left(\frac{4\pi\sigma_w m\tau_\mathrm{s}}{\lambda}\right)^2\right]. \tag{2.14}$$

Summations are inconvenient as they require numerical evaluation, but this expression can be closely approximated by:

$$M_{\mathrm{I},S} \simeq \left[\left(M\left[\left(\frac{4\pi^{\frac{1}{2}}\sigma_w\tau_s}{\lambda}\right)^{-8}+1\right]^{-\frac{1}{8}}\right)^{\frac{7}{4}}+1\right]^{\frac{4}{7}}. \tag{2.15}$$

In the specific case of $M \gg M_{\mathrm{I},S} \gg 1$, this can be simplified further to obtain

$$M_{\mathrm{I},S} \simeq M\,\frac{4\pi^{\frac{1}{2}}\sigma_w\tau_\mathrm{s}}{\lambda}, \tag{2.16}$$

which is sometimes expressed as the 'time to independence':

$$\tau_\mathrm{I} = \frac{M}{M_{\mathrm{I},S}}\tau_\mathrm{s} \simeq \frac{\lambda}{4\pi^{\frac{1}{2}}\sigma_w}. \tag{2.17}$$

Figure 2.1 shows a comparison between the numerical evaluation of (2.14) and the analytical approximations given by (2.15) and (2.16), for $M = 1000$. Clearly (2.15) provides an excellent approximation to the full solution. The spectral width σ_w can be measured routinely by a radar with Doppler capability, so in practice it could be used with (2.15) to estimate $M_{\mathrm{I},S}$ and hence (as we shall see) the precision of the measured reflectivity factor.

For a spaceborne radar the time to independence again depends on the observed Doppler width, but this time it is predominantly due to the velocity of the satellite relative to the cloud and the finite beamwidth of the instrument, rather than the variation of vertical velocity within the radar

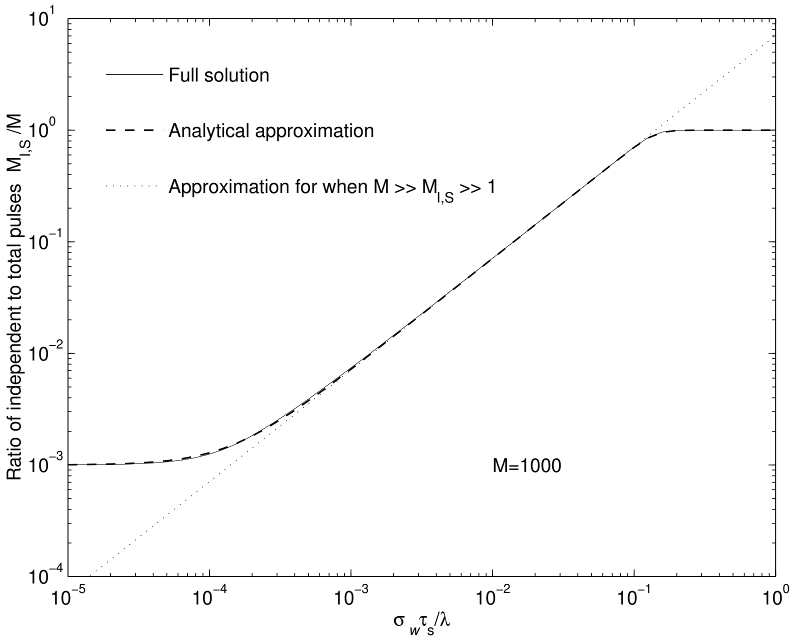

Figure 2.1: The ratio of independent to total pulses (in the absence of noise) versus $\sigma_w\tau_s/\lambda$ (see text for definitions). The three lines correspond to the full solution (Eq. 2.14), the analytical approximation given by (2.15) and the simple approximation for the case when $M \gg M_{I,S} \gg 1$, given by (2.16). In this particular case there were a total of 1000 pulses.

pulse volume. If the velocity of the satellite is v and the main beam of the radar in the direction of flight can be represented by a Gaussian weighting function with a standard deviation of σ_θ radians, then the observed Doppler spectral width is simply $v\sigma_\theta$. However the breadth of the weighting function is usually expressed in terms of the beamwidth θ, defined as the angular distance between the points on each side of the beam where the weighting function falls to half its peak value. Hence $\theta = 2\sqrt{2\ln 2}\,\sigma_\theta$, and from (2.17) we obtain:

$$\tau_I = \sqrt{\frac{\ln 2}{2\pi}}\frac{\lambda}{v\theta} \simeq \frac{1}{3}\frac{\lambda}{v\theta}. \tag{2.18}$$

The spaceborne cloud radar proposed by IGPO (1994) would have a beamwidth of 0.2° (corresponding to a 1 km footprint), a wavelength of 3.2 mm, and being on a polar-orbiting satellite would have a surface-relative velocity of 7 $\mathrm{km\,s^{-1}}$. This results in a time to independence of 0.05 ms. Since the pulse repetition frequency (PRF) would have to be less than 3 kHz to avoid misinterpreting 'mirror-image' cloud signals that have been reflected from the ground, every pulse of a spaceborne system can be considered independent.

The noise $\hat{N}$ estimated from the cloud-free gates in the stratosphere is subtracted from $\bar{P}$:

$$\hat{S} = \bar{P} - \hat{N}; \qquad \Delta\hat{S}^2 = \Delta P^2 + \Delta\hat{N}^2. \tag{2.19}$$

However $\hat{N}$ is typically calculated by averaging the power from 50 or so gates, resulting in $\Delta\hat{N}$ being around 7 times less than ΔN, so in fact $\Delta\hat{S} \simeq \Delta P$. From (2.3) we see that $\Delta Z/Z = \Delta\hat{S}/\hat{S}$ and hence from (2.12) we have in logarithmic units

$$\Delta Z_{\mathrm{dB}} = \frac{10}{\ln 10}\frac{\Delta\hat{S}}{\hat{S}} = 4.343\left(\frac{1}{M_{\mathrm{I},S}} + \frac{1}{M}\left[\frac{1}{\mathrm{SNR}^2} + \frac{2}{\mathrm{SNR}}\right]\right)^{\frac{1}{2}}. \tag{2.20}$$

If all pulses are independent then this reduces to

$$\Delta Z_{\mathrm{dB}} = \frac{4.343}{\sqrt{M}}\left(1 + \frac{1}{\mathrm{SNR}}\right). \tag{2.21}$$

Meneghini and Kozu (1990) considered the case when noise was estimated from only one gate and all pulses were independent.

There is a limit to how far below the noise level we can extract the meteorological signal. Since after averaging the standard error of the mean noise power $\bar{N}$ is ΔN, to be confident that a measured power contains a signal from clouds, we must reject all those returns for which the power is less than $\bar{N} + \eta\Delta N$. Hence the minimum measurable signal is $\bar{S}_{\mathrm{min}} = \eta\Delta N$. If η is set too high then useful data is lost, and if it is set too low then anomalous points of cloud are evident in the final reflectivity field in regions of the sky which obviously should be cloud-free.

Illingworth et al. (1997) considered a value of $\eta = 2$ for a spaceborne radar, which since the signal in regions of noise is distributed normally, would reject 97.73% of cloud-free data. For the interpretation of ground-based radar data in Chapter 6, the higher threshold of $\eta = 3$ has been used, which in accordance with statistical theory is found to reject 99.87% of cloud-free data.

Since $\Delta N = \bar{N}/\sqrt{M}$, the minimum signal-to-noise ratio for cloud detection is

$$\begin{aligned} \mathrm{SNR}_{\mathrm{min}} &= \frac{\eta}{\sqrt{M}}; \\ \mathrm{SNR}_{\mathrm{min,dB}} &= 10\log_{10}\left(\frac{\eta}{\sqrt{M}}\right) \end{aligned} \tag{2.22}$$

which tells us the sensitivity gained by subtracting noise. At this threshold, the standard error in the measured signal is given by

$$\Delta Z_{\mathrm{dB}} \simeq \frac{4.343}{\eta}. \tag{2.23}$$

2.3 Application to real data

In the summer of 1996, around 800 hours of data were recorded by the 35 GHz Rabelais radar and the 94 GHz ESTEC Galileo radar at Chilbolton, including over 100 hours during which the instruments were operating simultaneously. The antennae were colocated and vertically-pointing, and recorded uncalibrated reflectivity factor to the nearest 0.01 dB. Each ray of data consisted of a ten-second average of Z at each of 199 range-gates. The range-gate spacing was 75 m and the maximum range was 15 km. Although the pulse repetition frequencies were 3125 Hz at 35 GHz and 5000 Hz at 94 GHz, the recording system was not fast enough to average every pulse, so Z was in fact an average of 3125 evenly spaced pulses at 35 GHz and 10 000 at 94 GHz. Hence from (2.22) we calculate that the respective minimum detectable reflectivities at 35 and 94 GHz were 12.7 and 15.2 dB lower than the noise level, respectively.

2.3.1 Averaging

It can be seen from (2.20) and (2.22) that both radar accuracy and sensitivity increase as the square root of the number of samples. Therefore if the radar is to be used in a role for which resolution is not a priority, then there is much to be gained by averaging the data in both time and range before subtracting the noise. For instance, comparison of radar measurements with the hourly analyses from a forecast model would only require a resolution of one hour and, say, 300 m. Therefore 1440 pixels of the original 10 s/75 m data could be averaged resulting in a further 15.8 dB increase in sensitivity. Studies of cloud microstructure on the other hand would require much higher spatial resolution.

It might be expected after inspection of Fig. 2.2 that because the mean noise $\bar{N}$ varies appreciably as low clouds pass overhead in addition to the instantaneous noise N fluctuating from pulse to pulse, one should definitely not average over much longer than a few minutes. This is not the case. The standard error after averaging is increased somewhat by this variation, but in the example of Fig. 2.2, even for an averaging time of an hour the slow variation ($\sim \pm 0.5$ dB) is considerably less than the pulse-to-pulse fluctuation ($\pm$ 5.6 dB) It also turns out that because in linear space the slow variation in the noise level is a multiplicative rather than an additive effect to the pulse-to-pulse fluctuation, the noise is *still* independent every pulse. If during the averaging time the standard deviation of the slow variation (in linear units) is σ_{N_0}, then the standard error of the mean noise is

$$\Delta N = \sqrt{\frac{\bar{N}^2 + \sigma_{N_0}^2}{M}}, \tag{2.24}$$

which reduces to a form similar to (2.7) when σ_{N_0} is small.

2.3.2 Calibration

Calibration is frequently a problem for meteorological radars, but the solution in this case has been to use range-height scans (RHIs) through low cloud (taken on 1 August 1996) with the colocated 3 GHz antenna in operation. The 3 GHz radar has itself been calibrated to an accuracy of better than 0.5 dB from the consistency of differential reflectivity and differential phase measurements in moderate rain (Goddard et al. 1994b), but at vertical incidence it is of little use because of severe ground clutter. After matching 35 and 3 GHz reflectivities, the 35 GHz noise at 1 km was found to be -34 dBZ. It is reasonable to assume that this would be approximately the same at vertical incidence, so the radar was calibrated on other occasions simply by adjusting the reflectivity so that the mean value of N was -34 dBZ.

The same RHIs suggested that the equivalent value at 94 GHz was -23 dBZ, although hardware problems with this instrument caused its sensitivity to vary with temperature. For this reason, wherever possible the 94 GHz radar was calibrated by matching reflectivity with the 35 GHz radar in regions of unattenuated Rayleigh scattering.

2.3.3 Attenuation correction

Attenuation by liquid water, water vapour and oxygen becomes important at millimetre wavelengths. The total two-way gaseous attenuation at 10 km amounts to about 1 dB at 35 GHz and 3 dB at 94 GHz. Radar measurements are corrected using the line-by-line model for millimetre-wave propagation of Liebe (1985), coupled with the temperature, pressure and humidity diagnosed by the mesoscale version of the UKMO Unified Model. In warm clouds if dual-wavelength radar were to be used to measure liquid water attenuation, then the removal of attenuation from other sources would be an essential step, but in cirrus where the vapour densities of water vapour and oxygen are much lower this is a minor adjustment.

2.3.4 Ground clutter

Until a rigid arm had been fabricated to secure the 94 GHz next to the 35 GHz radar on the side of the main 25 m dish at Chilbolton to allow for scanning and comparison with the 3 GHz radar, these two radars were operated from the ground in a fixed vertically-pointing configuration. When they were mounted on the main dish however, the corruption of the data by ground clutter increased, especially at 35 GHz where it was significant up to 2 km on some occasions. Ground clutter at vertical incidence is caused by power from the feed spilling out over edges of the antenna and impinging on the ground beyond. If the antenna is raised up then the ground a given distance away will subtend a greater angle at the feed of the radar and so more sidelobe power will be returned from it. Future observational campaigns will use a specially constructed skirt of absorbing material around the 35 GHz antenna to greatly reduce this problem.

2.3.5 Hardware problems

A number of hardware problems were apparent in the data and were corrected for where possible. Nothing could be done about the sensitivity loss at 94 GHz of 10 to 15 dB compared with the 35 GHz radar, which was due to a drift of the transmit frequency of the gun diode with temperature. This meant that there was a need to periodically retune the instrument so that the beat frequency after the returned signal was mixed with the signal from the Stable Local Oscillator was matched with the frequency of the low-pass filter. The instrument will be Dopplerised before the next recording campaign, with the useful spin-off that the transmit frequency will be fixed.

Two other problems showed up in parts of the data as systematic biases which varied with range. The first was due to the fact that range calibration was initially carried out to only the nearest 0.25 dB. The effect of this was removed by examining a long period of completely cloud-free data to obtain the bias at each gate, and then subtracting this (in log space) from data which contained cloud before performing the noise subtraction. The second problem was caused by interference in the received signal by an 80 kHz oscillator (with harmonics) somewhere in the hardware, and manifested itself as a periodic variation with range, with a wavelength of 1.875 km. Since its relative magnitude varied as the contribution from noise changed, it was not a constant offset and could not be removed in the same way as the range calibration problem. The best solution was found to be to use the noise observations in the cloud-free stratosphere to determine the shape of the oscillation for one wavelength, and to assume that this shape was repeated through the whole depth of the atmosphere. In this way the contribution from the oscillator could be incorporated into the estimated noise, which was then subtracted from the measured signal.

Naturally, estimation of biases such as these is less accurate than estimating thermal and instrument noise alone, so the threshold for data rejection usually had to be set a little higher than would have been possible with a completely ‘clean’ signal, and consequently the accuracy and sensitivity of Z were not as good as they might have been.

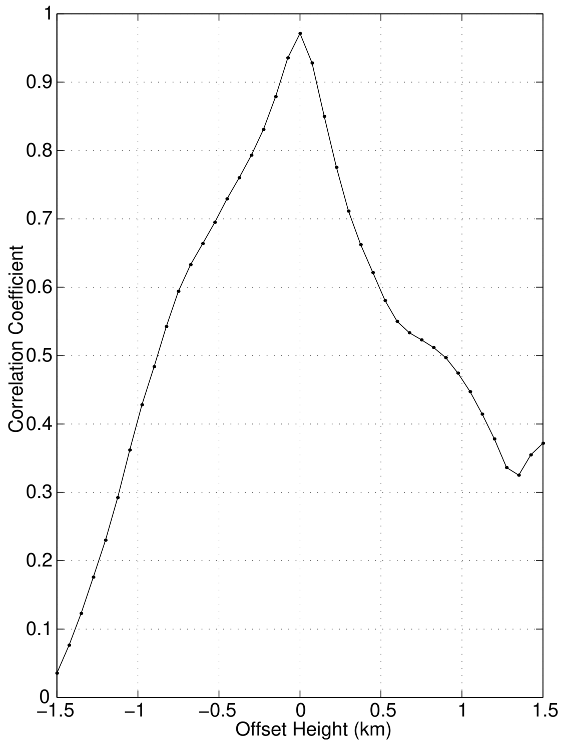

Figure 2.3: The correlation of 35 and 94 GHz reflectivity data in cirrus on 22 June 1996, as a function of offset distance and offset time.

2.3.6 Dual-wavelength considerations

During the 1996 campaign, the two radars operated continuously and recorded data in 10-second dwells, but the start time of each dwell was not synchronised between the two radars, there usually being an offset of around 4 seconds. Interpolating the data from one of the radars on to the time grid of the other was found to noticeably reduce the scatter in the dual-wavelength ratio.

To verify that the two radars were optimally coaligned, Fig. 2.3 shows the correlation of 35 and 94 GHz reflectivity fields in cirrus taken on 22 June 1996, after being offset temporally and spatially. It is clear that there is no systematic offset in the alignment of the radars in range or time. However the wind at cirrus altitudes on this day was from the north, and it is conceivable that the radar beams were mismatched in an east-west direction which would only be revealed by performing the same experiment in an Easterly or Westerly wind. The best way to confirm alignment however would be to scan across the sun; this was done with the 3 and the 35 GHz radars at Chilbolton and confirmed that the two radars are coaxially aligned to better than 0.1° (Illingworth et al. 1995).

CHAPTER THREE

Two methods to deduce the liquid water content of stratocumulus clouds

3.1 Introduction

Of all clouds, low-level stratus and stratocumulus have the most profound impact on the earth's radiation budget because of their high optical depth and large global coverage. Their abundance over large areas of the ocean is readily apparent from satellite imagery, particularly over the eastern parts of the subtropical Atlantic and Pacific, where large-scale subsidence from the descending arm of the Hadley Circulation occurs over relatively cold sea surface temperatures. Arctic stratus is an even more persistent feature which occurs over the polar oceans, and where in the summer months the total mean cloud cover can exceed 90% (Vowinckel and Orvig 1970).

Stratus and stratocumulus clouds have an overall cooling effect on climate since they reflect most of the incoming solar radiation back into space, yet emit in the long-wave at a similar brightness temperature to the surface (Randall et al. 1984). Their climatic importance was demonstrated by Slingo (1990), who found that a modest 15–20% increase in the total global coverage of these clouds (equivalent to only 5% more of the earth's surface being covered) would offset the increase in mean global temperature caused by a doubling of the amount of carbon dioxide in the atmosphere. The same effect could be achieved by increasing liquid water path by 20–35% on average, or decreasing the mean droplet radius by 15–20%. Clearly it is crucial to our understanding of climate change that the behaviour of low clouds in response to other changes in the climate system is understood.

Passive instruments have the capability to retrieve vertically-integrated properties of stratocumulus clouds, but they invariably encounter problems in multi-layered cloud systems. White et al. (1995) used a ground-based microwave radiometer to measure liquid water path and shortwave radiometers for optical depth, from which the mean effective radius through the depth of the cloud was derived. Similar techniques can be used from satellites; for instance Greenwald et al. (1993) demonstrated the use of the Special Sensor Microwave/Imager (SSM/I) to obtain liquid water path, although their method relied on the emissivity of the surface being known, so was only reliable over oceans free from sea-ice. A more advanced technique was used by Han et al. (1994) to obtain effective radius at cloud top, using data from the Advanced Very High Resolution Radiometer (AVHRR). However to measure the vertical profile of cloud properties and to cope with multi-layered cloud requires active instruments. Lidar suffers severe attenuation in liquid water cloud, so there is a need to explore the potential of radar for this purpose.

It is invariably more difficult to make good measurements of liquid-phase clouds than of cirrus using radar, principally because the small liquid droplets tend to have a much lower radar reflectivity than the much larger ice crystals found in cirrus. Furthermore, the data in the lowest few kilometres is often contaminated by birds and insects (sometimes collectively referred to as 'atmospheric plankton') and ground clutter; this is clearly apparent in Fig. 2.2. Insects are not found in clouds, but their presence in the surrounding air can make cloud boundaries difficult to identify. Algorithms to reject non-meteorological atmospheric targets have been developed which use their characteristic Mie scattering or depolarisation properties to distinguish them from low cloud (e.g. Lohmeier et al. 1997). Single wavelength, single polarisation radars could only expect to be able to reject insects by relying on their characteristically intermittent returns, although the data would have to be recorded at a high temporal resolution which is expensive in terms of data storage if the radar is to be left unattended for long periods of time. Ground clutter can be rejected using its Doppler signature (Passarelli et al. 1981), but one should note that it is a problem which decreases with increased frequency, and for a ground-based vertically-pointing 94 GHz radar is only really significant in the lowest few hundred metres.

It was shown by Fox and Illingworth (1997b) that simple power-law relationships between radar reflectivity and liquid water content (LWC), such as proposed by Atlas (1954), would be very inaccurate for estimating LWC because of the ubiquitous presence of occasional drizzle drops a few hundred microns in diameter which dominate the reflectivity but contribute negligibly to LWC. The droplets which contain the bulk of the liquid water and dominate the radiative properties of the cloud are in fact those smaller than 50 μm. The existence of two distinct components in the distribution reflects the two very different physical processes that are occurring. When a cloud first forms, droplets grow by vapour deposition for which the rate of increase in diameter D is proportional to D^{-1}. Therefore after an initial rapid increase, D tends to level-out at a few tens of microns, which corresponds to a terminal fall speed of a few centimetres per second. Once the cloud is reasonably thick a few of the largest droplets have an appreciable fall speed relative to the smaller droplets, and can grow rapidly by collision and coalescence to form drizzle. Note that in cirrus the dominant mode of crystal growth is by vapour deposition, so the distributions tend to be more monomodal.

In this chapter two new methods to measure LWC which circumvent the problem of drizzle are described and compared. The first uses dual-wavelength radar and exploits the fact that liquid-water attenuation at millimetre-wavelengths is proportional to LWC and increases with frequency. The second uses high-resolution Doppler spectra measured by a single millimetre-wave radar to isolate the cloud and drizzle components of the spectrum, and rather than attempting to 'deconvolve' the spectrum to determine the size distribution (e.g. Gossard 1994), it has been found that the reflectivity of the cloud component alone is closely related to LWC. Aircraft size spectra obtained during the Atlantic Stratocumulus Transition Experiment (ASTEX) have been analysed to estimate the errors associated with these two techniques.

Finally we explore the potential of Doppler-spectra measured simultaneously at two different wavelengths to retrieve even more information about the size distribution in stratocumulus. This approach could also prove useful in mixed-phase clouds. Validation of the ideas presented in this chapter, using coincident observations by radar and aircraft, is seen as essential.

3.2 Retrieval of LWC using differential attenuation

3.2.1 Background

A useful property of liquid-phase hydrometeors is that, provided they are small enough to attenuate in the Rayleigh regime, their attenuation of microwave radiation is exactly proportional to LWC and increases with frequency. It is simple in principle therefore to use the difference in the reflectivity factor measured at two different wavelengths to deduce LWC, without the need to resort to any empirical relationships. A further advantage is that the method is insensitive to the absolute calibration of the radars; only the ability to measure differences in reflectivity is required. The use of attenuation to measure LWC was first suggested by Atlas (1954), but it was not until the development of 35 GHz radars that attenuation has really been measurable in non-precipitating clouds. Eccles and Mueller (1971) proposed the use of coincident 3 and 10 GHz radars to estimate the mass of liquid precipitation during convective storms, but a number of factors made it difficult to implement:

- The algorithm failed if any hail was present because of the contribution of Mie scattering to the reflectivity difference.
- It was found that radars with wavelengths large enough to penetrate most storms were only capable of measuring attenuation over relatively long paths, such that the very large rainfall rates from intense but localised events would be 'smeared out'. Differential reflectivity (Z_{DR}) is a better parameter for providing extra information on the size distribution since, like reflectivity, it is a point measurement.
- The drops contributing most to the attenuation in heavy rain are several millimetres in diameter, so at a frequency of 10 GHz the Rayleigh approximation no longer holds and the attenuation is not directly proportional to LWC. Moreover, it is generally the rainfall rate which is required, so empirical relationships between this and LWC must be used.

However in clouds it *is* LWC which is of interest, and the droplets contributing most to the attenuation (i.e. those containing the bulk of the liquid water) are typically no more than 30 μm in diameter, so even at 94 GHz are two orders of magnitude smaller than the wavelength and firmly in the Rayleigh regime.

Recently Martner et al. (1993) attempted to measure LWC from horizontal scans of a dual-wavelength radar at 10 and 35 GHz. The attenuation at 35 GHz was measurable only at a resolution of 4 km or worse, suggesting that these frequencies could not be used to obtain vertical profiles of LWC in stratocumulus. They used the technique in supercooled clouds and reported occasions when the 10 GHz reflectivity decreased more sharply with range than that at 35 GHz, indicating that Mie scattering by large ice crystals was occurring.

Other more complicated algorithms using attenuation to measure LWC have been been proposed in the literature. Gosset and Sauvageot (1992) described a method for determining both the liquid and ice water contents of mixed-phase clouds using dual-wavelength radar (also at 10 and 35 GHz), which made the assumption that below 0°C, small liquid-phase droplets dominated LWC while only ice crystals several hundred microns in diameter made a significant contribution to the reflectivity. Since it has been shown by Fox and Illingworth (1997b) that liquid drizzle drops as large as this are common in stratocumulus, there is a clear danger that this algorithm may wrongly interpret a reflectivity of greater than around −18 dBZ to indicate the presence of ice when in fact all the reflectivity can be attributed to liquid water. However at present not enough is known about mixed-phase clouds to state whether this is a significant possibility. Testud and Amayenc (1989) proposed the 'stereoradar' technique in which an airborne dual-beam radar at a single attenuated wavelength observes precipitation from two different angles. Then in theory both the 'true' (i.e. unattenuated) reflectivity and attenuation-coefficient fields can be determined by solving a fairly simple differential equation. This applicability of this concept has recently been extended to non-precipitating clouds, using a frequency of 94 GHz (Guyot and Testud 1998).

In this section we examine the feasibility of using dual-wavelength radar to measure vertical profiles of LWC in non-precipitating stratus and stratocumulus. In choosing the most appropriate frequencies for this application, there is a balance to be struck between the advantages of increased radar sensitivity and large liquid-water attenuation which are to be gained by using high frequencies, and the need for the Rayleigh approximation to be valid at both frequencies so that differences in reflectivity can be confidently attributed to attenuation alone. There is also the possibility that strong water vapour and liquid water attenuation could lead to a complete loss of signal at very high frequencies such as 215 GHz (Mead et al. 1989). We shall consider the combination of 35 and 94 GHz, which requires that the droplets contributing most to the reflectivity must be smaller than around 0.3 mm, but for which the attenuation is sufficiently large that it can be measured along a vertical path. At these frequencies and a temperature of 10°C, the two-way differential attenuation per $\mathrm{g\,m^{-3}}$ of liquid water is 7.1 $\mathrm{dB\,km^{-1}}$, which is clearly measurable. However gaseous attenuation (predominantly by water vapour and oxygen) is a correction which has to be made by assuming that all regions where cloud is detected are saturated, and taking the temperature from radiosonde ascents or a forecast model. The differential attenuation due to gases at 10°C and mean sea level pressure is 0.5 $\mathrm{dB\,km^{-1}}$. The possibility of errors in LWC caused by errors in the assumed temperature is examined later.

To detect differential attenuation over relatively short distances, reflectivity factor needs to be measured to an accuracy much greater than is usually necessary with weather radars, and this is achieved by averaging over a large number of independent pulses. Naturally it is important that the beams of the two radars are closely aligned so that they are observing the same region of cloud.

3.2.2 Theory

At an attenuating frequency f and an altitude z, the measured reflectivity factor Z_f is related to the unattenuated reflectivity factor at centimetre wavelengths Z (in conventional logarithmic units) by

$$Z_f[\mathrm{dBZ}] = Z[\mathrm{dBZ}] + 10\log_{10}\left(\frac{|K_f|^2}{0.93}\right) - 2\int_0^z (\alpha_{\mathrm{g},f} + \alpha_{\mathrm{l},f})\,dz \tag{3.1}$$

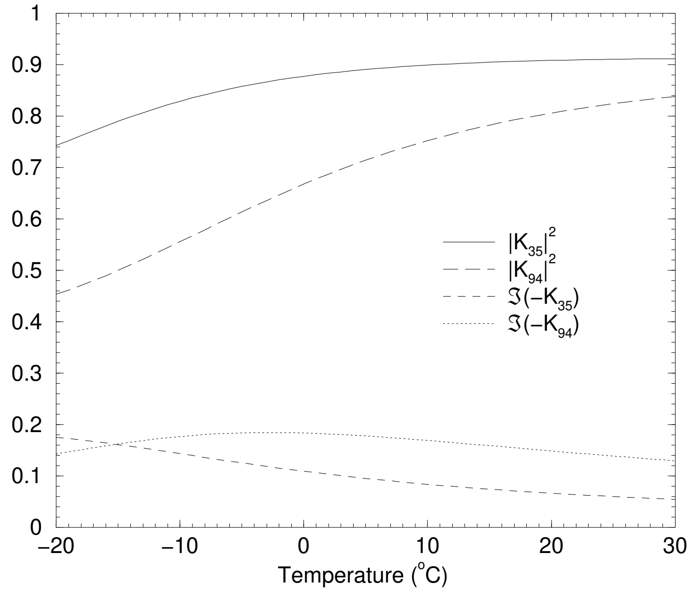

Figure 3.1: The variation of four dimensionless dielectric parameters with temperature.

where $\alpha_{\mathrm{g},f}$ and $\alpha_{\mathrm{l},f}$ are the one-way specific attenuation coefficients in dB km^{-1} due to atmospheric gases (predominantly molecular oxygen and water vapour) and liquid water respectively. No other atmospheric constituents significantly attenuate the radar beam at frequencies below 350 GHz. The second term on the right accounts for the fact that at millimetre wavelengths the dielectric parameter $|K|^2$ is less than its centimetre-wavelength value of 0.93, and is a function of temperature. K is related to the complex permittivity of water ε by

$$K = \frac{\varepsilon - 1}{\varepsilon + 2} \tag{3.2}$$

The double-Debye formulation of Liebe et al. (1989) is used to calculate ε as a function of temperature for both frequencies. A plot of the variation of $|K|^2$ with temperature, for both 35 and 94 GHz, is shown in Fig. 3.1. Also shown is $\Im(-K)$ (where $\Im$ denotes the imaginary part), a parameter which is important in determining the attenuation.

Line-by-line calculations have been carried out to determine the specific attenuation of atmospheric gases at each frequency as a function of the atmospheric thermodynamic variables, using the model described by Liebe (1985). The reduced line base was used (valid for frequencies less than 300 GHz) which consists of 34 oxygen lines, 3 water vapour lines, and oxygen and water vapour continua. Usually we will be interested in the attenuation of air saturated with respect to liquid water, and values of $\alpha_{\mathrm{g},f}$ for saturated air at 1013 mb are given in Table 3.1.

Extinction by hydrometeors is due to absorption and scattering. In the Rayleigh regime the cross-sections of absorption (σ_a) and scattering (σ_s) for a single droplet of diameter D are given by

T °C	$\lvert K_{35}\rvert^2$	$\lvert K_{94}\rvert^2$	$\alpha_{g,35(\text{saturated})}$ dB km^{-1}	$\alpha_{g,94(\text{saturated})}$ dB km^{-1}	$k_{l,35}$ dB km^{-1}/g m^{-3}	$k_{l,94}$ dB km^{-1}/g m^{-3}
−20	0.7427	0.4534	0.0541	0.1128	1.672	3.674
−10	0.8287	0.5555	0.0620	0.1785	1.371	4.539
0	0.8771	0.6675	0.0843	0.3230	1.044	4.710
10	0.8989	0.7520	0.1355	0.6358	0.802	4.341
20	0.9081	0.8058	0.2455	1.3101	0.637	3.816
30	0.9116	0.8380	0.4773	2.7544	0.524	3.328

Table 3.1: Temperature dependent parameters at 1013 mb. The attenuations are one-way.

(Doviak and Zrnić 1993):

$$\sigma_a = \frac{\pi^2 D^3}{\lambda}\Im(-K) \qquad \mathrm{m}^2; \tag{3.3}$$

$$\sigma_s = \frac{2}{3}\frac{\pi^5 D^6}{\lambda^4}|K|^2 \qquad \mathrm{m}^2. \tag{3.4}$$

The *one-way* absorption or scattering coefficient for a population of droplets is related to the cross-section of a single droplet by

$$\alpha_i = 4.343\times 10^3 \sum_{\text{vol}} \sigma_i \qquad \mathrm{dB\,km^{-1}} \tag{3.5}$$

(where the summation is over 1 m^3 of volume). Therefore

$$\alpha_a = 8.186\times 10^{-2}\frac{\Im(-K)}{\lambda}\mathrm{LWC}, \tag{3.6}$$

$$\alpha_s = 8.860\times 10^{-13}\frac{|K|^2}{\lambda^4}Z, \tag{3.7}$$

where LWC has the units g m^{-3}, Z has the units mm^{6}m^{-3}, the wavelength λ is in metres and the density of water has been taken to be 10^6 g m^{-3}. Absorption will dominate scattering at both frequencies provided $Z \ll 300\,\mathrm{LWC}$, which is invariably satisfied for warm clouds, and in any case since Z is measured it would be a simple matter to calculate the effect of scattering and remove it. Hence from (3.6) we have

$$\alpha_{l,f} \simeq \alpha_a = k_{l,f}\mathrm{LWC}, \tag{3.8}$$

where $k_{l,f}$ is the one-way attenuation coefficient per unit liquid water content (in dB km^{-1}/g m^{-3}), for which values can be found in Table 3.1.

We are now in a position to derive an expression for the mean LWC between two specified altitudes as a function of Z measured by both radars at these heights. Defining the dual-wavelength ratio as

$$\mathrm{DWR} = Z_{35}[\mathrm{dBZ}] - Z_{94}[\mathrm{dBZ}] \quad \mathrm{dB}, \tag{3.9}$$

from (3.1) we have

$$\mathrm{DWR} = 10\log_{10}\left(\frac{|K_{35}(T)|^2}{|K_{94}(T)|^2}\right) + 2\int_0^z (\alpha_{g,94} - \alpha_{g,35}) + (\alpha_{l,94} - \alpha_{l,35})\,dz \quad \mathrm{dB}, \tag{3.10}$$

where it has been assumed that beams and sample volumes are perfectly matched. If we measure DWR at altitudes z_1 and z_2, then

$$\mathrm{DWR}_2 - \mathrm{DWR}_1 = \beta + 2\int_{z_1}^{z_2} (\alpha_{g,94} - \alpha_{g,35}) + \mathrm{LWC}(k_{l,94} - k_{l,35})\,dz, \tag{3.11}$$

where

$$\beta = 10\log_{10}\left(\frac{|K_{35}(T_1)|^2}{|K_{35}(T_2)|^2}\frac{|K_{94}(T_2)|^2}{|K_{94}(T_1)|^2}\right) \quad \mathrm{dB}. \tag{3.12}$$

Therefore the mean liquid water content between the two heights is

$$\overline{\mathrm{LWC}} = \frac{\mathrm{DWR}_2 - \mathrm{DWR}_1 - \beta - 2\int_{z_1}^{z_2} (\alpha_{g,94} - \alpha_{g,35})\,dz}{2\int_{z_1}^{z_2} (k_{l,94} - k_{l,35})\,dz} \quad \mathrm{g\,m^{-3}}. \tag{3.13}$$

Assuming that the attenuation coefficients are constant over the depth of the layer, this simplifies to

$$\overline{\mathrm{LWC}} = \frac{1}{k_{l,94} - k_{l,35}}\left(\frac{\mathrm{DWR}_2 - \mathrm{DWR}_1 - \beta}{2(z_2 - z_1)} - \alpha_{g,94} + \alpha_{g,35}\right) \quad \mathrm{g\,m^{-3}}. \tag{3.14}$$

The parameter β is a small but necessary adjustment which accounts for the difference in air temperature at the two heights. For example, if $\mathrm{T}_1 = 11°\mathrm{C}$ and $\mathrm{T}_2 = 9°\mathrm{C}$, then $\beta = +0.06\,\mathrm{dB}$.

The attenuation coefficients and β are functions of temperature, and the attenuation of atmospheric gases is also dependent on pressure and humidity, so an independent measure of the vertical profiles of these variables over the site would be needed.

3.2.3 Error estimates

The precision to which we can determine LWC is limited to the accuracy of our values for temperature and reflectivity factor.

The effect of errors in reflectivity factor

We shall first assume that the temperature and relative humidity (and therefore the gaseous attenuation and β) are known exactly, and consider only the effect of errors in reflectivity. If the range-gate spacing is δ and n gates are averaged for increased sensitivity (such that $z_2 - z_1 = n\delta$), then from (3.14) and (3.9) we see that the error in LWC is given by

$$\Delta\mathrm{LWC} = \frac{\sqrt{2}\,\Delta\mathrm{DWR}}{2(k_{\mathrm{l},94} - k_{\mathrm{l},35})n\delta} = \frac{\sqrt{2}\left(\Delta Z_{35}{}^2 + \Delta Z_{94}{}^2\right)^{\frac{1}{2}}}{2(k_{\mathrm{l},94} - k_{\mathrm{l},35})n\delta} \tag{3.15}$$

Since the clouds are so close to the radar we can take the limit of large signal-to-noise ratio, and from (2.21) and (2.17) we obtain

$$\Delta Z \simeq \frac{4.343}{\sqrt{M_\mathrm{I}}} = 4.343\left(\frac{\tau_\mathrm{I}}{n\tau_\mathrm{d}}\right)^{\frac{1}{2}} = 4.343\left(\frac{\lambda}{4\pi^{\frac{1}{2}}\sigma_w n\tau_\mathrm{d}}\right)^{\frac{1}{2}} \quad \mathrm{dB}, \tag{3.16}$$

where we have assumed that σ_w is small enough that successive pulses are not independent (or equivalently that PRF $> 4\pi^{\frac{1}{2}}\sigma_w/\lambda$). Hence

$$\Delta\mathrm{LWC} = \frac{4.343}{2(k_{\mathrm{l},94} - k_{\mathrm{l},35})\delta}\left(\frac{\lambda_{35} + \lambda_{94}}{2\pi^{\frac{1}{2}}\sigma_w n^3\tau_\mathrm{d}}\right)^{\frac{1}{2}}. \tag{3.17}$$

Alternatively this can be expressed the dwell time τ_d required to obtain LWC to a particular accuracy:

$$\tau_\mathrm{d} = \left(\frac{4.343}{2(k_{\mathrm{l},94} - k_{\mathrm{l},35})\delta\,\Delta\mathrm{LWC}}\right)^2 \frac{\lambda_{35} + \lambda_{94}}{2\pi^{\frac{1}{2}}\sigma_w n^3}. \tag{3.18}$$

Clearly after the dwell time and vertical averaging have been decided it is σ_w, the standard deviation of the reflectivity-weighted velocity distribution within the cloud, that determines how accurately we can measure LWC. This parameter has contributions from both turbulence and the differential fall speeds of the droplets. Figure 3.2 shows a scatterplot of still-air σ_w versus reflectivity for four flights during ASTEX, determined by calculating Doppler spectra from the observed size distributions (see Section 3.3.2). It would appear that virtually all clouds with a reflectivity greater than part of the error associated with, for example, an overestimate of temperature will be caused by overestimating the amount of the attenuation which is due to absorption by water vapour, resulting in an underestimate of LWC.

By differentiating (3.14) with respect to temperature, an expression for the systematic error in LWC associated with an error of in temperature of ΔT is obtained:

$$\Delta\mathrm{LWC} = (A + B\,\mathrm{LWC} + C\,\Gamma)\;\Delta T \qquad \mathrm{g\,m^{-3}} \tag{3.19}$$

where Γ is the lapse rate (in $^\circ\mathrm{C\,km^{-1}}$). A, B and C are due to the temperature dependencies of the differential attenuation of atmospheric gases at saturation, the differential attenuation of liquid water per $\mathrm{g\,m^{-3}}$, and the parameter β respectively. At 10°C, these coefficients have the values $A = -0.011, B = 0.0084$ and $C = -0.00023$, and at 20°C they have the values $A = -0.025, B = 0.012$ and $C = -0.00016$. In a worst-case scenario in which the temperature of a 10°C cloud was wrongly thought to be 15°C, for lapse rate of $-6^\circ\mathrm{C\,km^{-1}}$ and an LWC of 0.5 $\mathrm{g\,m^{-3}}$, we underestimate LWC by 0.04 $\mathrm{g\,m^{-3}}$. At higher temperatures an error in temperature has a larger effect on specific humidity and therefore the estimate of gaseous attenuation, and wrongly taking the temperature of a 20°C cloud to be 25°C would result in LWC being underestimated by $0.1\mathrm{g\,m^{-3}}$. However, we can realistically expect the temperature to be known to better than ± 2°C, so in general the errors should be acceptably low and typically smaller than those due to errors in reflectivity.

The effect of Mie scattering

Even though the cloud can be considered to be attenuating in the Rayleigh regime (because it is the very small cloud droplets which actually do the attenuating), the drops which dominate the reflectivity may be scattering in the Mie regime, which would bias the retrieved LWC. Figure 3.3 shows DWR due to Mie scattering versus diameter for individual spherical drops at 0°C, 10°C and 20°C. Clearly the presence of drops much larger that 800 μm would invalidate the algorithm, with Z_{94} drastically reduced below Z_{35}. Note that at higher temperatures there is also a 'resonance region' (see van de Hulst 1957) at around 700 μm where Z_{94} is in fact greater than Z_{35}. It may therefore be necessary to reject data from the base of clouds where the reflectivity exceeds around 0 dBZ, to minimise the probability of large drops contaminating the retrievals.

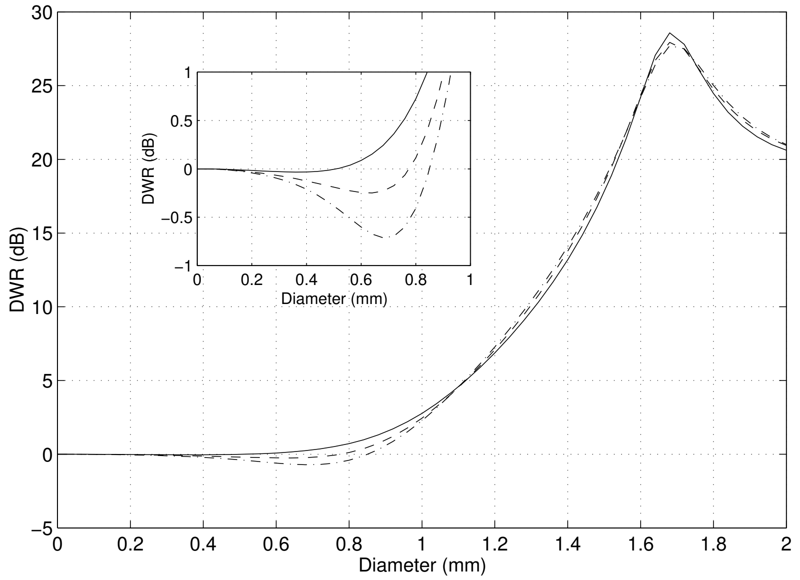

Figure 3.3: The dual wavelength ratio of single liquid water spheres due to Mie scattering at 0°C (solid line), 10°C (dashed line) and 20°C (dot-dashed line). The inset shows the resonance region where the 94 GHz reflectivity exceeds that at 35 GHz.

3.2.4 Simulation

The retrieval of LWC using vertically-pointing dual-wavelength radar has been simulated using an aircraft profile through stratocumulus from flight A209 of ASTEX. The cloud was around 700 m thick, and in the 4.2 minutes the aircraft took to descend through the cloud it travelled horizontally around 25 km. The top row of Fig. 3.4 shows vertical profiles of the spectral density of LWC as a function of diameter, and the parameter σ_w. The presence of drizzle droplets up to a few hundred microns in diameter is clearly apparent, and it is these which allow σ_w to attain a value of nearly 40 cm s^{-1}. We can also see that only the cloud droplets smaller than 40 μm in diameter contribute significantly to LWC.

Gaseous attenuation has been simulated by assuming a surface temperature of 10°C, a lapse rate of -6°C km^{-1}, and a relative humidity of 100% below 800 m and 50% above. The bottom row of Fig. 3.4 shows the reflectivity and DWR profiles that would be measured for this cloud, along with the separate contributions to DWR from liquid water attenuation, gaseous attenuation and Mie scattering. We see that in this case Mie scattering contributes only 0.1 dB to DWR in the light precipitation at the base of the cloud, whereas the total attenuation by atmospheric gases is over half as much as that due to liquid water.

Next the dual-wavelength retrieval of LWC was simulated and compared with the true LWC profile. Figure 3.5 shows two plots with the true profile overlayed by error bars indicating the performance of the radars both for no spatial averaging (75 m resolution) and 2-gate averaging (150 m resolution), and a one minute dwell. The higher resolution scenario captures the features of the profile slightly better, but the random errors to be expected are a factor of $2^{\frac{3}{2}}$ larger. A reduced resolution of 300 m would allow the dwell time to be reduced, but there would only be three points through the depth of the cloud.

At the base of the cloud, the DWR due to Mie scattering has wrongly been attributed to liquid water attenuation, resulting in an overestimate in LWC of 0.08 g m^{-3}.

This example suggests that a dual-wavelength radar has the potential to measure vertical profiles of LWC rather well, but the accuracy indicated by the error bars is not the best that can be achieved. Until now, differentiation of DWR with height has been performed in the simplest manner possible, by simply taking the centred-difference between adjacent points in the profile. If instead a smooth two-dimensional function was fitted through a time-height field of DWR, the errors in the retrievals of LWC could be reduced, essentially by relying on the similarity between successive profiles to minimise statistical fluctuations in the radar measurements. This variational approach has been proposed previously by Testud and Amayenc (1989) to estimate attenuation from stereoscopic radar observations of rain and cloud, for which the natural fluctuation of spatial derivatives of reflectivity is large.

3.3 Inferring LWC from the reflectivity of cloud droplets using Doppler spectra

3.3.1 Background

The main problem with using radar to make quantitative measurements in stratus or stratocumulus is that, when the size spectrum is weighted by the sixth power of diameter, the reflectivity is dominated by the contribution from the occasional drizzle drops larger than 50 µm which contain very little of the liquid water and contribute negligibly to the radiative properties of the cloud. A means is required to isolate the contribution to Z from the important droplets smaller than 50 µm.

Doppler radars have the capability of measuring the Doppler spectrum, which is the reflectivity-weighted velocity spectrum of the particles in the pulse volume. For a vertically-pointing radar this velocity consists of the sum of the terminal fall speeds of the particles and the vertical velocity of the air. Since for liquid droplets the terminal velocity is monotonically and precisely related to size, it is possible in theory to 'deconvolve' the Doppler spectrum to recover the complete size distribution, and thus LWC. The problem is that the mean vertical velocity of the air must first be determined and subtracted, and there is always a certain amount of turbulence which acts to smear out the features of the spectrum. Algorithms able to cope with these effects have been developed for both cloud and precipitation retrievals (e.g. Gossard 1994), and usually assume that the size distribution can be represented by the superposition of two gamma or lognormal distributions. These are then fitted to the observed Doppler spectrum, from which all the required parameters can be computed.

Using a 915 MHz wind profiler, Gossard et al. (1990) observed two distinct drop regimes in the Doppler spectra of stratiform rain: the drizzle drops several hundred microns in diameter which they interpreted as having grown out of the cloud regime via collision and coalescence, and the larger rain drops several millimetres in diameter, which originated from the melting snow. Similarly in stratocumulus clouds, Gossard et al. (1997) used a 35 GHz Doppler radar with a much higher spectral resolution and were able to detect the same drizzle component, but also the component corresponding to the much smaller cloud droplets that we are concerned with. Considerable success was achieved in fitting idealised distributions to the observed rain and drizzle spectra, since the effect of turbulence was small compared to the intrinsic width of the spectra. However the cloud component proved to be more problematic since, with such small intrinsic fall velocities, most of the observed spectral width was due to turbulence. Part of the deconvolution technique was to estimate the magnitude of the turbulence and remove its effect, but it was found to be difficult to do this accurately. Indeed, Gossard et al. (1997) stated that *'A limitation in size information is found at a diameter of about* $D_M = 40\,\mu m$*, regardless of the turbulence intensity'* (where D_M is the diameter corresponding to the peak in the Doppler spectrum). Work is still in progress to try to extract the important cloud parameters from the spectrum, but realistically any fitted function for the size distribution is likely to be in error because of the uncertainty regarding the magnitude of the turbulence.

So can LWC be derived at all from Doppler spectra? In this section a much simpler idea than deconvolution is considered; if we can separate the two components of the distribution using Doppler spectra, then the reflectivity of the cloud droplets alone may be directly related to LWC, since these are the droplets which contain most of the liquid water. This has the advantage that it is virtually unaffected by turbulence (provided that turbulence is not so strong that the cloud mode has not been smeared away so much as to be unidentifiable), and is completely independent of vertical velocity. This principle was first suggested by Fox and Illingworth (1997a), but here we examine more closely the problem of turbulence.

Good correlations between LWC and the reflectivity of the smaller droplets in boundary-layer clouds have been noted before. Paluch et al. (1996) examined data from an FSSP (which measures number concentration up to a diameter of 50 μm) from flights through non-precipitating Florida cumulus and reported a fairly constant value for b in the relationship $\mathrm{LWC} = aZ^b$ of 0.85. Fox and Illingworth (1997a) also used only the FSSP, and obtained a value of $b = 0.86$ from predominantly stratocumulus during ASTEX (although they presented their results in terms of an expression of the form $Z = c\mathrm{LWC}^d$). They also binned their observations by reflectivity to obtain the mean value of LWC for a given Z, and the result of a regression between the Z value corresponding to the centre of each bin and the mean LWC of that bin was $b = 0.64$. Sauvageot and Omar (1987) used a maximum diameter of 100 μm to isolate the cloud droplets in flights through both cumulus and stratocumulus, and reported best-fit lines equivalent to values for b of between 0.52 and 0.75. However a diameter of 100 μm is somewhat larger than the natural watershed between cloud and drizzle droplets (which can be identified from Doppler spectra), and the poorer correlations reported by Sauvageot and Omar must have been due to the inclusion of drizzle drops in their analysis. Much earlier, Atlas (1954) proposed the relationship $Z = 0.048\mathrm{LWC}^2$, i.e. $b = 0.5$. These differences are quite significant, so if we are to be able to measure LWC accurately with this method it is important to distinguish between the natural variations between clouds of the same type, systematic differences between clouds of a different type (e.g. cumulus, stratocumulus and stratus), and artifacts of the data, for instance caused by a failure to screen out drizzle drops.

3.3.2 Theory

The Doppler spectrum

The Doppler spectrum can be calculated by taking the Fourier Transform of a time series of M samples of the complex voltage V output from the radar receiver at a particular range gate (see Chapter 2). This provides the reflectivity spectral density at M equally spaced velocities between $-v_\mathrm{a}$ and $+v_\mathrm{a}$, where v_a is the unambiguous velocity and is equal to $\mathrm{PRF}\,\lambda/4$. Hence the spectral resolution is given by

$$\Delta v = \frac{2v_\mathrm{a}}{M} = \frac{\lambda}{2}\frac{\mathrm{PRF}}{M} = \frac{\lambda}{2\tau_\mathrm{d}}, \tag{3.20}$$

where τ_d is the dwell time.

To resolve the small velocities of the cloud droplets requires that the spectral resolution is at most a few mm s^{-1}, and that the dwell time is not so long that the vertical velocity of the air has been able to vary enough to smear out the cloud peak. It is also important to note that in the nature of Fourier Transforms, the raw spectrum tends to be rather noisy and thus some spectral resolution will need to be sacrificed in exchange for a smoother spectrum. Supposing we required a spectral resolution of $\Delta v = 0.5\ \ \mathrm{mm\,s^{-1}}$, then for the 3, 35 and 94 GHz radars at Chilbolton for example, the required dwell times would be 100, 8.6 and 3.2 seconds respectively. Clearly higher frequencies are much more suitable for measuring Doppler spectra in stratocumulus.

Calculating Doppler spectra from aircraft measurements

To simulate what a vertically-pointing radar would observe, Doppler spectra have been calculated from size distributions obtained by the Forward Scattering Spectrometer Probe (FSSP) and the 2D cloud probe aboard the UKMO C-130 aircraft during ASTEX. This is the same data that was used by Fox and Illingworth (1997a,b). These instruments provide the number density $n(D)$ in 42 bins ranging in mean diameter from 6.5 to 800 µm, from which the spectral density of Z is calculated:

$$S(D) = n(D)D^6. \tag{3.21}$$

The Doppler spectrum is then simply given by

$$S(w_\mathrm{f}) = S(D)\frac{dD}{dw_\mathrm{f}}. \tag{3.22}$$

The droplet fall velocity w_f was calculated as a function of D from the semi-empirical formulae of Beard (1976), and is plotted in Fig. 3.6 for three different ambient pressures.

Next we calculated w_t, the velocity corresponding to the trough in the Doppler spectrum between the two peaks. Since the two peaks are nearly always present, w_t is simply taken to be where $S(w_\mathrm{f})$ falls to a minimum between the velocities of 1 and 30 $\mathrm{cm\,s^{-1}}$. Then the reflectivity of the cloud droplets alone is defined as

$$Z_\mathrm{c} = \int_0^{w_\mathrm{t}} S(w_\mathrm{f})\,dw_\mathrm{f} \tag{3.23}$$

It is this parameter which we shall relate to LWC, and which could be determined easily from a measured Doppler spectrum in quiescent air.

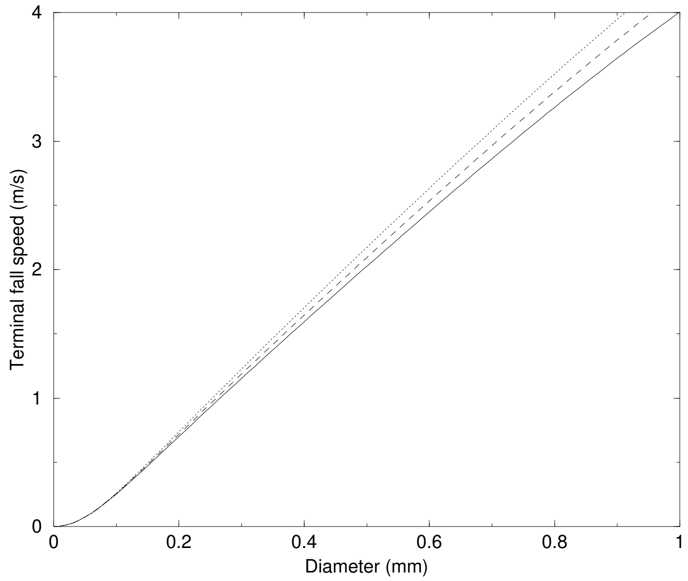

Figure 3.6: Cloud droplet terminal fall speed as a function of diameter for a temperature of 10°C and pressures of 1000 mb (solid line), 900 mb (dashed line) and 800 mb (dotted line), and calculated according to the formulae of Beard (1976).

3.3.3 Turbulence considerations

Turbulence is a major consideration since it could in theory smear out the cloud component so that the clearly defined minimum between the cloud and the drizzle is lost. An example is shown in Fig. 3.7; the left plot shows a 1-minute averaged size spectrum from flight A209 of ASTEX and the right plot shows the corresponding Doppler spectrum. The two modes of the spectrum are clearly apparent, and in this case w_t has the value 15 cm s^{-1}. It should be noted that the measured spectrum at the largest drop sizes can be significantly in error because of the low number of samples, and in this example the three largest bins each registered only a single drop. Also shown is the same Doppler spectrum after broadening by Gaussian air-turbulence with standard deviations (σ_a) of 2.5, 10 and 25 cm s^{-1}. In each of these cases the cloud mode is still identifiable and the technique could still be applied. However Fig. 3.8 shows a size distribution and Doppler spectrum for a cloud with a much weaker cloud mode, and it can be seen that a turbulence of $\sigma_a = 10$ cm s^{-1} is sufficient to smear out the cloud peak completely and thus make the technique unworkable.

We need to determine how likely this is to occur by examining many spectra and comparing with typical measured values of σ_a found in stratocumulus. We define a 'critical' air vertical-velocity standard deviation σ_c to be that which causes the minimum between the two peaks in the spectrum to just disappear, leaving only a 'shoulder' in the spectrum where both dS/dw and d^2S/dw^2 are zero. This parameter has been estimated from Doppler spectra calculated from three

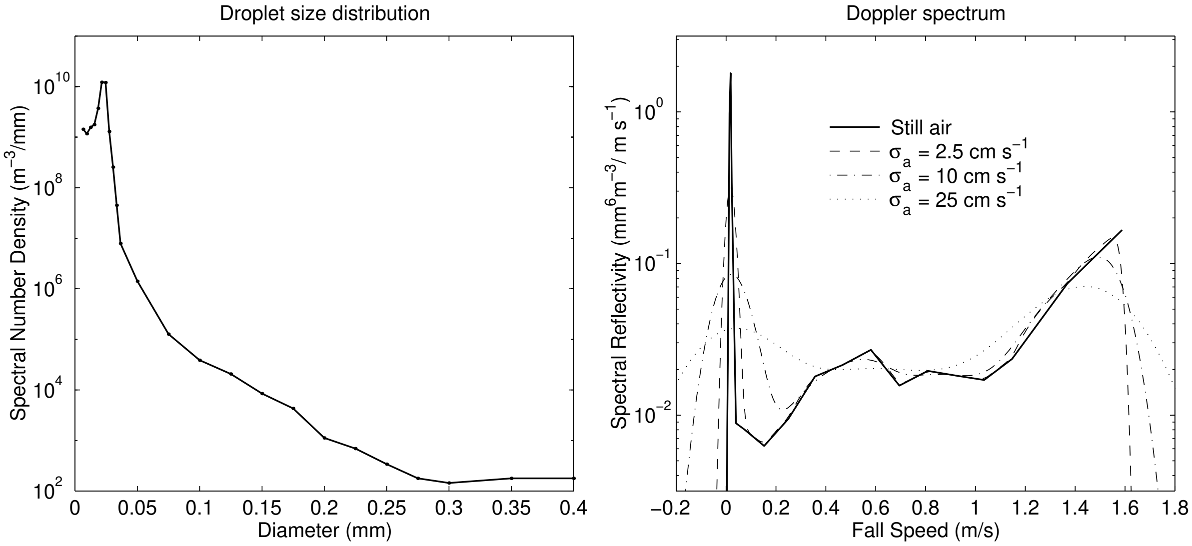

Figure 3.7: A stratocumulus droplet size distribution from flight A209 of ASTEX (12 June 1992), with the corresponding Doppler spectrum. The reflectivity is $-11.5\,\mathrm{dBZ}$ and the liquid water content is $0.59\ \mathrm{g\,m^{-3}}$. Also shown are the Doppler spectra that would be measured in the presence of turbulence with velocity standard deviations of 2.5, 10, and $25\ \mathrm{cm\,s^{-1}}$.

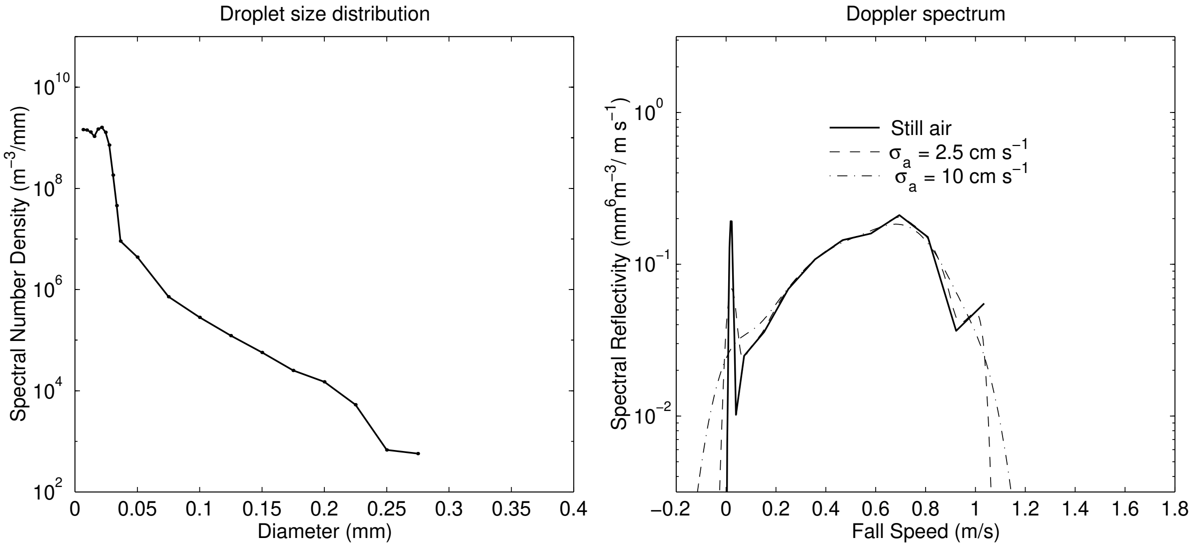

Figure 3.8: A droplet size distribution and Doppler spectrum from flight A212 (16 June 1992). The reflectivity is $-9.6\,\mathrm{dBZ}$ and the liquid water content is $0.14\ \mathrm{g\,m^{-3}}$. Also shown are the Doppler spectra that would be measured in the presence of turbulence.

flights during ASTEX. To get reliable samples of the larger drizzle drops, the number distributions were averaged over 100 seconds. Four parameters were calculated from each Doppler spectrum: the reflectivity of the cloud droplets Z_c, the reflectivity of the drizzle drops, the reflectivity-weighted mean velocity of the drizzle drops and the standard deviation of the velocity of the drizzle drops. These parameters were used by a simple algorithm which calculated σ_c iteratively by assuming that

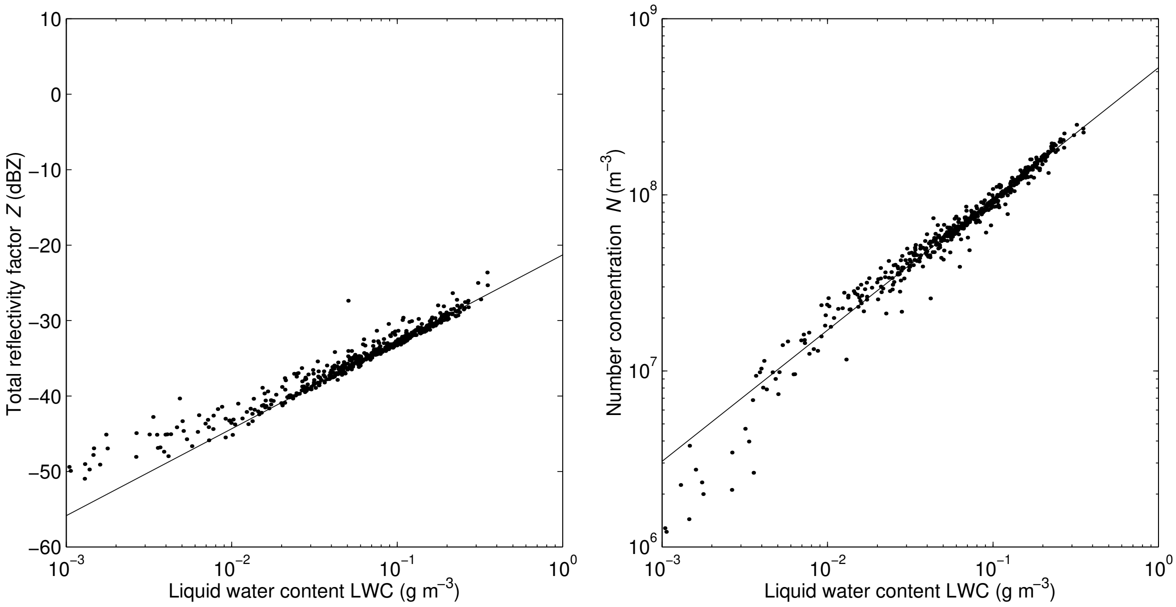

Figure 3.10: Scatterplot of total reflectivity factor and total number density against LWC for the whole of flight A169. The data have been averaged every 10 seconds.

value for a large fraction of the stratocumulus observed in these three flights, but it is not certain how representative it is and there is very little more in the literature to indicate the range of values of σ_a that should be expected in stratocumulus. The problem of turbulence is even more important for the deconvolution method (in which the entire number distribution is retrieved), because it is likely to get more and more inaccurate as σ_a increases. The effect of turbulence can be reduced by minimising the volume of air that is sampled by the radar, so it is advantageous for a cloud radar with the capability of measuring Doppler spectra to have a short pulse length, a narrow beamwidth and a short dwell time. One should be aware that Gossard et al. (1997) expressed turbulence intensity in terms of the half width to the e^{-1} point of the velocity probability distribution function, which is equal to $\sqrt{2}\,\sigma_a$.

Gossard et al. (1997) also reported that in their system, imperfect matching of the in-phase and quadrature channels resulted in the observed Doppler spectrum in fact consisting of the true spectrum plus its own reflection about the zero velocity point, but 10 dB down. In some cases this could conceivably lead to the wrong peak being identified as the cloud component. They state that in very high quality systems the artificial image can be 30–40 dB weaker.

3.3.4 Error estimates

Drizzle-free clouds

We first examined data from flight A169, which consisted of over four hours of measurements through a continental stratocumulus layer 200 to 300 metres thick, and contained very little in the way of drizzle drops larger than 50 µm in diameter. The minority of clouds in which drizzle is not significant would in practice be identifiable from the small spectral width of the Doppler spectrum.

Total reflectivity factor and LWC were calculated from this data in the form of 10 second averages, and exhibit excellent correlation (Fig. 3.10). The best fit regression has the form

$$\mathrm{LWC} = 70.5\,Z^{0.87} \qquad \mathrm{g\,m^{-3}} \tag{3.24}$$

where Z is in linear units. This is in very good agreement with the aircraft measurements of Paluch et al. (1996) in drizzle-free cumulus over the coast of Florida, who found a consistent value for b in the $\mathrm{LWC} = aZ^b$ relationship of 0.85, and were also able to parameterise a as a function of the height above cloud base.

In previous work developing radar retrieval algorithms for stratocumulus it has often been assumed (e.g. Atlas 1954, Frisch et al. 1995, 1997) that the number concentration of droplets (N) in a given cloud is constant. Observations of constant droplet number concentration with height have been reported in the literature (e.g. Slingo et al. 1982, Martin et al. 1994). Since $Z \propto D^6$ and $\mathrm{LWC} \propto D^3$, one would then assume that $\mathrm{LWC} \propto Z^{\frac{1}{2}}$. The reason that the exponent is found to be larger than one half in this case is that the number concentration is changing as well. A scatterplot of total number density versus LWC is also shown in Fig. 3.10, and again there is a strong correlation, with the best fit given by

$$\mathrm{LWC} = 1.97 \times 10^{-12}\,N^{1.34} \qquad \mathrm{g\,m^{-3}} \tag{3.25}$$

where N has units of $\mathrm{m^{-3}}$. Paluch et al. (1996) reported an exponent of 1.25 in such a relationship, and explained these correlations as due to mixing in of dry air from the surroundings. They considered two extremes. The first, *inhomogeneous mixing* (Baker et al. 1980), assumes that droplet evaporation occurs much faster than turbulent mixing, so that at the interface between the dry and cloudy air the droplets evaporate completely until the entrained air is saturated. Therefore the remaining droplets have the same size, and effectively only dilution has occured, which results in a simple proportionality between N, LWC and Z. The opposite extreme is *homogeneous mixing*

(Paluch and Baumgardner 1989), for which it is assumed that turbulent mixing occurs much more rapidly than droplet evaporation. Hence all the droplets evaporate somewhat in response to the reduction in humidity immediately after entrainment and mixing, and the relationship between LWC and N (and hence between LWC and Z) depends on the mixing proportions, the temperature and humidity of the entrained air, and the cloud liquid water content.

Martin et al. (1997) presented aircraft measurements through a stratocumulus cloud which had underlying cumulus penetrating through it from beneath. Cumulus clouds have stronger updraughts than stratocumulus, and so tend to activate more of the cloud condensation nuclei, resulting in both larger N and LWC. On this particular flight leg their observations showed an apparent correlation between these two parameters. It would appear therefore that the clouds in flight A169 had the characteristics of cumulus, and may have formed from the spreading-out of an earlier cumulus cloud field, although puzzlingly the flight log indicated that the cloud was fairly uniform with no rising cumulus beneath. From a theoretical point of view there is no reason to believe that the absence of drizzle should always be an indication of a correlation between N and LWC, and in flight A169 the reason for the absence of drizzle was that the cloud was in a continental airmass and had a large aerosol concentration, so consequently the droplets could not attain a sufficient size to begin the collision and coalescence process. Flight A169 may therefore be representative of cumulus rather than drizzle-free stratocumulus.

We calculated the standard deviation of the true LWC from that given by (3.24) in a number of LWC bins, and from this Fig. 3.11 gives an indication of the error of an LWC measurement derived using this relationship. We see that the error is between 5% and 10% when LWC is greater than 0.01 g m^{-3}, indicating that Z alone can provide an excellent means of estimating LWC, provided the cloud is free from drizzle, a criterion which can be determined using Doppler spectra. Other flights in which drizzle is not observed would need to be analysed to verify the representativity of these findings.

Clouds containing drizzle

It is much more common for stratocumulus clouds to contain drizzle, in which case simple Z-LWC relationships are very inaccurate. Figure 3.12 shows scatterplots of total reflectivity factor and total number concentration against LWC for three flights (lasting a total of 16.9 hours) containing drizzle. As expected, there is no correlation between Z and LWC. We can also see that, unlike in flight A169, there is little correlation between N and LWC; rather the droplet number concentration tends to have a constant value of around 1.5×10^8 m^{-3}, indicating that little entrainment is

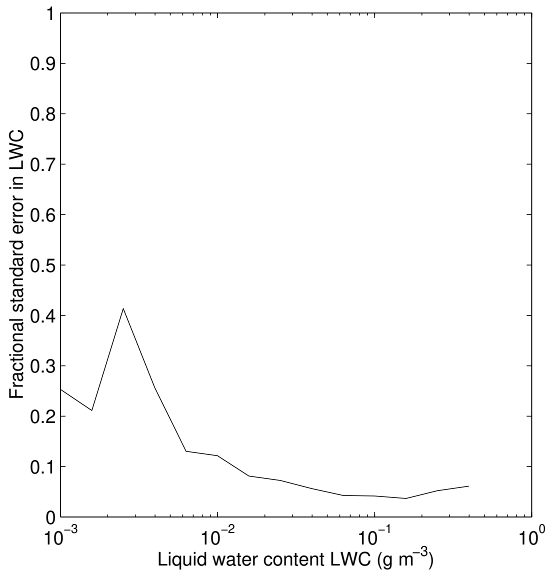

Figure 3.11: The fractional error in LWC measured using (3.24), versus reflectivity factor.

occurring.

This time we calculate Z_c (as defined in Eq. 3.23), and Fig. 3.13 shows a scatterplot of Z_c against LWC. There is a much better correlation than for Z, and the regression line has the form

$$\mathrm{LWC} = 4.77 Z_c^{0.52} \qquad \mathrm{g\,m^{-3}}. \tag{3.26}$$

It is interesting to note that this is much closer to $\mathrm{LWC} \propto Z^{\frac{1}{2}}$ because the assumption of constant number concentration is much more valid. However, algorithms that assume this relationship are still likely to fail if they have no way of removing the effects of drizzle.

Note that this gives the most probable value of LWC for a given measured Z_c (which is what we want), which partially explains the difference between this and the expression found by Fox and Illingworth (1997a) who calculated their regression with the parameters switched, which in effect gave the most likely value of Z_c for a given LWC. If this is done for our data the exponent becomes 0.59. Furthermore, they used the diameter threshold of 50 µm to reject the drizzle drops (i.e. the data from the FSSP only), whereas here the Doppler spectrum was used to determine the natural division between the two droplet regimes, and usually it was at smaller sizes than this. They also included the drizzle-free flight A169 in their analysis. Sauvageot and Omar (1987) calculated regressions for each of 11 flights and reported the predominant cloud type for each one. Most commonly they found $Z \propto \mathrm{LWC}^{1.7}$, equivalent to an exponent in (3.26) of 0.59, but no obvious difference between the relationships for cumulus and stratocumulus was apparent. This could be due to the fact that their diameter threshold was 100 μm which meant that some drizzle drops must have been included in their calculations.

Also shown in Fig. 3.13 is the fractional error in LWC measured using this method, as a function of LWC. The error is greater than for drizzle-free clouds, but is still less than 10% for clouds with LWC greater than 0.1 g m^{-3} and less than 30% when LWC is greater than 0.01 g m^{-3}.

Even if the turbulence is not sufficient to completely smear out the cloud mode, it would result in the some of the drizzle reflectivity being attributed to the cloud droplets or vice versa, which could slightly bias the results. However a good correlation between Z_c and LWC is found despite the fact that the natural position of the trough varies considerably, having a mean of around 5.5 cm s^{-1} (corresponding to a diameter of 45 μm), but ranging between 3.5 and 12 cm s^{-1} (diameters of 30 to 70 μm respectively). Hence a blurring of the boundary between the two droplet regimes by turbulence should not drastically increase the errors.

3.4 Dual-wavelength Doppler spectra

The first method presented in this chapter was found to be somewhat in error when any Mie scattering was occurring at 94 GHz. In the simulation of Section 3.2.4, the resulting error in LWC was only 0.08 g m^{-3}, but if rain drops (or even ice crystals) were present the effect could be much more substantial. A possible solution is to combine the two techniques presented so far in this chapter, and retrieve Doppler spectra simultaneously at two wavelengths. This could have many advantages.

Separating the effects of attenuation and Mie scattering

The first obvious benefit is that the contribution to DWR from Mie scattering would be clearly identifiable from comparison of the two Doppler spectra, since the spectra would match up closely for droplets smaller than 800 μm (corresponding to a fall velocity of 3 m s^{-1}), but diverge at larger sizes. The offset between the spectra for the Rayleigh scattering droplets only could then be used to determine the attenuation coefficient and hence LWC, rather than relying on the difference between the total measured reflectivity. In theory the technique would then be applicable to precipitating clouds. Furthermore, if the problem of Mie scattering can be removed then there is no reason to restrict ourselves to using 94 GHz as the higher frequency; it may well be advantageous to use 140 or even 215 GHz instead. This would result in an increase in the differential attenuation per unit LWC by a factor of 1.8 and 2.5 respectively, thereby enabling LWC to be retrieval more accurately or at a higher spatial or temporal resolution.

Lhermitte (1988) presented some interesting measurements of Doppler spectra in rain at 94 GHz, in which the very distinct Mie minimum which occurs for drops of diameter 1.67 mm at this frequency (corresponding to a terminal velocity of around 6 m s^{-1} depending on the air density) was clearly visible. By comparing the observed position of the minimum to the predicted, it was possible to determine and subtract the vertical velocity of the air, and then calculate the full size distribution of the precipitation.

Mixed-phase clouds

The second possibility is that mixed-phase clouds could be distinguished from clouds composed only of supercooled liquid water, and maybe even the ice/liquid water ratio could be deduced. It can be safely assumed that if ice is present it will be in the form of crystals much larger than the liquid-phase droplets, but the problem is in identifying them as ice rather than drizzle. A number of properties of ice crystals could be exploited using dual-wavelength Doppler spectra to make this distinction. The major difference is that ice crystals have a much lower fall speed for a given size, so after estimating the vertical velocity of the air from the position of the cloud mode, the velocity corresponding to the onset of Mie scattering (i.e. where Z_{35} and Z_{94} begin to diverge) would clearly indicate whether ice or drizzle was being observed. This is demonstrated in Fig. 3.14. Plot (a) shows an idealised size distribution consisting of the superposition of three components: a lognormal distribution of cloud droplets and two exponential distributions corresponding to drizzle- and precipitation-sized particles. The cloud and drizzle components of the spectrum are intended to be typical of stratocumulus size distributions such as those in Figs. 3.7 and 3.8. The precipitation component of the distribution is that given by Marshall and Palmer (1948) corresponding to a rainfall rate of 0.02 mm hr^{-1}. Plot (b) shows the corresponding Doppler spectrum for the case when the drizzle- and precipitation-sized particles are in the liquid phase, and plot (c) shows the spectrum for the case when these particles are ice crystals. In the latter case the Locatelli and Hobbs (1974) velocity-diameter and density-diameter relationships corresponding to 'aggregates of unrimed bullets, columns and side-plates' have been assumed:

$$w_\mathrm{f} = 0.69D^{0.41} \quad \mathrm{m\,s^{-1}} \tag{3.27}$$

$$\rho = 0.07D^{-1.1} \quad \mathrm{g\,cm^{-3}} \tag{3.28}$$

where ρ is the density and the diameter D is in millimetres. The onset of Mie scattering occurs at very different velocities relative to the cloud peak; for drizzle the 94 GHz spectral reflectivity falls

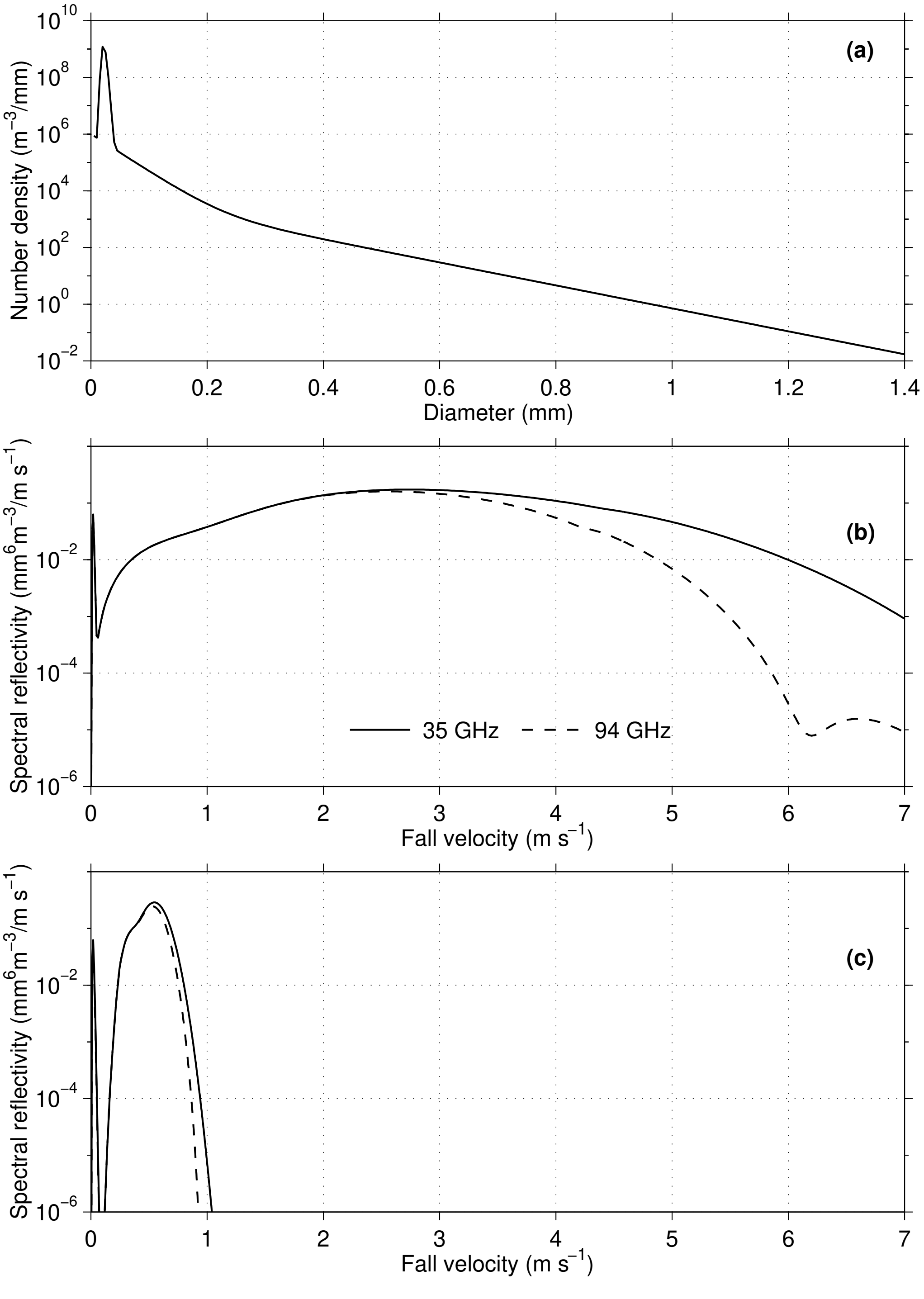

Figure 3.14: Simulation demonstrating the difference between ice and drizzle for Doppler spectra. (**a**) Idealised size distribution consisting of contributions from a lognormal distribution of cloud droplets and two exponential distributions of larger particles of unspecified phase. **(b)** The corresponding Doppler spectrum at 35 and 94 GHz for the case in which the larger particles are liquid-phase drops. **(c)** The Doppler spectrum for the case when the larger particles are ice crystals.

to 3 dB below that at 35 GHz for a velocity of 4 m s^{-1}, whereas for ice this occurs at a velocity of only 0.7 m s^{-1}.

It should also be noted that ice has the same value for $|K|^2$ at 35 and 94 GHz, whereas for liquid water it is 1.2 dB larger at 35 GHz at 0°C, and 1.7 dB larger at -10°C (see Fig. 3.1). Therefore if the two spectra were matched in the liquid water regime, the ice component of the Doppler spectrum would be slightly greater at 94 GHz. It is doubtful whether such differences would be detectable given the intrinsic errors in measured Doppler spectra. A further point is that the well-defined spectral-reflectivity minimum at 94 GHz due to Mie scattering would be much more diffuse in ice because each crystal type has a different velocity-diameter relationship, and a volume of ice cloud typically contains a number of different crystal habits. Turbulence would also modify the measured spectra a little, although not enough to have much effect on retrieved parameters because the intrinsic spectral width is so much larger.

If a mixed-phase cloud was diagnosed from the Doppler spectrum then LWC could be determined either from differential attenuation or from the reflectivity of the cloud-peak in the spectrum, and the ice water content could be estimated by fitting the appropriate idealised size distribution to the part of the Doppler spectrum corresponding to the ice crystals. Very little is known about mixed-phase clouds, and this is a problem for atmospheric models, where usually the ice/liquid water fraction is parameterised as a simple (but arbitrary) function of temperature between around -15°C and 0°C.

3.5 Conclusions

Two potential methods to measure LWC in stratocumulus clouds have been described, both of which are to a large extent unaffected by the presence of drizzle.

The first utilises the difference in liquid water attenuation at 35 and 94 GHz, and for most clouds is shown to be able to measure LWC to an accuracy of ± 0.05 g m^{-3} at a vertical resolution of 150 m and a dwell time of one minute. Mie scattering at 94 GHz has the potential to bias the retrievals somewhat at cloud base, although reflectivity is a good indicator of the larger particles and therefore could be used to reject observations for which the technique is likely to be in error.

The second method uses Doppler spectra to extract the contribution to the total reflectivity from the cloud droplets Z_c, which is found to be well correlated with LWC. Values of water content obtained in this way should have an error of less than 10% where LWC is greater than 0.1 g m^{-3}, and less than 30% when it is greater than 0.01 g m^{-3}. In the minority of clouds with no drizzle, the data analysed suggested that an accuracy of 10% is achievable down to 0.01 g m^{-3}. Clouds containing no drizzle should be clearly identifiable by their small Doppler spectral width. However, it is uncertain whether flight A169 was representative of stratocumulus clouds containing no drizzle or clouds with cumulus-like properties. More work is required to establish the most appropriate functional relationship between Z_c and LWC for stratocumulus. It may be that the difference between relationships reported in the literature is a symptom of the fact that there exists a continuum of clouds between the extremes of those with constant number concentration and those such as observed in flight A169 which were probably dominated by mixing effects. If this is the case then a single relationship will not be generally applicable, in the same way that the relationship between Z and rainfall rate was found to vary considerably (Joss et al. 1970).

There may therefore be the need to make an additional independent measurement to improve the accuracy of the retrievals. One possibility is to measure liquid water path using one or more coincident microwave radiometers, and then to use Z_c measured by the radars to partition the liquid water between the various heights. A similar concept was described by Frisch et al. (1997), except that they used Z rather than Z_c which could clearly result in an inaccurate profile of LWC being derived in clouds containing drizzle. Alternatively one could make the assumption that total number concentration N is constant with height, and use a lidar together with the Doppler radar to estimate N at cloud base. This would provide the parameter a in the relationship LWC $= aZ_c^{\frac{1}{2}}$ which would be used through the remainder of the profile to determine LWC.

A large number of Doppler spectra were analysed to estimate the strength of turbulence sufficient to smear out the peak associated with the cloud droplets, since this would make the technique unworkable. It was found that the cloud mode would still be identifiable in virtually all spectra with an LWC greater than 0.1 g m^{-3} for a turbulence standard deviation (σ_a) of less than 10 cm s^{-1}. It would be identifiable in only 70% of clouds (again with LWC >0.1 g m^{-3}) for $\sigma_a = 15$ cm s^{-1}, and in 50% for $\sigma_a = 20$ m s^{-1}. In some clouds with lower values for LWC, the reflectivity of the drizzle was over 40 dB more than that of the cloud droplets, and for these very little turbulence would be necessary to smear away the cloud peak. It is difficult to translate these findings into the fraction of clouds for which this technique would work since there is little in the literature about the the range of σ_a that one should expect in stratocumulus, and of course this parameter is also a function of the dimensions of the radar averaging volume.

Lastly the considerable potential of dual-wavelength Doppler spectra was outlined, in particular its ability to identify mixed-phase clouds about which very little is currently known. It should also be possible to use such measurements to divide the contributions to the dual-wavelength ratio between Mie scattering and attention, thereby enabling differential attenuation (and hence LWC) to be measured in the presence of precipitation-sized particles.

The guiding principle behind the work in this chapter is the perception that drizzle is common in stratocumulus, and that there is consequently a need to develop new radar retrieval techniques which avoid the erroneous assumption that stratocumulus size spectra can be well represented by idealised monomodal distributions. Drizzle was found to be ubiquitous in the clouds sampled during ASTEX, but since the ASTEX flights took place predominantly in marine stratocumulus, they cannot necessarily be considered to be globally representative of all stratiform clouds. It is conceivable that most of the low clouds observed by a ground-based radar far from any oceans could be drizzle-free, but the fact that stratiform clouds over land certainly *can* contain drizzle, even if the probability of occurrence is not well known, means that the value of any radar algorithm which depends on drizzle being absent is doubtful. This is especially true given that only around one fifth of all stratus and stratocumulus occurs over land (e.g. Heymsfield 1993), and therefore the most useful location for the deployment of a cloud-profiling radar would be a coastal region in order that marine stratocumulus, the most radiatively important of all cloud types, would constitute the dominant fraction of all cloud observations. More work is required to characterise the occurrence of drizzle, particularly in continental stratocumulus, and it would be useful to learn more about its vertical distribution. On this last point it is clearly not appropriate to assume that drizzle is only a problem at cloud base; in the example of Fig. 3.4 it can be seen that in all but the very top of the cloud the reflectivity is dominated by droplets larger than 100 µm.

It is important to consider whether techniques such as those presented in this chapter could be feasible from a spaceborne platform. Existing proposals for a spaceborne radar (e.g. IGPO 1994, Illingworth et al. 1997) have shown that with a present technology it should be possible to construct such an instrument at 94 GHz with a minimum detectable reflectivity of -30 dBZ and a range resolution of 500 m. Clearly this is insufficient resolution for measuring attenuation since many stratiform clouds are thinner than 500 m. The gate-spacing could of course be reduced to 250 m, but at the expense of 6 dB of sensitivity. Drizzle drops have the beneficial effect of making the majority of stratocumulus clouds detectable with a minimum sensitivity of -30 dBZ, but with a sensitivity of only -24 dBZ, random errors at low signal-to-noise ratio would clearly make the detection of differential attenuation impossible. One should also be aware that a one minute dwell corresponds to a swath length of 400 km.

The measurement of Doppler spectra from space is even less feasible; for a radar of the conventional pulse type, the PRF must be less than around 3 kHz to avoid mirror image returns, and the speed of the satellite is such that every pulse is independent and Doppler measurements are impossible. A pulse compression system could make Doppler measurements, but a long coded pulse would be required, which would result in a blind zone near the surface which could cause easily cause the signal from low clouds to be corrupted. Even then only the mean Doppler velocity would be measurable because the typical satellite velocity of 7 $\mathrm{km\,s^{-1}}$ coupled with a radar beamwidth of around 0.2° would introduce a broadening of the spectrum with a standard deviation of around 10 $\mathrm{m\,s^{-1}}$. Given the important of low clouds in climate it is vital that algorithms are developed to measure the important cloud parameters from space. At this stage it is difficult to conceive how a spaceborne radar could provide any more than a means of cloud detection.

However the focus of this chapter is on the potential of ground-based radars for measuring LWC in stratocumulus, and two promising avenues for research have been discussed which attempt to overcome the largest problem for radar observations of stratocumulus which is that of drizzle. Since both depend on certain atmospheric conditions being satisfied, namely that Mie scattering is negligible (for the differential attenuation technique) and that turbulence is small (for the Doppler spectrum technique), it is not until real data is analysed that the true potential of these approaches can be accurately assessed.

CHAPTER FOUR

Ice crystal density and the CIRRAD flight

4.1 Introduction

Perhaps the greatest difficulty for the measurement and modelling of cirrus microphysics stems from the multitude of crystal habits which are present. A common approach in modelling radiative transfer in the visible, infrared and microwave regions of the spectrum is to assume that ice crystals can be approximated as spheroids consisting of a homogeneous mixture of ice and air. To simplify matters further it is usual to adopt an idealised size distribution, and assume density and aspect ratio can be expressed as functions of size only. Microwave scattering calculations comparing realistic crystal shapes, such as hexagonal columns and plates (Schneider and Stephens 1995) and dendritic snowflakes (O'Brien and Goedecke 1988), with their equivalent spheroids show that the errors associated with the spheroidal approximation are in general less than 15% (0.6 dB), provided maximum dimension, aspect ratio and total ice mass are maintained. However it is not obvious where the spheroidal surface enclosing a complex dendrite or polycrystal should lie, or whether it is necessarily the same in the visible and the microwave regions of the spectrum.

In this chapter the issue of crystal density is addressed. Knowledge of the density of crystals is important for numerous remote retrieval algorithms, including the dual-wavelength method for deducing the size of ice crystals in cirrus, which will be covered in the next two chapters; in Section 6.2.1 it is shown how errors in the knowledge of this parameter translate directly into errors in retrieved size and ice water content. Other cloud radar techniques have been presented in the literature which are also sensitive to assumed density (Matrosov et al. 1996, Matrosov 1997, Ryzhkov et al. 1998). Similarly Aydin and Tang (1997) presented theoretical calculations of advanced radar parameters for idealised cirrus distributions and found them to be particularly sensitive to density and aspect ratio. In addition to its importance for remote sensing, this issue is also relevant to parameterisations of effective radius (r_e) which, it turns out, is intimately related to density. The link between these two parameters has not been made before, and it is important to ensure that independent estimates of them are consistent with each other.

Firstly in this chapter the existing methods to derive density from aircraft are examined, and a discrepancy is found which is believed to relate to the ability of aircraft probes to accurately determine the volume of non-spherical crystals. A new expression for density is proposed from reinterpretation of existing work in the literature. Secondly, results are presented from an intercomparison flight of the UK Meteorological Office C-130 aircraft over the Chilbolton radars (the CIRRAD flight). Both reflectivity Z and differential reflectivity Z_{DR} were calculated from 2D cloud probe data using the established and the newer density assumptions, and compared with the values measured by the 3 GHz radar at Chilbolton.

The aim of CIRRAD was threefold: to validate the use of aircraft data to evaluate the potential of cloud radar techniques, to validate the dual-wavelength technique for sizing ice crystals, and to measure ice crystal density unambiguously. The first of these objectives was achieved quite satisfactorily, the second was not possible because the 94 GHz radar was not operational during the flight, and the third was difficult due to the possibility that significant canting could be occurring which made the interpretation of Z_{DR} ambiguous. However this study suggests that a future flight with both the 35 and 94 GHz radars in operation should hopefully be able to achieve both the second and third objectives at the same time.

4.2 Background

4.2.1 Formulae for crystal density

The obvious way to determine density is from simultaneous measurements of crystal mass and crystal volume. Before the advent of aircraft-borne imaging probes the usual procedure was to collect crystals and measure their dimensions manually both before and after melting. The first extensive study was carried out by Nakaya and Terada (1935) who related the terminal fall velocity of naturally-occurring snowflakes to both the mass and the maximum crystal dimension. A similar study by Magono and Lee (1966) categorised the observed crystals into 80 different types and determined the optimum relationship for each. Since their main interest was fall velocity there was no attempt to derive density. Clearly the fact that such a diverse range of crystal types has been observed, each with its own relationship between mass and maximum dimension, means that any expression for density as a function of diameter is likely to be at best an average of the densities of all different crystal types. It is important to note however that the early studies were of all types of ice-phase precipitation; this was predominantly snow but also included hail and graupel. Since we are interested in cirrus clouds which have a far greater global importance for the radiation budget than snow, the relevance of studies which involved collecting crystals at the ground at temperatures greater than $-20°$C is doubtful.

The best means of making in situ measurements of both mass and volume in cirrus clouds is using aircraft. Brown and Francis (1995) analysed data from flights of the UKMO C-130 aircraft through cirrus, and compared a bulk measure of ice water content obtained using the Total Water Probe (Brown 1993) with that derived from size spectra measured by the combination of the 2D cloud and precipitation probes. The principle behind the 2D probes is described more fully later on, but basically they collect two-dimensional images of the crystals from which some measure of size can be calculated. Therefore with a sufficiently large number of images the full size spectrum is obtained. Brown and Francis (1995) binned their observations by D_{m}, the mean of the maximum dimensions of the crystal measured parallel and perpendicular to the 2D photodiode array. The best agreement was found to be for crystal mass M (in grams) given by the expression of Locatelli and Hobbs (1974) for 'aggregates of unrimed bullets, columns and side-plates':

$$\begin{aligned} M &= 4.82 \times 10^{-13} D_{\mathrm{m}}^{3}; \quad D_{\mathrm{m}} < 100\,\mu\mathrm{m} \\ M &= 7.38261 \times 10^{-11} D_{\mathrm{m}}^{1.9}; \quad D_{\mathrm{m}} \geq 100\,\mu\mathrm{m} \end{aligned} \tag{4.1}$$

where D_{m} is in microns. Locatelli and Hobbs had in fact defined D_{m} to be the maximum dimension of the crystal.

If one assumes that the crystals in the Brown and Francis study were spherical, then the density ρ is given as a function of diameter D (in millimetres) by

$$\rho = 0.07 D^{-1.1} \ \ \mathrm{g\,cm^{-3}} \tag{4.2}$$

although it is not allowed to exceed the density of solid ice, 0.917 $\mathrm{g\,cm^{-3}}$. This form has been used in a number of areas of cloud research, including those not involving aircraft data, such as the interpretation of radar measurements in cirrus.

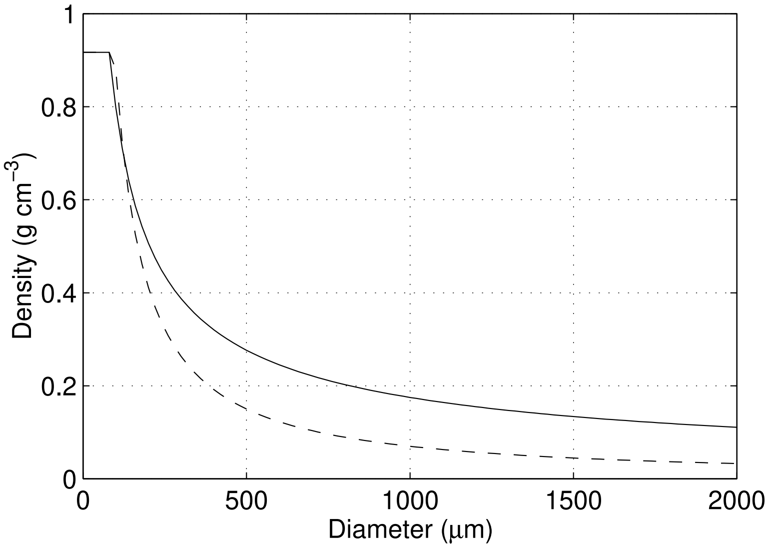

Figure 4.1: Density as a function of diameter, as given by Eq. 4.4 (solid line) and Eq. 4.2 (dashed line).

An alternative formula for mass was later derived from essentially the same data by Francis et al. (1998), who discretised the size spectra according to the crystal cross-sectional area $\mathcal{A}$ measured directly by the probes, rather than by D_m, and again compared ice water content with that from the Total Water Probe. The result was expressed as a relationship between D_eq, the diameter of a water droplet with the same mass as the ice crystal (in millimetres), and $\mathcal{A}$:

$$\begin{aligned} D_\mathrm{eq} &= 1.097\mathcal{A}^{0.50}; \quad \mathcal{A} \leq 0.0052\,\mathrm{mm}^2 \\ D_\mathrm{eq} &= 0.615\mathcal{A}^{0.39}; \quad \mathcal{A} > 0.0052\,\mathrm{mm}^2 \end{aligned} \tag{4.3}$$

which is a modification of the form of Cunningham (1978). The first of these two expressions is present so that the small crystals do not have a density exceeding that of solid ice. In this case when one assumes spherical crystals, and hence $\mathcal{A} = \pi(D/2)^2$, the following formula for density is obtained:

$$\rho = 0.175D^{-0.66} \;\; \mathrm{g\,cm}^{-3} \tag{4.4}$$

(again up to a maximum of 0.917 $\mathrm{g\,cm}^{-3}$). The density functions (4.2) and (4.4) are plotted in Fig. 4.1, and a significant discrepancy between the two is apparent. Since the formulae were derived from the same data we can only conclude that the problem lies with the assumption of sphericity.

4.2.2 Theoretical examination of the interpretation of 2D probe data

In order to determine density independently of shape we require a relationship between crystal mass and either volume V or equivolumetric diameter D_v. Since the 2D probes offer only a silhouette

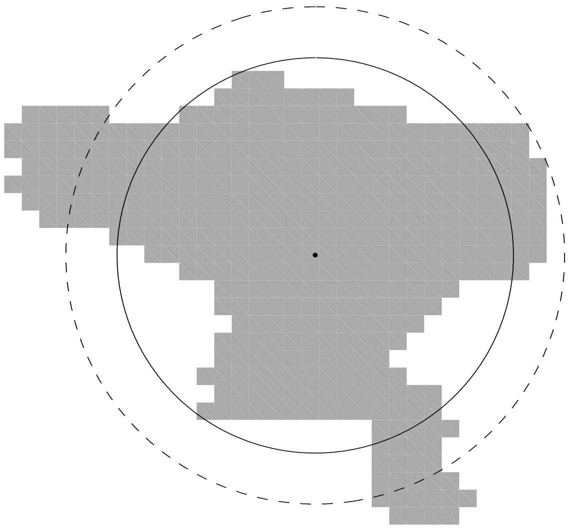

Figure 4.2: A typical crystal image from the 2D cloud probe. The solid circle has an area equal to that of the image and its diameter (D_a) is 566.3 µm. The dashed circle has a diameter equal to the mean of the maximum dimensions of the image (D_m), which in this case is 712.5 µm. This is a difference of 26% which is equivalent to a difference in the estimated crystal volume (and therefore density) of a factor of two.

image of the crystal, neither V nor D_v can be derived exactly, but it seems intuitive that these three-dimensional quantities should be estimated more accurately using all the two-dimensional information available, rather than just the length and width of the image. We define D_a to be the diameter of a circle with the same area as the crystal image $\mathcal{A}$. To illustrate the difference between the two definitions of size, a typical image from the 2D cloud probe is shown in Fig. 4.2, and overlayed are circles with diameters of D_a (solid line) and D_m (dashed line). In this example D_m is 26% larger than D_a, which when cubed implies a difference of a factor of two in the estimate of volume. This in turn implies a difference in density of a factor of two which would explain the disparity between (4.2) and (4.4).

By considering a range of different oblate and prolate spheroids we shall determine whether D_m or D_a provides the best approximation to D_v. D_m and $\mathcal{A}$ were calculated for idealised spheroidal crystals with aspect ratios ranging from 0.1 to 10, at all possible orientations with respect to the probe photodiode array. By assuming that ice crystals are randomly oriented when passing through the 2D probe, the mean values $\bar{D}_\mathrm{m}$ and $\bar{\mathcal{A}}$ were obtained by numerically integrating over all orientation angles. $\bar{D}_\mathrm{a}$ was then calculated from $\bar{\mathcal{A}}$.

The ratios $D_\mathrm{a}/D_\mathrm{v}$ and $D_\mathrm{m}/D_\mathrm{v}$ are shown in Fig. 4.3, as a function of aspect ratio for the case of random orientation. Clearly both D_m and D_a overestimate D_v for non-spherical crystals, but the error in the estimate from D_m is more than that from D_a, especially for very prolate crystals. To determine the ratio of the volume estimated by the two methods to the true volume, and hence the

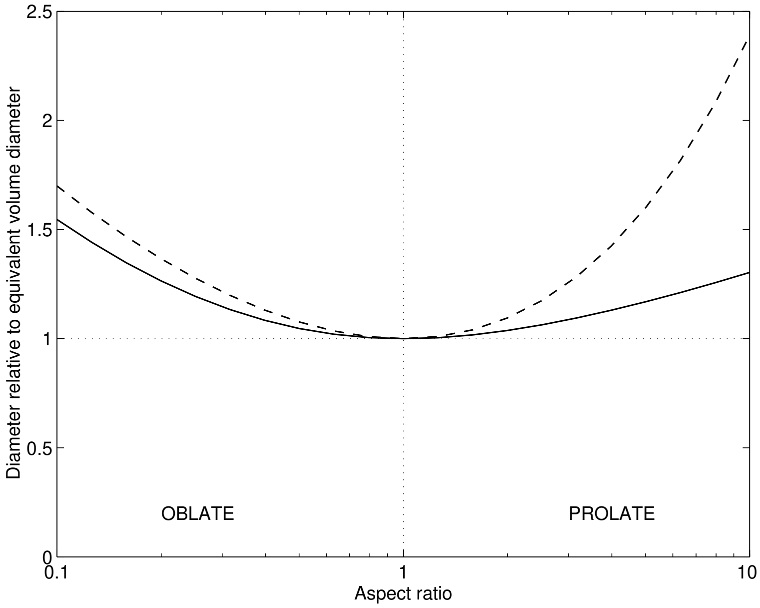

Figure 4.3: The ratios D_a/D_v (solid line) and D_m/D_v (dashed line) for randomly-oriented spheroids as a function of aspect ratio.

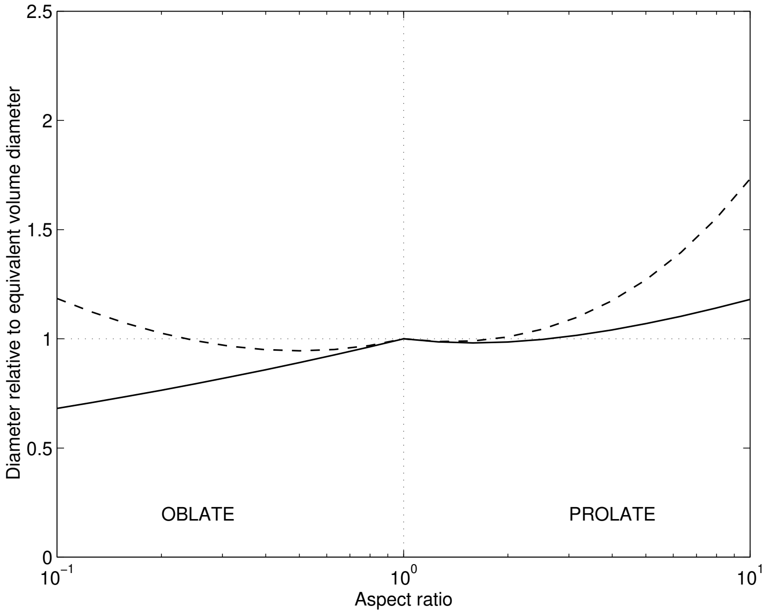

Figure 4.4: As for Fig. 4.3 but with horizontally aligned crystals.

error in density, the ordinate of Fig. 4.3 should be cubed. It is this power of three which makes the estimate of density so sensitive to how one defines diameter.

We also considered crystals aligned with their longest axis in the horizontal, but with a random azimuthal orientation (with the probe viewing the crystals from the side), which is believed to be the natural fall mode of pristine crystals (Liou 1986). The results are plotted in Fig. 4.4. D_m is still always larger than D_{a}, but the systematic error in the estimate of D_{v} is less, and unlike before it is possible to underestimate D_{v}. It is important to know to whether turbulence generated as air is drawn into the probe is sufficient to tumble crystals which would otherwise exhibit horizontal alignment. It will be shown later from real 2D probe data that turbulence *is* in fact strong enough to set the crystals tumbling, and therefore the situation is much closer to that indicated by Fig. 4.3 than Fig. 4.4.

It is obvious that D_{m} is determined by the extremities of the crystal and therefore is nearly always larger than D_{v}. The reason why the area method also systematically overestimates D_{v} (for random orientation) can be explained conceptually as due to the fact that for a fixed crystal volume, the surface area increases as the crystal becomes more aspherical, and hence on average the measured cross-sectional area will also be larger than that of a sphere with the same volume.

These findings are applicable to simple crystal habits such as columns and plates, but more commonly 2D probes images tend to be rather irregular in appearance (such as the example in Fig. 4.2). Irregular crystals can have even more disparate values for D_{m} and D_{a}, but it is more difficult to determine how these are likely to compare with D_{v}.

We are forced to conclude that (4.4) is a better estimate of density than (4.2), but the fact that the assumptions that went into this derivation may still be based on a systematic overestimate of volume means that it is possible that the true density lies somewhere between (4.4) and that for solid ice. There is a clear need for more work to try to determine the most accurate way to measure crystal volume from aircraft.

This finding has implications for radar calculations from aircraft data. As well as the density function in (4.2) being inappropriate, the size parameter into which the crystals are binned is not equivalent to D_{v}, and it is D_{v} that should be used in radar calculations. Computations in the Rayleigh scattering regime (where D is much less than the wavelength) should remain largely unchanged, since radar reflectivity factor is proportional to $\rho^2 D^6$, or simply mass squared, and the mass of each crystal can be still be calculated fairly accurately from (4.1). In the Mie regime however (where D is of the same order as the wavelength) the diameter dependence of reflectivity changes considerably from D^6, and so it is necessary to know both density and equivolumetric diameter.

Both density functions were derived to provide the maximum agreement with the ice water content (IWC) indicated by the Total Water Probe, so will be only be strictly applicable at the sizes which contribute significantly to IWC. For radar however it is the density of those crystals which contribute most to Z which is important, and the diameter of these will naturally be somewhat larger than the diameter of those which contribute most to IWC. The density formulae will therefore not necessarily be applicable to the very large crystals that the radar is sensitive to at the base of thick clouds. Moreover these crystals may have grown by aggregation, in which case their density would no longer decrease with increasing diameter. It would clearly be desirable for the density which is to be used in cloud radar algorithms to have been derived using radar.

4.2.3 Effective radius

The most basic cloud parameters required by radiation schemes are the short-wave volume extinction coefficient β_{vis} and the infrared volume absorption coefficient β_{ir}. Since atmospheric models carry IWC, it is usual to parameterise an effective radius r_{e} such that radiation schemes can easily relate IWC to β (Foot 1988):

$$r_{\mathrm{e}} = \frac{3}{2}\frac{\mathrm{IWC}}{\rho_{\mathrm{i}}\beta_{\mathrm{vis}}} = \frac{3}{4}\frac{\mathrm{IWC}}{\rho_{\mathrm{i}}\beta_{\mathrm{ir}}}. \tag{4.5}$$

where ρ_{i} is the density of solid ice. It is common to assume in both the visible and the infrared that ice crystals are large compared with the wavelength, and hence make the geometric optics approximation. Hence extinction coefficient is proportional to the cross-sectional area of the crystals and

$$r_{\mathrm{e}} = \frac{\int_0^\infty \rho(D) n(D) D^3\, dD}{2\rho_{\mathrm{i}} \int_0^\infty n(D) D^2\, dD}. \tag{4.6}$$

If we assume that density has the form $\rho = aD^b$, then for a monodisperse distribution

$$r_{\mathrm{e}} = \frac{aD^{1+b}}{2\rho_{\mathrm{i}}}. \tag{4.7}$$

Effective radius is plotted as a function of D in Fig. 4.5 for both monodisperse and exponential distributions, and the densities given by (4.2) and (4.4) . It is immediately apparent for monodisperse distributions that r_{e} is equal to the physical radius for the small, solid ice crystals (as expected), but above $D = 100\,\mu\mathrm{m}$ where (4.2) begins to drop-off as $D^{-1.1}$, we find r_{e} decreasing as $D^{-0.1}$. In fact for this density function, r_{e} can never exceed $50\,\mu\mathrm{m}$, even when the physical diameter exceeds a millimetre, and the same is true for polydisperse distributions. This is somewhat disconcerting but perhaps in cirrus it is not appropriate to regard r_{e} as a legitimate measure of the actual physical size of the particles (as is the case in liquid water clouds), but rather as the ratio of two important parameters which just happens to have the units of length. Of course if this density function is true, and

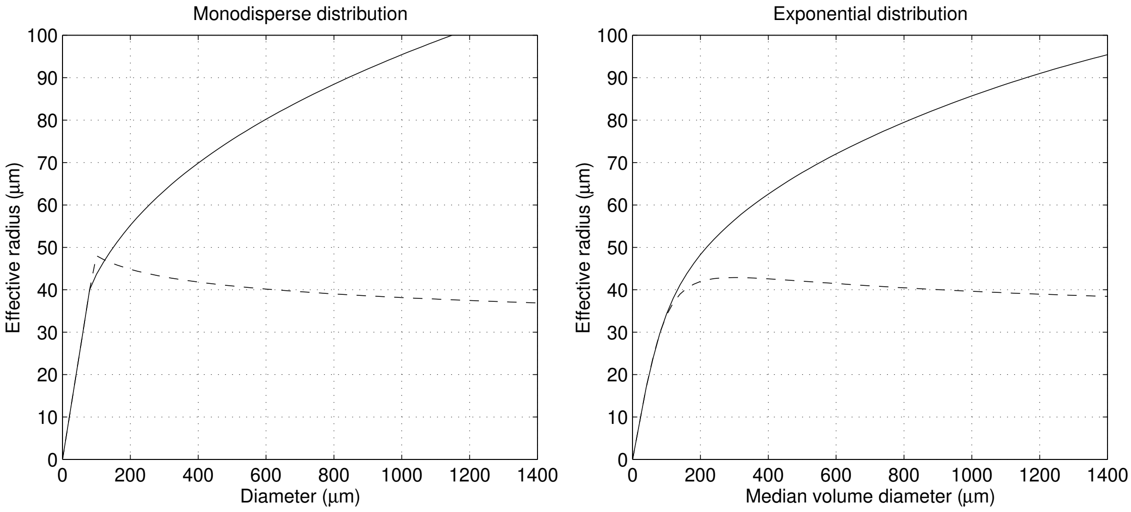

Figure 4.5: Effective radius as a function of diameter for both monodisperse and exponential distributions, and the density functions given by Eq. 4.4 (solid lines) and Eq. 4.2 (dashed lines).

r_e really can never exceed 50 μm, then a simple parameterisation of $r_e = 40\,\mu$m in cirrus radiation schemes would be an excellent approximation.

This possible asymptotic behaviour of r_e was noted recently by McFarquhar and Heymsfield (1998), who listed nine different expressions that have been used in the literature for deriving r_e from populations of non-spherical crystals. When applied to real measured size distributions, r_e was found to asymptote to a constant value between 20 and 80 μm for some of the expressions, whereas for others it could attain values of many hundreds of microns. Part of the problem was that some implicitly assumed that ice crystals have a certain specific shape (e.g. hexagonal columns) or a certain orientation (e.g. random), and to apply these blindly to all data naturally produced anomalous values for r_e. In any case it is fairly clear that the asymptotic behaviour of r_e in Fig. 4.5 is erroneous. Fundamentally it is based on the assumption that the cross-sectional area $\mathcal{A}$ (from which β is calculated) is equal to $\pi D_m^2/4$, but it is clear from the example in Fig. 4.2 that these two areas are very different. In fact this is the very reason why Francis et al. (1998) derived a mass-area relationship in the first place; they needed to use the true value of $\mathcal{A}$ to derive β, but did not want to bin the data by D_m as well to derive mass. Francis et al. (1994) used area to derive β and reported r_e to be on average around 50 μm, and at the base of thick clouds it was sometimes found to exceed 200 μm.

Hence the solid line in the right plot of Fig. 4.5 represents the most realistic relationship between D_0 and r_e, and it allows the numerous size retrieval algorithms which operate in terms of D_0 to determine r_e as well. Since this relationship contains incomplete gamma functions and must be calculated numerically, a fifth order polynomial has been fitted to it which is accurate in the range $0 < D_0 < 1$ mm, and has been constrained such that $r_e = 0$ at $D_0 = 0$:

$$r_e = 0.452D_v - 1.503D_v^2 + 2.742D_v^3 - 2.423D_v^4 + 0.819D_v^5 \tag{4.8}$$

where both r_e and D_v are in millimetres.

It would be interesting to use r_e retrieved by radiometric methods to imply a density. A number of observational studies have suggested that r_e is typically very small, with reported values varying between 11 and 26 µm (Stephens et al. 1990, Parol et al. 1991), although one should be aware that values derived from satellite may not be representative of the whole depth of the cloud, and for large optical depths are likely to only reflect the properties of the cloud top. Ackerman et al. (1990) obtained values up to 40 µm, and Landsat observations by Wielicki et al. (1990) indicated a figure of 60 µm, although the concurrent aircraft measurements produced a value of 200 µm. However the problem is that invariably the reported value of r_e is not accompanied by a physical size, so it is impossible to infer a corresponding density.

4.3 Methodology

The findings of the previous section are next applied to the interpretation of data from the CIRRAD flight. In this experiment we compare three radar parameters, each with a different sensitivity to density, to the values derived from the aircraft 2D cloud probe. These are reflectivity Z, differential reflectivity Z_{DR} and specific differential phase K_{DP}.

The PMS 2D cloud probe mounted on the UKMO C-130 aircraft is based on the instrument described by Knollenberg (1970), and basically consists of a laser which illuminates a linear array of 32 photodiodes. When the aircraft is in flight, air is drawn through the instrument, between the laser and the array, and atmospheric particulates of sufficient size cast a shadow on one or more of the photodiodes. The instrument records ‘image slices’ in quick succession, so that as the particles pass through a two-dimensional image is recorded from which size, aspect ratio and other parameters can be determined. The diode array is sampled at a rate which is slaved to the true airspeed of the aircraft, in order that the pixels in the resulting images can be considered square. The resolution of the cloud probe is 25 µm, so the maximum measurable dimension of a crystal in the array-parallel direction is 800 µm.

A number of procedures need to be applied to the data, the main one of which is to weight each measured particle according to its sample volume. Sample volume is determined by considering two opposing effects: the increase in the depth of field with size, and the decrease with size due to the fact that large particles are more likely to occlude the edge of the array and therefore be rejected from the analysis (Knollenberg 1970). There is also a need to reject false images, such as 'streakers' caused by particles colliding with the instrumentation and passing through the beam of the laser much more slowly, and at certain sizes diffraction can cause single particles to cast two distinct shadows on the array.

A number of comparisons have taken place previously between radar and aircraft derived Z and Z_{DR}, although most have been concerned with precipitation (in both the liquid and the ice phase) rather than clouds (e.g. Bringi et al. 1984, Cherry et al. 1984, Bader et al. 1987, Brown and Swann 1997). Thomason et al. (1995) found from coincident radar and aircraft measurements that solid ice was a poor assumption for snowflakes larger than 500 μm in diameter, and that a constant density of 0.1 $\mathrm{g\,m^{-3}}$ provided much better agreement between the radar and aircraft. Recently, Matrosov et al. (1998) compared aircraft IWC in cirrus with that derived using a colocated Doppler radar and infrared radiometer. Their remote retrieval technique required the radar to be vertically pointing, so comparison was only possible when the aircraft was directly overhead.

4.3.1 Calculation of reflectivity from the 2D cloud probe

Reflectivity was calculated from aircraft spectra using (1.4), although Rayleigh scattering was assumed since the wavelength of the radar is 10 cm and therefore much larger than any of the crystals found in cirrus (i.e. $\gamma = 1$). The 2D probe data were binned by both D_{m} and $\mathcal{A}$, and reflectivity was calculated separately for each:

$$Z_{\mathrm{m}} = \int_0^\infty \frac{|K(\rho_{\mathrm{m}})|^2}{0.93} n(D_{\mathrm{m}}) D_{\mathrm{m}}^6 \, dD_{\mathrm{m}} \tag{4.9}$$

$$Z_{\mathrm{a}} = \int_0^\infty \frac{|K(\rho_{\mathrm{a}})|^2}{0.93} n(D_{\mathrm{a}}) D_{\mathrm{a}}^6 \, dD_{\mathrm{a}} \tag{4.10}$$

where ρ_{m} and ρ_{a} denote the density functions given by (4.2) and (4.4) respectively, and

$$K = \frac{\varepsilon - 1}{\varepsilon + 2} \tag{4.11}$$

where ε is the complex dielectric constant of the ice-air mixture and was calculated at 3 GHz and a temperature of $-30°$C using the formulae of Liebe et al. (1989) and Meneghini and Liao (1996), the latter of which is given in Section 5.2.2. In fact ε is virtually independent of temperature. Since $|K|^2$ is approximately proportional to ρ^2, reflectivity in the Rayleigh regime is essentially proportional to the sum of the square of the masses of the crystals in a unit volume, and as both methods can produce an unbiased estimate of crystal mass, we do not expect Z_{m} and Z_{a} to differ by very much.

4.3.2 Calculation of aspect ratio from the 2D cloud probe

Several possible methods exist to calculate the aspect ratio of a particle from a 2D probe image. Frost (1991) used a technique which found the centre of area of each image and then calculated the distance $R(\Theta)$ from this point to the perimeter along 64 equally-spaced radials. The mean particle diameter was taken to be $\bar{R}$, and the second harmonic of a Fourier analysis of $R(\Theta)$ was used to estimate aspect ratio. Particle classification was possible by using the sixth harmonic to detect the hexagonal symmetry typical of stars and plates, and higher harmonics provided an index to the 'roughness' of the particle, thereby enabling discrimination between aggregates and smoother particles such as drops and graupel.

Since we are dealing with ice-phase cirrus there is no need to classify particles, and only equivolumetric diameter and aspect ratio are important. Therefore we shall estimate aspect ratio using a much simpler scheme. For each image, two vectors x and y are defined which contain the array-perpendicular and array-parallel coordinates of each shadowed diode. Hence the 'centre of gravity' is at $(\bar{x}, \bar{y})$. The vectors are first normalised so that the centre of gravity lies at $(0,0)$. We need to find the major axis of the image, such that the sum of the squares of the shortest distance from every shadowed diode to this axis is minimised. If the major axis is defined by

$$y = mx \tag{4.12}$$

then it can be shown that the closest distance from it to the point (x_i, y_i) is given by

$$l_i = \sqrt{\left(1 - \frac{1}{m\left[m + \frac{1}{m}\right]}\right) x_i^2 + \left(1 - \frac{m}{m + \frac{1}{m}}\right) y_i^2 - \left(\frac{2}{m + \frac{1}{m}}\right) x_i y_i} \tag{4.13}$$

and m can be found by solving

$$\frac{d}{dm} \sum_{i=1}^{N} l_i^2 = 0. \tag{4.14}$$

The solution is

$$m = -\gamma - \sqrt{\gamma^2 + 1} \tag{4.15}$$

where

$$\gamma = \frac{\sum_{i=1}^{N} x_i^2 - \sum_{i=1}^{N} y_i^2}{2 \sum_{i=1}^{N} x_i y_i}. \tag{4.16}$$

The gradient of the minor axis is similarly given by

$$m' = -\gamma + \sqrt{\gamma^2 + 1} = -\frac{1}{m}. \tag{4.17}$$

Defining σ to be the standard deviation of the closest distance from each point to the major axis and σ' to be the same but for the minor axis, a measure of the aspect ratio can be given by the following if each diode is assumed to be a circle with a radius R:

$$\alpha = \frac{\sigma}{\sigma'} = \left(\frac{\bar{l^2} + \frac{R^2}{4}}{\bar{l'^2} + \frac{R^2}{4}} \right)^{\frac{1}{2}}. \tag{4.18}$$

In order that simple images have their correct aspect ratios (i.e. a 3×1 image, say, has an aspect ratio of $\frac{1}{3}$), it is found that R must have the value $1/\sqrt{3}$ (in pixel units). It should be noted that hereafter we use the convention of greater-than-unity aspect ratios, so a 3×1 image would be assigned an aspect ratio of 3.

4.3.3 Calculation of differential reflectivity and specific differential phase from aspect ratio

Differential reflectivity provides a measure of the shape and alignment of the hydrometeors, and is defined as

$$Z_{\mathrm{DR}} = 10 \log_{10} \left(\frac{Z_{\mathrm{H}}}{Z_{\mathrm{V}}} \right) \quad \mathrm{dB} \tag{4.19}$$

where Z_{H} and Z_{V} are the reflectivities measured with horizontally and vertically polarised radiation respectively. In the Rayleigh scattering regime the forward and backward scattering amplitudes (denoted by f and b respectively) are equal. Seliga and Bringi (1976) used an extension to Rayleigh scattering theory developed by Gans (1912) for oblate spheroids to demonstrate the potential of Z_{DR} to measure the shape and hence size of raindrops. They showed that when the wavelength of the radiation is much larger than the size of the particle, the scattering amplitudes for a single horizontally-aligned spheroid with equivolumetric diameter D_{v}, are given by

$$\begin{aligned} f_{\mathrm{H}} = b_{\mathrm{H}} &= \frac{2}{3}\frac{\pi^3}{\lambda^2} D_{\mathrm{v}}^3 \left(\frac{\varepsilon - 1}{4\pi + [\varepsilon - 1]P'} \right) \\ f_{\mathrm{V}} = b_{\mathrm{V}} &= \frac{2}{3}\frac{\pi^3}{\lambda^2} D_{\mathrm{v}}^3 \left(\frac{\varepsilon - 1}{4\pi + [\varepsilon - 1]P} \right) \end{aligned} \tag{4.20}$$

where

$$P = \frac{4\pi}{e^2}\left(1 - \frac{\alpha}{e}\sin^{-1} e\right)$$
$$P' = \frac{4\pi - P}{2}$$
$$e^2 = 1 - \alpha^2. \tag{4.21}$$

In these equations e is the eccentricity, α is the ratio of the minor to major axis of the particle and ε is the complex dielectric constant. The suffixes H and V denote horizontally and vertically polarised radiation respectively, and the radar is assumed to be viewing the particle from the horizontal. The backscattering cross-section for horizontally polarised radiation is given by

$$\sigma_{\mathrm{H}} = 4\pi|b_{\mathrm{H}}|^2, \tag{4.22}$$

and similarly for vertically polarised radiation. We write the differential reflectivity as

$$Z_{\mathrm{DR}} = 10\log_{10}\left(\frac{\sum_{\mathrm{vol}}\sigma_{\mathrm{H}}}{\sum_{\mathrm{vol}}\sigma_{\mathrm{V}}}\right) \quad \mathrm{dB}. \tag{4.23}$$

This form will be used to calculate Z_{DR} from the 2D cloud probe images. Figure 4.6 shows a contour plot of Z_{DR} as a function of aspect ratio and ice fraction for single horizontally-aligned crystals. This is re-plotted in Fig. 4.7 as Z_{DR} against ice fraction for a number of different aspect ratios and can be seen that Z_{DR} increases with both density and aspect ratio, and for a single crystal is completely independent of diameter. Hence in theory we can use the crystal images measured by the 2D cloud probe to determine aspect ratio, and find the density function that produces values for differential reflectivity which best agree with the radar observations. However an orientation for the crystals would have to be assumed.

Another parameter which has some dependence on density and aspect ratio is specific differential phase, K_{DP}. In an environment where the hydrometeors have their longest axis in the horizontal, the horizontally polarised radiation travels slightly slower than the vertically polarised radiation, and this difference can be measured by comparing the phases of the returned signal at both polarisations. Specific differential phase is the rate at which one phase lags behind the other with distance, and is related to the size distribution by

$$K_{\mathrm{DP}} = \frac{360\times 10^3}{\pi}\lambda\sum_{\mathrm{vol}}\Re(f_{\mathrm{H}} - f_{\mathrm{V}}) \quad {}^\circ/\mathrm{km} \tag{4.24}$$

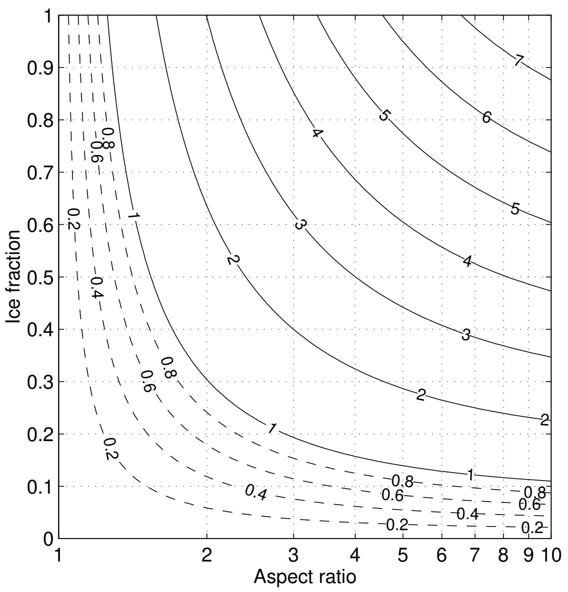

Figure 4.6: Contour plot of Z_{DR} in dB, as a function of aspect ratio and ice fraction for single spheroidal crystals aligned with their major axes in the horizontal.

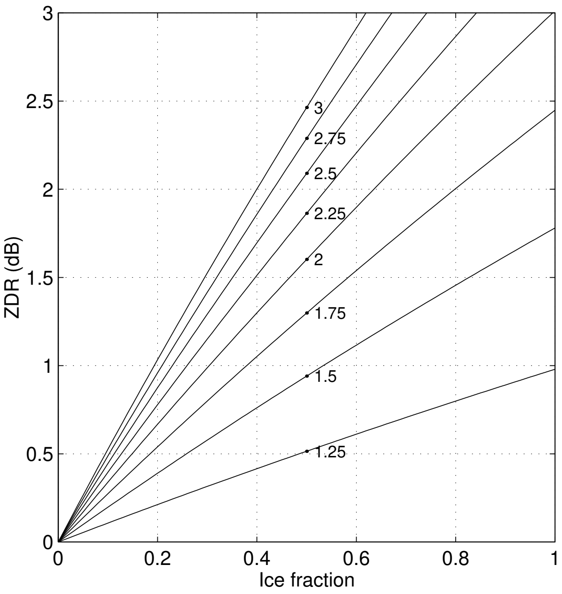

Figure 4.7: Z_{DR} as a function of ice fraction for crystals with aspect ratios ranging between 1.25 and 3.

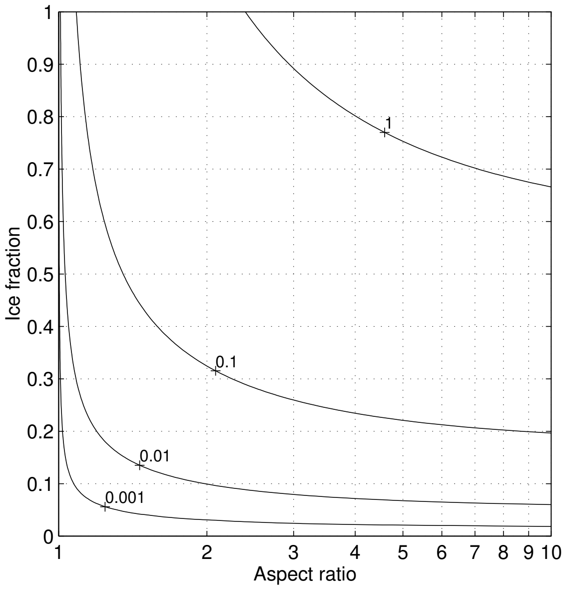

Figure 4.8: Contour plot of K_{DP} in °/km for 100 µm crystals at a concentration of $10^6\,\mathrm{m}^{-3}$, as a function of aspect ratio and ice fraction.

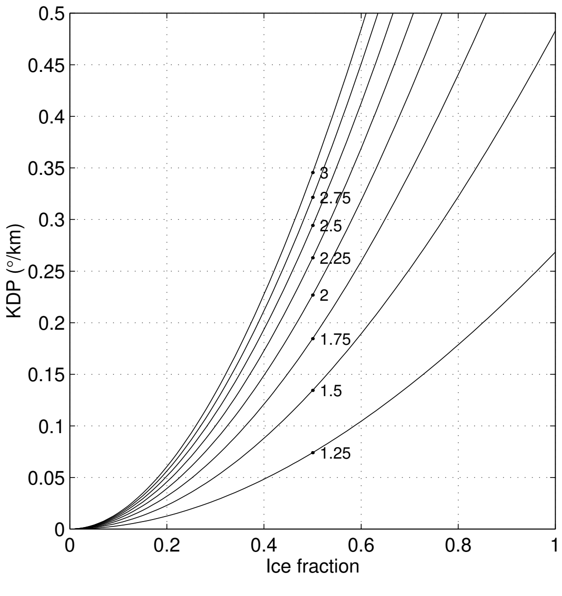

Figure 4.9: K_{DP} as a function of ice fraction for 100 µm crystals at a concentration of $10^6\,\mathrm{m}^{-3}$ and aspect ratios ranging between 1.25 and 3.

where λ, f_H and f_V are in metres. Note that this is the *two-way* specific phase shift. The main difference between K_{DP} and Z_{DR} as a measure of oblateness is that K_{DP} is also proportional to concentration. Figures 4.8 and 4.9 show K_{DP} as a function of aspect ratio and ice fraction for 100 µm crystals at a concentration of 10^6 m^{-3}. It turns out that K_{DP} is approximately proportional to the square of density so has the potential to be even more useful than Z_{DR} for our purposes. It also has the advantage that it does not need to be calibrated, although being a volume integrated effect, any radar/aircraft comparisons would rely on the total number concentration measured by the aircraft being accurate. However at 3 GHz it is rather small and may not be measurable along a path length of a few kilometres in cirrus.

4.4 Results

4.4.1 The CIRRAD flight

On 8 October 1997, a flight of the UKMO C-130 aircraft took place over Chilbolton. Both the 3 and the 35 GHz radars were in operation, and coincident radar-aircraft measurements were taken through stratiform precipitation and cirrus.

Rather than using the usual antenna scan rate of $1°\mathrm{s}^{-1}$, the scan was performed in two sections, from zenith to an elevation of 30° at a scan rate of $0.5°\mathrm{s}^{-1}$, and from here to horizontal at a scan rate of $0.25°\mathrm{s}^{-1}$, resulting in a total scan time of 4 minutes. In this way it was hoped that the radar beam would be sufficiently close to the aircraft for comparison to be possible throughout the duration of scan.

An azimuth of 259° was selected and the aircraft flew along it throughout the flight. The wind at cirrus altitudes was south-westerly and varied in strength between 45 and 50 m s^{-1}. Between 1100 and 1245 UTC the aircraft maintained an altitude of around 4 km and performed 8 runs towards and away from the radar in stratiform precipitation, mostly above the melting layer. It was found afterwards that the precipitation probe data from the flight was unreliable, so unfortunately none of these runs could be used.

However at around 1245 UTC, a thick layer of cirrus between 8 and 11 km was advected in from the south west, and between 1330 and 1500 UTC, 5 successful aircraft runs took place at altitudes of between 8.2 and 8.8 km. Figure 4.10 shows a scan of Z and Z_{DR} at 3 GHz for the first of these (Run 6.2), with the path of the aircraft shown by a black horizontal line. Ground clutter was removed to a large extent by rejecting all data where the linear depolarisation ratio was greater than -10 dB, although there is still a suggestion of non-meteorological echos just above the precipitation cells. The clutter was very strong at a range of 12 km (for all elevations), and so unfortunately some of the signal from the cirrus cloud was lost in the rejection. This was a symptom of the chosen azimuth, so was evident in all scans taken during the experiment. The reflectivity of the cirrus

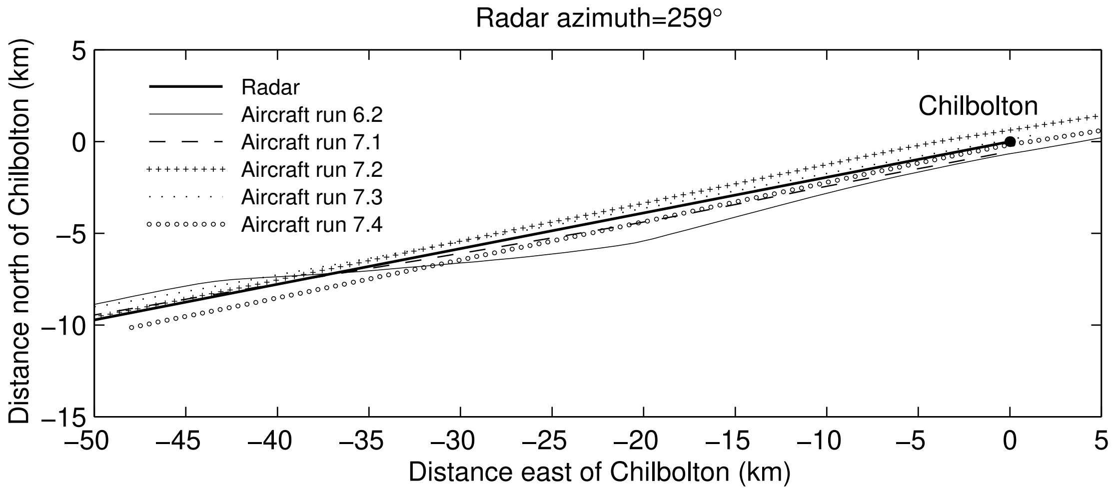

Figure 4.12: The flightpath of the C-130 aircraft on each of the five runs. The thick line indicates the azimuth of the radar.

to the right show distance from Chilbolton versus time for the aircraft and the radar beam at the altitude of the aircraft. It is immediately apparent that on some occasions the radar and aircraft sample the same region of space several minutes apart, in which time the cloud would have been advected many kilometres towards the radar, so direct comparison is difficult. It has therefore proved necessary to change the coordinate systems of both the radar and the aircraft to a 'true' distance scale, which corresponds (as well as is possible with this data) to a snapshot of the cloud without the effects of a finite sampling time. For this a constant wind speed of 48 m s^{-1} directly towards the radar has been assumed. Naturally the cloud would have had time to evolve somewhat in the intervening period.

The effect of the strong wind on the progress of the aircraft is clearly apparent in the distance-time graphs, with the aircraft taking approximately twice as long to travel a given distance on the outbound runs than on the inbound. It is clear for future campaigns that it would be extremely beneficial to have a continuously-varying scan rate such that the radar could track the path of the aircraft closely and account for the different ground-relative speeds on the inbound and outbound runs.

The coincidence of the radar and the aircraft in the horizontal has also been examined; Fig. 4.12 shows a plan view with the azimuth along which the radar was scanning as a solid black line, and the flight paths of the aircraft for each run superimposed. The worst deviation of the aircraft from this azimuth was 1.5 km during Run 6.2, but after this the aircraft was always within 500 m of the correct azimuth.

The aircraft data has been used to calculate Z_{m} using (4.9) and Z_{a} using (4.10) as 5-second averages, and these are shown in Fig. 4.11 by the dashed and solid black lines respectively. As expected there is very little difference between the two, because the two density functions have each been tuned to give the best crystal mass for their two different measures of crystal volume. However, where they do differ, it is usually Z_m which is slightly larger.

The aircraft and radar appear to match up exceptionally well, especially given the completely different methods by which they were derived and the lack of exact coincidence between the radar and the aircraft. This gives us considerable confidence in the technique of using aircraft data to test the feasibility of cloud radar retrieval algorithms, such as was done by Brown et al. (1995) and Hogan and Illingworth (1998). However this applies only in the Rayleigh scattering regime so aircraft comparisons with a 94 GHz radar would be required to truly validate the technique when Mie scattering is occurring.

It is interesting to note that the fact that sampling the same region of cloud but up to three minutes apart does not seem to have been crucially important, although it was very fortuitous that the wind direction was very close to being along the flight path of the aircraft. The poorest agreement is between 20 and 25 km of Run 6.2, and although this is where the radar and aircraft samples were very close in time, Fig. 4.12 shows that this is where they were displaced most in the transverse direction. The most likely explanation for the mismatch is that at higher reflectivities (such as those that were observed in Run 6.2) a significant contribution to the returned signal can be from crystals larger than 800 μm, and these were not detected by the aircraft because the precipitation probe was unavailable during the flight. In fact it can be shown using aircraft data from EUCREX (used extensively in the following chapter) that when $Z \simeq -15$ dBZ, the omission of precipitation-sized particles has little effect on the calculation of reflectivity, but when true Z is around -5 dBZ, this omission has the effect of underestimating Z by around around 3 dB.

Despite the apparent agreement between radar and aircraft, and excepting differences which are explainable by the limitations of the instruments, there are nonetheless uncertainties regarding the calibration of both the 2D cloud probe and the radar. The radar was calibrated using the method of Goddard et al. (1994b) which utilises the fact that in rain, Z, Z_{DR} and K_{DP} are not independent, and therefore only the correct calibration for Z will allow the three parameters to be consistent. This technique is supposed to be accurate to ± 0.5 dB, but the nearest calibration event occured nearly three months later, on 5 January 1998, and it is conceivable that the radar calibration could have drifted in the intervening time.

It should also be noted that there are alternative ways to analyse 2D cloud probe data. The standard procedure used at the UKMO Meteorological Research Flight (MRF) is to classify crys-

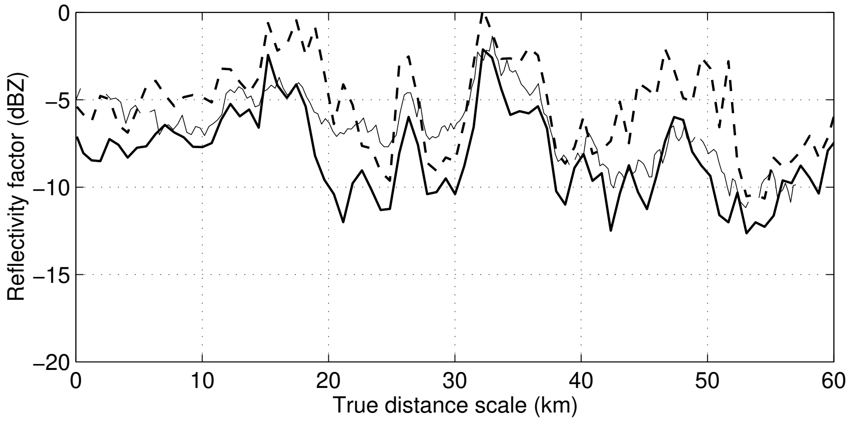

Figure 4.13: Comparison of aircraft Z for Run 6.2 calculated from spectra in which crystals were not classified by type, which is the same as in Fig. 4.11 (thick solid line), and from spectra in which they were (thick dashed line). The radar-measured Z is shown by the thin line. Both spectra were in terms of D_{m}, although the results for area are very similar.

tals by habit which then enables the appropriate relationship from the literature to be applied (see Heymsfield and Baumagardner 1985 and references therein). However, so far in this chapter the algorithm used by Brown (1993) and Brown and Francis (1995) has been implemented, in which D_{m} is defined consistently as the mean of the maximum crystal dimensions in each direction and applied to all crystals, with the exception of needles in which D_{m} is taken to be the crystal length. They justified the use of a simpler scheme on the grounds that it is crystals smaller than 150 μm which contribute most to IWC, and these are inadequately resolved by the probe to be accurately categorised.

When the standard MRF procedure was applied and the spectra again binned by D_{m}, IWC calculated using the density function (4.2) was found to be almost identical to that using the simpler scheme. However it yielded a reflectivity which was systematically greater by 2.3 ± 1.6 dB; this is shown for Run 6.2 in Fig. 4.13. The reason for the difference is that the result of the classification was a tendency to put crystals in larger size bins, but the total number of large particles was slightly reduced, presumably because of different ways of calculating the depth-of-field of the instrument for the various crystal types. These two effects cancelled for IWC, but the size effect dominated for Z.

Given these uncertainties, it is clear that comparison of Z cannot be used to estimate density.

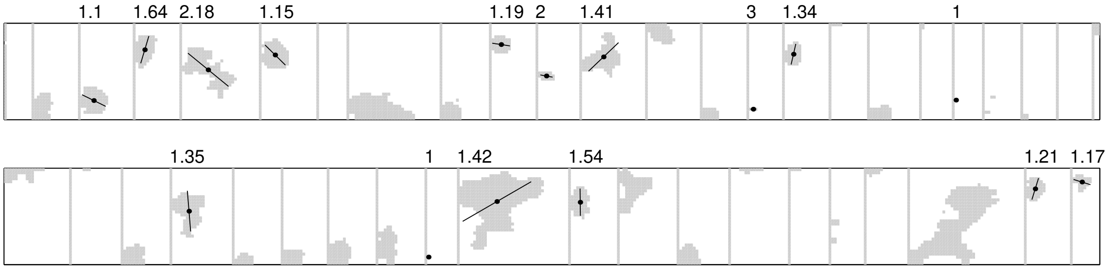

Figure 4.14: Example of the raw 2D cloud probe data, with each crystal overlayed by a point indicating the centre of gravity and a line indicating the longest axis. The aspect ratio is given above each image. Note that those images which occlude the edge of the array or due to diffraction have cast two shadows have been rejected from the analysis.

4.4.3 Comparison of differential reflectivity

The next step was to calculate Z_{DR} from the raw 2D cloud probe data and compare with that measured by the radar. In the low signal-to-noise ratios of clouds, Z_{DR} is noisier than it is in precipitation, and it was found that in all but Run 6.2 (in which the signal was on average 5 dB stronger), it was too noisy to be used reliably.

Figure 4.14 shows an example of the raw crystal images from the probe during this run, with their centres of gravity and longest axes (derived objectively using the method described earlier in this chapter) indicated by a point and a line. The aspect ratio is shown above each accepted image. In fact over half of the images have been rejected, usually because of edge-occlusion, although of course the sample volume has been reduced to take account of this. On average 50 whole images are recorded every second. The large crystal in the middle of the bottom row is the same as that shown in Fig. 4.2.

To get a feel for the characteristics of cirrus crystals observed using the 2D cloud probe, Fig. 4.15 shows scatterplots of aspect ratio and crystal orientation versus diameter for the 25 199 crystals observed during Run 6.2. Superimposed are probability density functions in arbitrary units. The mean aspect ratio is 1.6 and there is no apparent tendency for the larger crystals to be more aspherical than the smaller crystals, as is implied by the crystal length-width relationships derived by Auer and Veal (1970) and Heymsfield (1972); in fact the reverse is true. This could be an indication that the smaller crystals are pristine bullets, columns or plates (for which such length-width relationships were derived) while the larger crystals are aggregates or polycrystals. There is no distinct alignment of the particles in the horizontal, as might be expected for freely-falling crystals (e.g. Liou 1986), and this is probably because turbulence is generated in the intake of the probe which is sufficient to set the crystals tumbling. There is a suggestion that the largest particles ($\sim 500\,\mu$m)

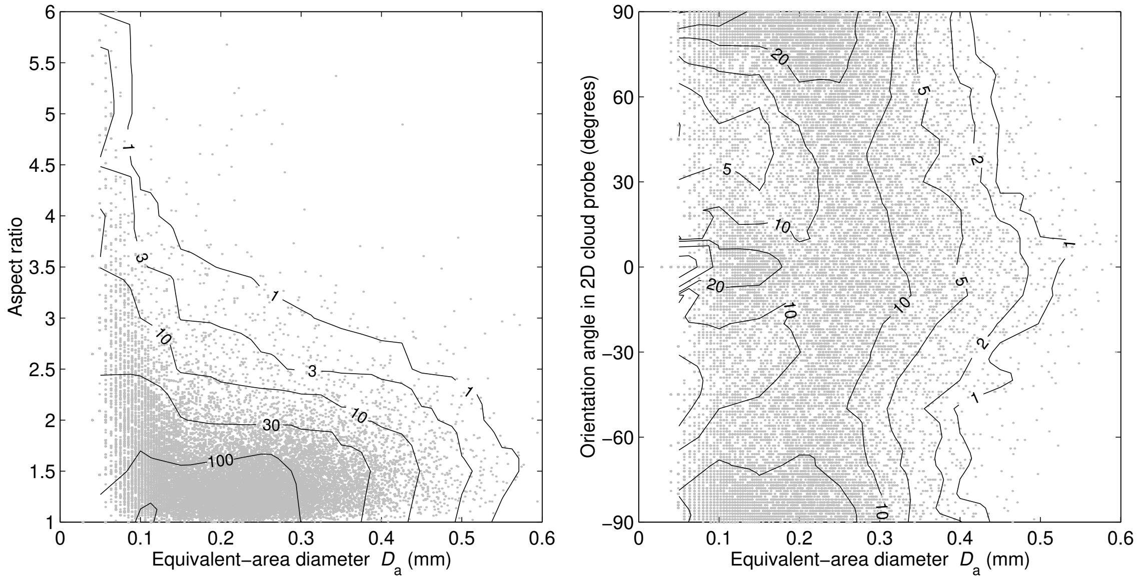

Figure 4.15: Scatterplots of crystal aspect ratio and orientation angle versus D_a, for the 25 199 images in Run 6.2. Contours of the corresponding probability densities are superimposed in arbitrary units. The orientation angle is taken to be relative to a horizontally-aligned crystal.

are more likely to be aligned horizontally, although this is probably because the probe can only measure particles with a vertical dimension of less than 800 µm, so the only way a crystal with a large *mean* size can be detected by the probe and not rejected is if it is close to horizontal alignment. Strangely the crystals around 200 µm in diameter appear to be twice as likely to be *vertically* aligned.

It is clear that the orientation observed by the probe offers no indication of the natural orientation at terminal fall speed. Therefore in the first instance for calculating polarimetric parameters we assume that all crystals are aligned exactly with their major axes parallel to the ground.

Radar-measured differential reflectivity was calibrated by examining those pixels in the light rain beneath the cirrus which had a reflectivity less than 0 dBZ, an LDR of less than −23 dB (to reject most pixels containing significant ground clutter), and specifying that the Z_{DR} of these points should be as near to 0 dB without any of them being less. In this way it is believed any bias in Z_{DR} is less than 0.05 dB.

Z_{DR} was interpolated on to the aircraft flight path in the same way as reflectivity, and is shown in Fig. 4.16 with that calculated from the aircraft using the two density functions. Both the aircraft and the radar data are noisy; the former because a 5-second average is not sufficient to get a good sample of the large crystals which Z_{DR} is most sensitive to, and the latter because Z_{DR} calculated from a only a few hundred pulses (with a large signal-to-noise ratio) will naturally fluctuate with a agreement with radar. There is of course the possibility that appreciable canting may be occurring, and to illustrate this the aircraft calculations were repeated with the crystals all aligned an angle of 33° from horizontal, as shown in plot (b) of each figure. This time there is good agreement with the higher density of the two instead. Unfortunately therefore the results of this comparison are inconclusive because the system is under-constrained; measurements of crystal alignment would be required as well for density to be derived. We can state however that the density given by (4.2) is the minimum possible to be consistent with these observations.

Given the compelling evidence to support the adoption of the higher density in the first half of this chapter, the findings of this comparison would seem to be at odds with the evidence in the literature which supports the contention that that free-falling ice crystals tend to be aligned horizontally. However most of these studies were concerned with pristine crystals such as columns (Jayaweera and Mason 1965, Ono 1969), whereas the large crystals in this study which dominated Z and Z_{DR} were predominantly polycrystalline and therefore akin to snowflakes, which have been shown to have a wide range of canting angles (Hendry et al. 1987). Moreover, lidar observations of horizontal crystal alignment in cirrus (Platt et al. 1978, Thomas et al. 1990) are at wavelengths much more sensitive to the smaller crystals which are more likely to be pristine columns or plates.

Again there is the possibility that large, non-spherical crystals were present which were not detected by the 2D cloud probe but contributed appreciably to Z, and accordingly to Z_{DR}.

4.4.4 Other parameters

Other parameters were measured during the CIRRAD flight, but none of them were found to add any more information to that given by Z and Z_{DR} at 3 GHz. The 35 GHz radar was in operation and measured both Z and Z_{DR}, but because it is around 7 dB less sensitive than the 3 GHz radar, much less of the cloud could be detected, and the lower signal-to-noise ratio meant that Z_{DR} was much noisier. Since cirrus crystals are typically less than 2 mm in diameter it also scatters mostly in the Rayleigh regime and so no reflectivity difference was apparent. Unfortunately the 94 GHz radar was not operational during CIRRAD, but in theory the sensitivity of the 35/94 GHz dual-wavelength sizing technique (see Chapter 6) to density could have been exploited to infer it without the problem of knowing crystal orientation.

The 3 GHz radar also measures linear depolarisation ratio (LDR), which was found to be very useful for eliminating ground clutter (which typically has a value of greater than -10 dB). However in this study LDR due to the cloud itself was found to be too low to be measurable.

Differential phase at 3 GHz was also measured, but no discernible gradient with range was

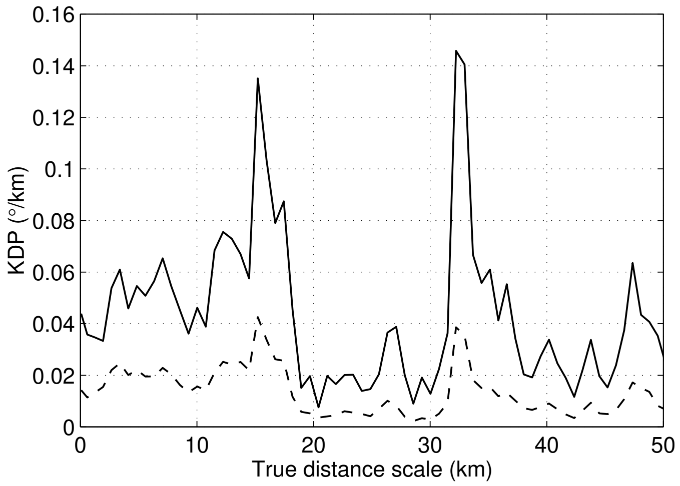

Figure 4.18: Two-way specific phase shift (K_{DP}) calculated from the aircraft data in Run 6.2 with the densities given by Eq. 4.2 (dashed line) and Eq. 4.4 (solid line).

apparent, even through the entire depth of the cloud. It was found to vary randomly from one gate to the next with a standard deviation of around 2°, in agreement with the findings of Li et al. (1994) for the same radar. Blackman (1996) also found in observations of anvil cirrus with a maximum reflectivity of 10 dBZ (i.e. much higher than in this study) that K_{DP} was too small to be measured at 3 GHz. K_{DP} has been calculated from the 2D probe data using (4.24) and is shown in Fig. 4.18. The two density functions produce very different values, but both are too small to be detected. Blackman (1996) also measured differential phase at 35 GHz and even at this higher frequency was unable to detect any propagation component. However there was a strong contribution from differential phase shift on backscatter, which occurs when non-spherical, non-Rayleigh scattering particles are present.

4.5 Conclusions

In the first half of this chapter evidence has been presented which indicates that the established formula for crystal density $\rho = 0.07D^{-1.1}$ is an underestimate, and that the expression $\rho = 0.175D^{-0.66}$ is likely to be much more accurate. The problem arose because the size used to classify crystals, D_{m}, is consistently larger than the equivolumetric diameter D_{v} and therefore should not be used to estimate crystal volume. The equivalent area diameter D_{a} on the other hand provides a much better estimate of D_{v}. The new density is larger than the old by around a factor of two at the sizes the radars are sensitive to, so has important implications for a number of cloud radar techniques, such as the dual-wavelength method for retrieving crystal size in cirrus that will be described in Chapter 6.

This conclusion does not affect the estimation of IWC from size spectra, provided the appropriate density is used with the size parameter that the spectra are binned by; hence the established density still gives an unbiased estimate of IWC if the spectra are binned by D_m, but it should not be used in any other context. Really it is misleading to regard it as a physical density, and it would be better to express the findings of Brown and Francis (1995) only as a mass-D_m relationship.

Radar-measured and aircraft-derived reflectivity factor obtained during the CIRRAD flight exhibited encouragingly good agreement given the lack of exact coincidence. This provides some validation to the technique of using aircraft data to estimate the errors associated with particular radar techniques, but is only applicable in the Rayleigh regime; an intercomparison flight with the 94 GHz radar at Chilbolton in operation would be required to validate the dual-wavelength technique for the sizing of ice crystals, which is of course dependent on non-Rayleigh scattering. In fact this was the original purpose of the flight.

The results of the comparison of Z_DR to infer density were unfortunately inconclusive because of the ambiguity surrounding the orientation of the crystals; if crystals were assumed to be aligned horizontally then the results pointed towards the lower of the two densities, whereas it was shown that with considerable canting it was possible for the results to be consistent with the higher of the two densities. It is also probable that crystals too large to be detected by the 2D cloud probe made a significant contribution to both Z and Z_DR.

Specific differential phase was found to be undetectable in cirrus, in agreement with the measurements of Blackman (1996). This suggests that the algorithm of Ryzhkov et al. (1998), which derives IWC on the assumption that it is proportional to the ratio of K_DP to $1 - 1/Z_\mathrm{DR}$ (with Z_DR in linear units), is only valid in snow and could not be applied to cirrus clouds.

The findings from this intercomparison flight point clearly to the need for a further flight with the following improvements in experimental technique:

- With both the 35 and 94 GHz radars in operation it should be possible to validate the dual-wavelength sizing technique, and additionally the dependence of the dual-wavelength ratio on both density and median volume diameter could make it a parameter from which density could be derived.

- A continuously-varying scan rate would allow the radar to track the aircraft much more precisely, minimising the uncertainties introduced by matching up non-synchronous data. This would also mean that the scan rate would be very low at long range, enabling more spatial averaging and therefore more accuracy and sensitivity. If possible the aircraft should fly along the azimuth corresponding to the direction of the wind.

- Radar calibration should ideally take place shortly before or soon after the flight itself, so that there is no possibility of calibration drift in the intervening time.

- The aircraft *must* carry a functioning precipitation probe.

- In any spare time between runs the radars should make long dwells at an angle of 45°, which would enable all parameters to be derived much more accurately, the 35/94 GHz dual-wavelength ratio to be measured independently of crystal alignment (Section 6.2.1), and possibly even LDR and K_{DP} to be detectable.

CHAPTER FIVE

The potential of spaceborne dual-wavelength radar to make global measurements of cirrus clouds

5.1 Introduction

The importance of ice clouds in the climate system is well recognised (Randall et al. 1989, Stephens et al. 1990), and attention recently has focussed on ways to globally measure the radiative properties and water content of these clouds using active instruments from space. Brown et al. (1995) analysed aircraft cloud probe data taken during EUCREX (the European Cloud Radiation Experiment) and CEPEX (the Central Equatorial Pacific Experiment) to determine how accurately a single 94 GHz radar could measure ice water content (IWC). They found that from radar reflectivity factor alone it should be possible to measure IWC with a standard error of $+85\%$ and -45% for IWC greater than 0.01 $\mathrm{g\,m^{-3}}$, but that if the median size of the ice crystal distribution could be derived using other instruments on board the satellite, then the error would be reduced to $+50\%$ and -35%. For IWC $=0.001\ \mathrm{g\,m^{-3}}$ these errors increase to between $+140\%$ and -60% when size is unknown, and $+80\%$ and -45% when size is known. The remaining error when size is known is due entirely to deviations of the crystal size distribution from exponential. They concluded that if no size information was available then the data from the radar would still provide a useful constraint for climate models, and with the proposed sensitivity threshold of -30 dBZ all but a few percent of radiatively significant clouds would be detected. A similar study was carried out by Atlas et al. (1995) using ity factor measured at this frequency ($Z_{\rm high}$) falls below that at the lower frequency ($Z_{\rm low}$), and the dual-wavelength ratio, defined as

$$\mathrm{DWR} = 10\log_{10}\left(\frac{Z_{\rm low}}{Z_{\rm high}}\right)\ \mathrm{dB}, \tag{5.1}$$

rises above 0 dB and is directly related to crystal size. This principle was first suggested by Matrosov (1993), and will be demonstrated using ground-based 35 and 94 GHz radars in the next chapter, although we shall see that DWR was observed to rise to only 7.5 dB, and random errors at low signal-to-noise ratios prevented size estimation in a significant fraction of detected cloud.

These problems would be much reduced by the use of higher frequencies. Gaseous attenuation normally precludes the use of frequencies higher than around 94 GHz for ground-based cirrus observations, but from space the attenuation is reduced to an acceptable level (see Section 5.4). The advantages of higher frequencies are:

1. A large increase in DWR for a given mean crystal size, enabling more accurate size retrieval and the ability to measure down to smaller sizes;
2. Higher sensitivity: in the Rayleigh regime, reflectivity increases as the fourth power of frequency for a fixed antenna size, although this is partially countered by increased thermal noise and reduced power output;
3. A smaller footprint;
4. For single frequency radars, the use of higher frequencies results in a closer correlation between IWC and Z (see Section 5.3.2).

The frequencies we shall consider in this chapter are 35, 79, 94, 140 and 215 GHz, chosen because they lie in the window regions of the atmospheric absorption spectrum. 35 and 94 GHz radars have been used in cloud research for over 10 years, but of the other frequencies I am aware of only a single 215 GHz radar in existence (Mead et al. 1989). This ground-based radar uses a similar transmitting tube to the 94 GHz radar of Lhermitte (1987), but the power output is less by 12.2 dB because of the higher operating frequency, which largely offsets the 14.4 dB increase in sensitivity due to increased scattering efficiency. The radar is restricted to probing low clouds because of the strong water-vapour attenuation in the boundary layer.

Radar reflectivity at these five frequencies, and the relevant microphysical parameters, have been calculated from the EUCREX and CEPEX datasets[1]. Firstly the accuracy of simple estim-

[1]EUCREX data provided by Philip Brown, CEPEX data by Andrew Heymsfield.

ates of IWC and visible extinction coefficient ($\beta_{\rm vis}$) from radar reflectivity alone are calculated for each wavelength. Then we compute the improved accuracy of these parameters using various combinations of these frequencies, and also the accuracy of retrievals of median volume diameter D_0. Lastly the effect of minimum detectability thresholds of both -30 and -40 dBZ is determined, by adding the appropriate random noise to DWR and recalculating the retrieved cloud parameters.

The magnitude of the attenuation by atmospheric gases is calculated for a number of standard atmospheres in Section 5.4, and is found to be acceptable down to the melting level, even at 215 GHz. We also calculate the attenuation by the ice crystals themselves for the EUCREX and CEPEX data. In Section 5.5 we estimate to what extent the different beamwidths of a dual-wavelength radar using the same antenna could cause errors in DWR while probing inhomogeneous cloud. This is achieved by using real cloud radar data to obtain the amplitude of reflectivity fluctuations at various spatial scales, and then simulating two-dimensional cloud fields with the same spectral properties. This method is also used to explore the feasibility of mounting the two radars of a dual-wavelength system on separate satellites in very close orbits. Other considerations such as calibration and the effects of non-spherical crystals are considered in Section 5.6.

This chapter is based on the paper Hogan and Illingworth (1998).

5.2 Theory

5.2.1 Cloud parameters

The most basic cloud parameters required by radiation schemes are the short-wave volume extinction coefficient $\beta_{\rm vis}$ and the infrared volume absorption coefficient $\beta_{\rm ir}$. It is common to assume in both the visible and the infrared that ice crystals are large compared with the wavelength, and hence make the geometric optics approximation:

$$\beta_{\rm vis} \simeq 2\int_0^\infty \mathcal{A}(D)\, n(D)\, dD \tag{5.2}$$

$$\beta_{\rm ir} \simeq \int_0^\infty \mathcal{A}(D)\, n(D)\, dD \tag{5.3}$$

where $\mathcal{A}(D)$ is the particle cross-sectional area as a function of diameter D, and $n(D)$ is the crystal number concentration per unit diameter.

For direct comparison with atmospheric models it is necessary for remote sensing techniques to measure ice water content. To calculate this from aircraft data, which consist of particle concentration in a number of size bins, we must prescribe a shape and density. For simplicity we assume spheres, and from the mass-diameter relationship of Brown and Francis (1995), density ρ is derived as:

$$\rho = 0.07 D^{-1.1} \ \mathrm{g\,cm^{-3}} \tag{5.4}$$

to a maximum of $0.917 \ \mathrm{g\,cm^{-3}}$, where the diameter D is in millimetres[2]. Brown and Francis found that their relationship maximised the agreement between the bulk measure of IWC from the Total Water Probe (Brown 1993) and that calculated from size spectra. This density function is also used in the calculation of radar reflectivity.

To assess the ability of the dual-wavelength method to estimate size, the median diameter of the volume-weighted size distribution, D_0, is used. This is often used as a parameter in idealised size distributions.

5.2.2 Radar parameters

Radars measure effective radar reflectivity, which for spherical particles at a frequency f is given by

$$Z_f = \int_0^\infty \frac{|K(\rho)|^2}{0.93} n(D)\, D^6 \gamma_f(D)\, dD \tag{5.5}$$

where γ_f is the ratio of Mie to Rayleigh backscatter. The parameter K is given by

$$K = \frac{\varepsilon - 1}{\varepsilon + 2} \tag{5.6}$$

where ε is the complex dielectric constant of the ice-air mixture. The dielectric constant of solid ice (ε_s) is calculated using the empirical expression of Liebe et al. (1989), and given the ice fraction of the crystal lattice (f_i), ε can be calculated using the formula of Maxwell-Garnet (1904), as modified by Meneghini and Liao (1996):

$$\varepsilon = \frac{(1 - f_\mathrm{i})\varepsilon_\mathrm{a} + f_\mathrm{i}\alpha\varepsilon_\mathrm{s}}{(1 - f_\mathrm{i}) + f_\mathrm{i}\alpha} \tag{5.7}$$

where

$$\alpha = \frac{2\varepsilon_\mathrm{a}}{\varepsilon_\mathrm{s} - \varepsilon_\mathrm{a}} \left[\frac{\varepsilon_\mathrm{s}}{\varepsilon_\mathrm{s} - \varepsilon_\mathrm{a}} \ln\left(\frac{\varepsilon_\mathrm{s}}{\varepsilon_\mathrm{a}}\right) - 1 \right] \tag{5.8}$$

[2] This form is used, despite the findings of Chapter 4, because the crystals have been binned by D_m rather than area; unfortunately the CEPEX data were not available in terms of area. The work for this chapter was completed and accepted for publication (Hogan and Illingworth 1998) before the issue of density had arisen, but it is not expected that this will significantly affect most of the results that follow because the crystal masses are still accurate, it is only their equivolumetric diameters which are slightly overestimated. Naturally more work is required to confirm this.

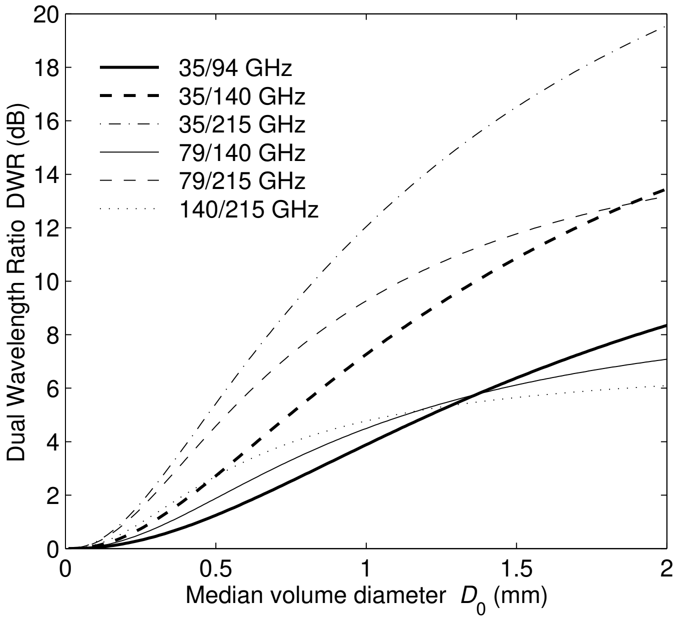

Figure 5.2: Dual-wavelength ratio as a function of median volume diameter for an exponential distribution.

and the dielectric constant of air (ε_a) is taken to be unity. It turns out that $|K|^2$ is approximately proportional to the square of density, and is virtually independent of frequency between 35 and 215 GHz. Because the radar measure of Z has no a priori knowledge of the phase of the target, and to enable comparison of different wavelengths, the factor 0.93 is present in (5.5) to make reflectivity factor relative to liquid water at centimetre wavelengths. Clearly Z is not directly proportional to any cloud parameter of interest, so it is necessary to derive empirical relationships from real data.

For dual-frequency radar, six combinations of frequencies are considered: 35/94, 35/140, 35/215, 79/140, 79/215 and 140/215 GHz. To illustrate the typical magnitude of DWR for each, Fig. 5.2 shows DWR as a function of D_0 for exponential distributions of spherical crystals.

5.2.3 Accuracy of radar parameters

A crucial concern for dual-wavelength radars is the extent to which various factors might introduce error into DWR. The problem of different beamwidths is explored in Section 5.5.1, and that of calibration in Section 5.6.2. Here we consider the random error in reflectivity measurements at low signal-to-noise ratios. For a single wavelength radar this is not usually of great importance, but for dual-wavelength radar it is what determines the lower size limit for the use of DWR.

Throughout this chapter we adopt the retrieval strategy suggested by Illingworth et al. (1997). They considered a nadir-pointing 79 or 94 GHz radar of the conventional pulsed type in a 500 km high orbit, and showed that at this altitude the maximum allowable Pulse Repetition Frequency to avoid mirror image cloud returns is 2830 Hz. In general, the noise component of the measured echo can be considered statistically independent every pulse, and for the cloud echo the decorrelation time is approximately equal to the reciprocal of the Doppler bandwidth within the mainbeam of the antenna. In the case we are considering, the decorrelation time is around 0.1 ms, so we can consider all pulses to be independent.

It was shown in Chapter 2 that for a radar with a noise-equivalent reflectivity (for a single pulse) N, the standard error of a reflectivity measurement averaged over M_{I} independent pulses is given approximately by

$$\Delta Z \simeq \frac{4.343}{\sqrt{M_{\mathrm{I}}}} \left(1 + 10^{0.1(N[\mathrm{dBZ}]-Z[\mathrm{dBZ}])}\right) \ \mathrm{dB}. \tag{5.9}$$

Hence for a 1 second dwell (7 km along-track averaging), $M_{\mathrm{I}} = 2830$, and in the limit of large signal-to-noise ratio, $\Delta Z \rightarrow 0.082\,\mathrm{dB}$.

It is necessary to define a threshold reflectivity for cloud detection. In Illingworth et al. (1997) the cloud was deemed detectable if the radiometric resolution, defined as

$$\gamma = 1 + \frac{1}{\sqrt{M}} \left(1 + 10^{0.1(N[\mathrm{dBZ}]-Z[\mathrm{dBZ}])}\right), \tag{5.10}$$

was less than 1.5. This is equivalent to setting $\eta = 2$ in (2.23), or setting the maximum allowable ΔZ to 2.25 dB, or specifying that in clear skies with only (normally-distributed) noise being detected, only 2.3% of the pixels would anomalously register as cloud. These could then be almost completely eliminated by rejecting all low reflectivity pixels not adjacent to any other pixel. At both frequencies of a dual-wavelength system we calculate ΔZ as a function of reflectivity and minimum detectable reflectivity, and from this the error in DWR:

$$\Delta\mathrm{DWR} = \left(\Delta Z_{\mathrm{high}}^2 + \Delta Z_{\mathrm{low}}^2\right)^{\frac{1}{2}} \ \mathrm{dB}. \tag{5.11}$$

Hence in the limit of large signal-to-noise ratio, $\Delta\mathrm{DWR} \rightarrow 0.12\,\mathrm{dB}$. It was stated in Illingworth et al. (1997) that with current technology a 79 or 94 GHz spaceborne radar could be built to have a minimum detectable reflectivity of -30 dBZ in this retrieval scenario. The precision of measured reflectivity for such a radar is plotted against reflectivity in Fig. 5.3.

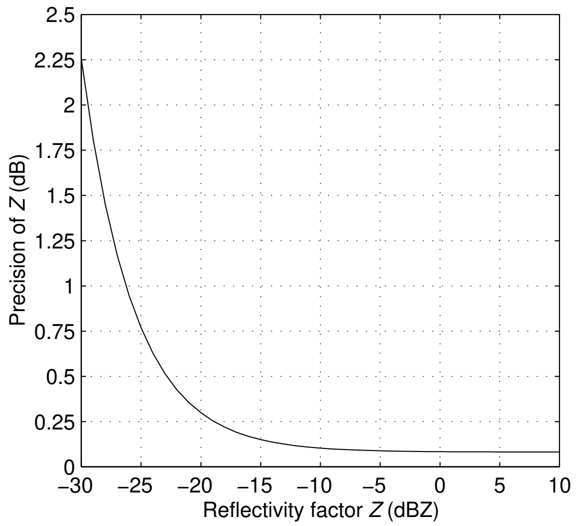

Figure 5.3: The precision of measured reflectivity for 2830-pulse averaging and a noise-equivalent reflectivity of -15.75 dBZ. This is the scenario envisaged for a spaceborne radar.

5.3 Accuracy of cloud parameters derived by spaceborne radar

5.3.1 Brief description of the aircraft data

The data used in this section comprise mid-latitude measurements from EUCREX and tropical measurements from CEPEX. They are the same as those used by Brown et al. (1995), but with a few additional mid-latitude flights which have been grouped together with the existing EUCREX data. See Brown et al. for more information. The EUCREX dataset consisted of over 10 000 5-second averaged size spectra discretised into 50 bins ranging from 25 to 6400 µm in diameter. The flights were by the UK Meteorological Office C-130 aircraft and took place in September and October 1993. The CEPEX dataset comprised a similar number of 10-second averaged size spectra in 28 bins between 45 and 2700 µm. The aircraft was a Learjet of Aeromet Inc. and the flights occured in March and early April 1993. In this study, observations at temperatures above $-20°$C were rejected because of the possibility of contamination from supercooled water droplets which would have biased the results.

Radar reflectivity at 35, 79, 94, 140 and 215 GHz was calculated from the spectra using Mie theory, along with the parameters IWC, β_{vis} and D_0. Histograms of the IWC observations are shown in Fig. 5.4.

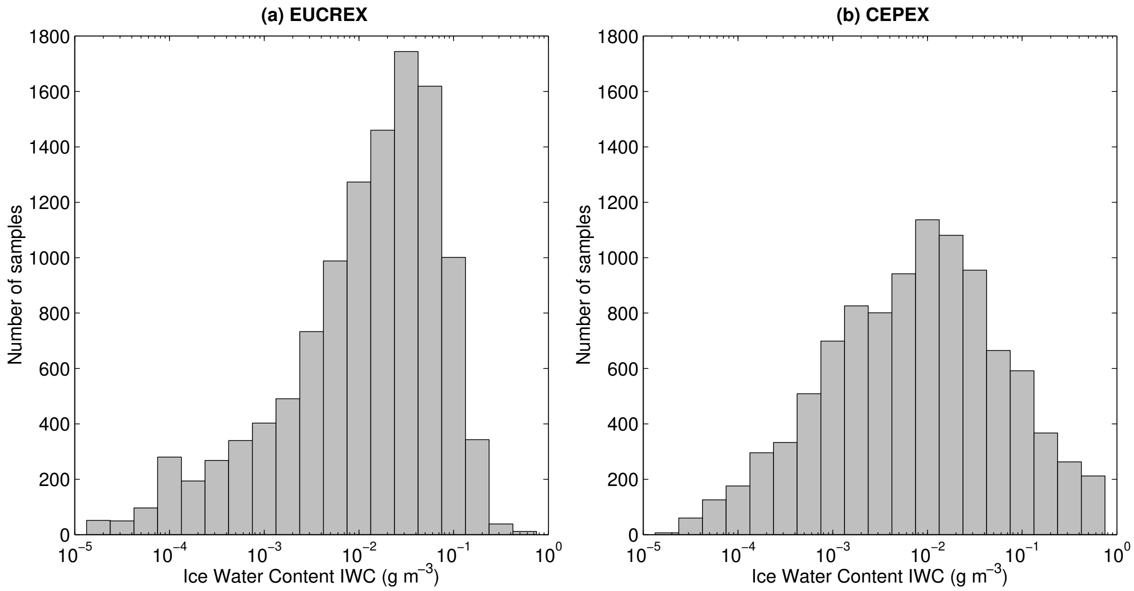

Figure 5.4: Histograms of the IWC observations for the EUCREX and CEPEX datasets.

	frequency	a	b
EUCREX	35 GHz	0.0619	−1.078
	79 GHz	0.0691	−0.888
	94 GHz	0.0706	−0.846
	140 GHz	0.0749	−0.713
	215 GHz	0.0820	−0.461
CEPEX	35 GHz	0.0617	−0.899
	79 GHz	0.0638	−0.834
	94 GHz	0.0647	−0.805
	140 GHz	0.0677	−0.700
	215 GHz	0.0734	−0.489

Table 5.1: Coefficients of the least squares fit $\log_{10}(\mathrm{IWC}) = aZ + b$, where Z is in dBZ and IWC is in g m^{-3}.

5.3.2 Accuracy of single wavelength measurements

Firstly the accuracy of simple empirical estimates of IWC from radar reflectivity were calculated for each wavelength as a function of IWC. The parameters of a least squares fit regression between Z and $\log_{10}(\mathrm{IWC})$ were computed, and are given in Table 5.1. At higher frequencies the effect of increased Mie scattering is to increase the slope of the lines of best fit. The small difference between the coefficients given for 94 GHz and those in Brown et al. (1995) are due mainly to the fact that they only performed regressions on part of the datasets in order to test their representativity, and

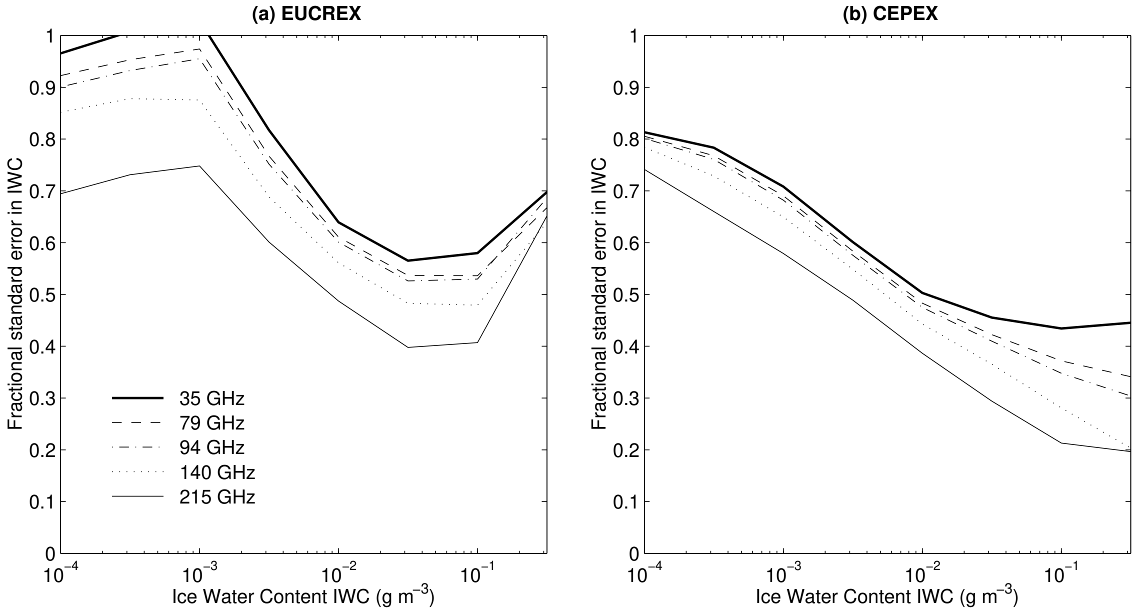

Figure 5.5: Error in ice water content estimated by radar reflectivity at five frequencies for the EUCREX and CEPEX datasets.

to explore how systematic differences in Z–IWC relationships from cloud to cloud could affect the accuracy of retrievals. However for determining the errors in IWC, the fit used was an interpolation between the mean of $\log_{10}(\text{IWC})$ in each 5 dB range of Z, which led to greater accuracy in the thickest and hence most radiatively important clouds.

Figure 5.5 shows the fractional standard error in IWC estimated from Z, as a function of IWC for the five frequencies. Fractional standard error is defined simply as the standard error of the natural logarithm. For small relative errors this is approximately equal to the standard error divided by the mean. It can be seen that accuracy improves with increased frequency. This is for the simple reason that the Mie scattering regime represents a transition between the Rayleigh scattering regime (where backscattered power is proportional to D^6) and the geometric optics regime (where backscattered power is proportional to D^2). Hence the return from frequencies which are backscattering further into the Mie regime has a diameter-dependence which is closer to that of IWC. The increase in fractional error at large IWC for the EUCREX case is partly a statistical effect due to the low number of samples; only 0.8% of the dataset had an IWC greater than 0.2 g m^{-3}. This is clearly apparent in Fig. 5.4.

The errors are due to the variation in mean size and the shape of the distribution, but do not include the effect of variation in density function, since it is very difficult to measure the density of individual crystals from aircraft.

Since the distinction between tropical and mid-latitude cirrus is somewhat artificial, it is con-

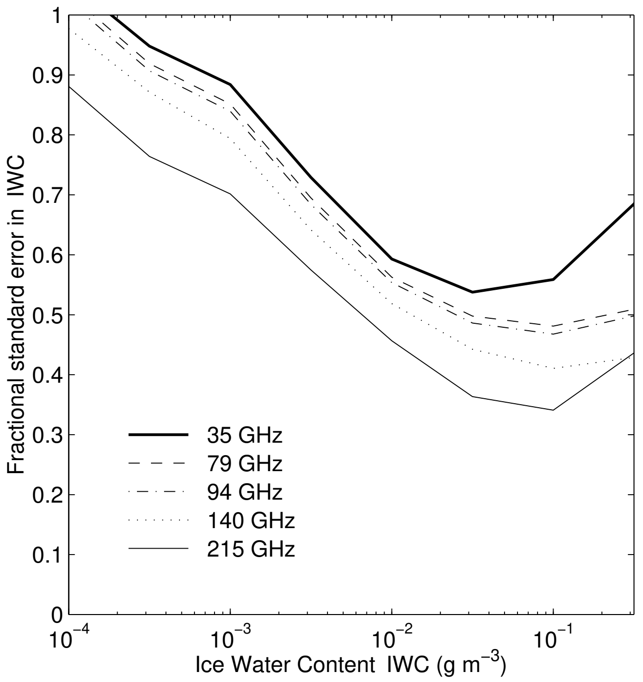

Figure 5.6: Error in ice water content estimated by radar reflectivity at five frequencies for the EUCREX and CEPEX datasets, using best fits calculated from the two datasets combined.

ceivable that using the wrong set of fits to a particular cloud could significantly increase the error. We therefore combined the two datasets and recalculated the errors in IWC. The results are plotted in Fig. 5.6. It would appear that the tropical and mid-latitude datasets are sufficiently similar that the use of a single Z–IWC relationship for all points on the globe does not lead to a significant loss of accuracy.

Visible extinction coefficient β_{vis}, defined in (5.2), can be more confidently calculated than IWC from aircraft size spectra alone because no assumption of density is required. However it was suggested by Arnott et al. (1994) that a sizeable number of crystals too small to be detected by the 2DC probe may contribute significantly to the extinction. More recent studies using a variety of instruments capable of measuring down to 5 µm (Mitchell et al. 1996, Kinne et al. 1997, McFarquhar and Heymsfield 1997) suggest that crystals smaller than 25 µm rarely dominate IWC or the radiative properties of cirrus.

Exactly the same procedure was carried out for β_{vis} as for IWC. The regression parameters are listed in Table 5.2, and the lines of best fit they represent are plotted in Fig. 5.7. The fractional error in β_{vis} as a function of β_{vis} is plotted in Fig. 5.8. The errors are slightly larger than for IWC, but again the highest frequencies are most accurate. It would be useful to compare visible or infrared radiometer measurements with radar derived optical depth using Z–β_{vis} relationships, with a

	frequency	a	b
EUCREX	35 GHz	0.0607	−2.493
	79 GHz	0.0677	−2.309
	94 GHz	0.0691	−2.268
	140 GHz	0.0732	−2.139
	215 GHz	0.0800	−1.894
CEPEX	35 GHz	0.0584	−2.306
	79 GHz	0.0603	−2.244
	94 GHz	0.0611	−2.217
	140 GHz	0.0640	−2.117
	215 GHz	0.0694	−1.917

Table 5.2: Coefficients of the least squares fit $\log_{10}(\beta_{\text{vis}}) = aZ + b$, where Z is in dBZ and β_{vis} is in m^{-1}.

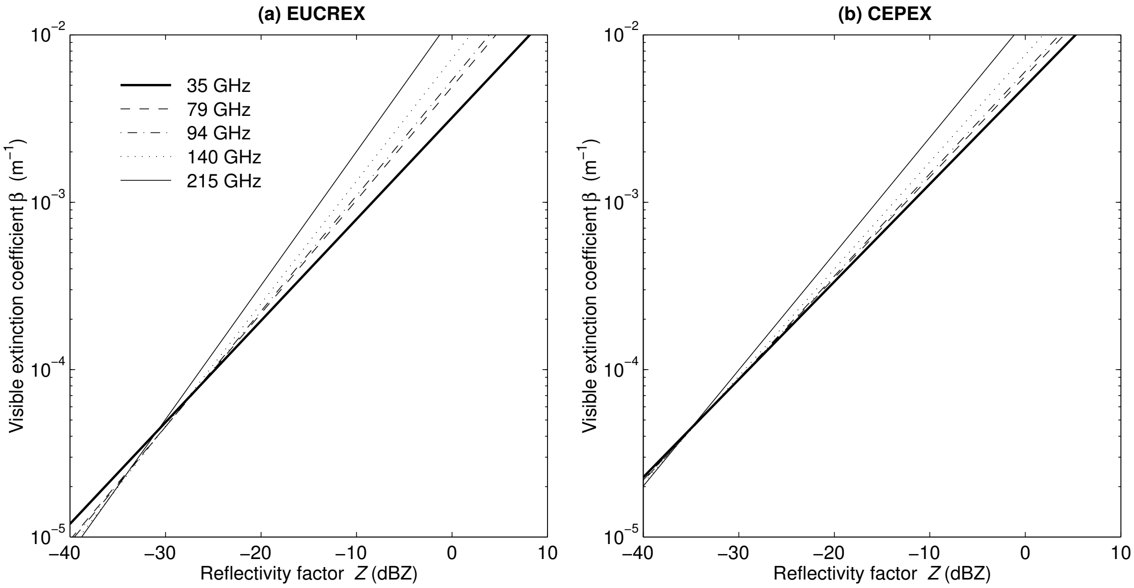

Figure 5.7: The regression lines relating Z to $\log_{10}(\beta)$ calculated from the coefficients in Table 5.2

view to exploring the ways an array of passive instruments along side the radar could validate and enhance the information provided by the radar.

One should be aware that through the depth of a particular cloud the errors in IWC or β_{vis} are likely to be in the same sense, since the relationships between these parameters and Z depend to some extent on the number concentration of ice nuclei. This can vary considerably but is likely to be correlated for a particular cloud. Hence vertically integrated quantities estimated from radar, such ice water path or optical depth, should be expected to have the same fractional error as IWC

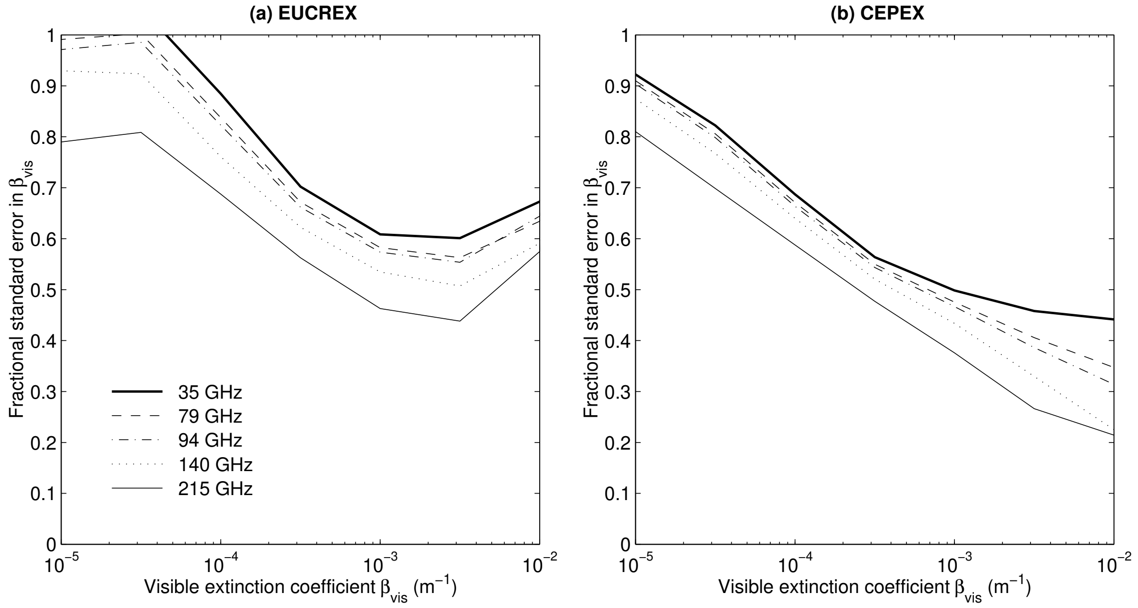

Figure 5.8: Error in the visible extinction coefficient estimated from radar reflectivity at five frequencies for the EUCREX and CEPEX datasets.

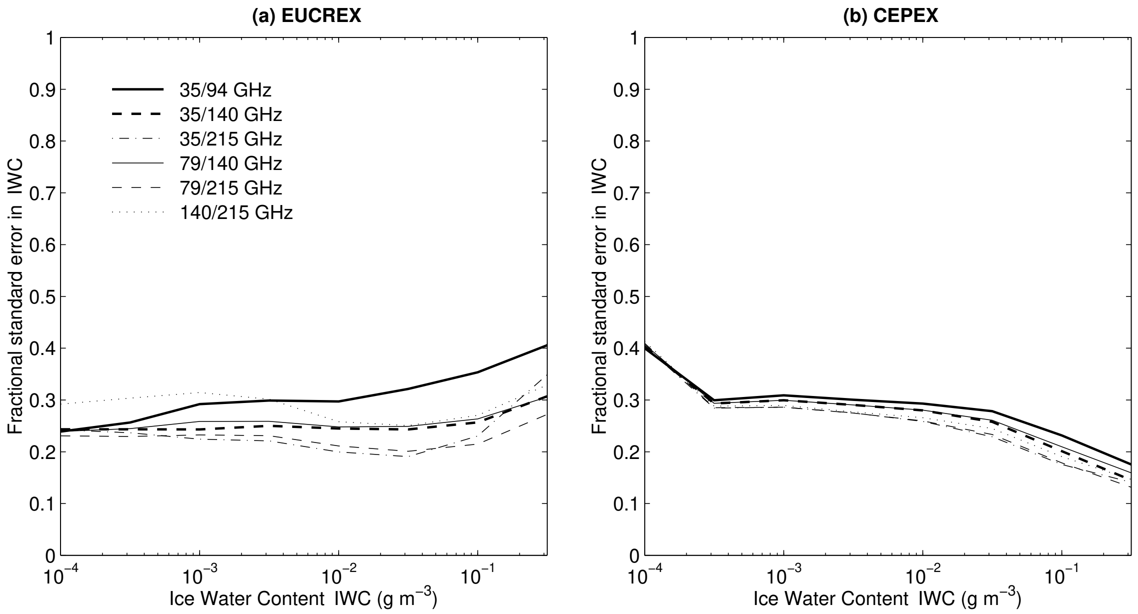

Figure 5.9: Error in IWC estimated by dual-wavelength radar for six frequency combinations.

and β_{vis}.

We conclude that if financial constraints were to restrict the satellite to carry only a single radar, then for estimating IWC and β_{vis} in cirrus, the highest frequencies are the best, although a judgement must be made as to whether attenuation by water vapour is too high at 140 and 215 GHz for these frequencies to be used if the detection of low clouds is also a priority.

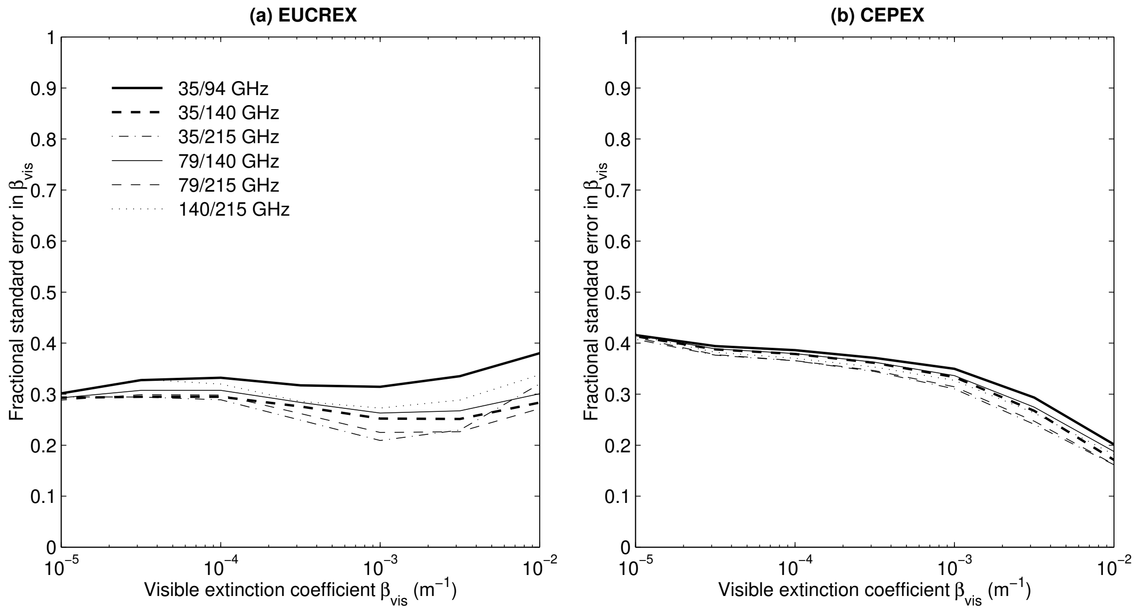

Figure 5.10: Error in β_{vis} estimated by dual-wavelength radar.

5.3.3 Accuracy of dual-wavelength measurements

Next we considered six dual-frequency combinations: 35/94, 35/140, 35/215, 79/140, 79/215 and 140/215 GHz. Firstly the accuracy of IWC was calculated assuming that DWR is known exactly, which would be the case for a radar with an infinite dwell time. The procedure was to calculate a best fit relating DWR to the ratio $g = \mathrm{IWC}/Z_{\mathrm{low}}$ and then to compare the true IWC with that given by $g \times Z_{\mathrm{low}}$, with g derived from DWR using the best fit. The fit was calculated in log-log space since the best fit between $\log(\mathrm{DWR})$ and $\log(g)$ is close to a straight line. The results are plotted in Fig. 5.9 and show considerable improvement over the single wavelength estimates. Essentially these findings are equivalent to those of Brown et al. (1995) for when some measure of mean size was known exactly. There is little difference between the various frequency combinations, although the 35/215 and 79/215 combinations exhibit slightly more accuracy. The remaining error of around 25–30% is due solely to the variation of the shape of the size distribution, and would be present for any technique which intrinsically assumes that one parameter (such as D_0) is sufficient to describe distribution shape. Improvements beyond this should only be possible with some path constraint provided by radiometers.

The same procedure was repeated for β_{vis}, and the results are plotted in Fig. 5.10. Again the error is a little higher than that for IWC. The error in measuring D_0 from DWR is shown in Fig. 5.11. Note that only 0.5% of the EUCREX data and 0.1% of the CEPEX data had D_0 greater than 800 μm.

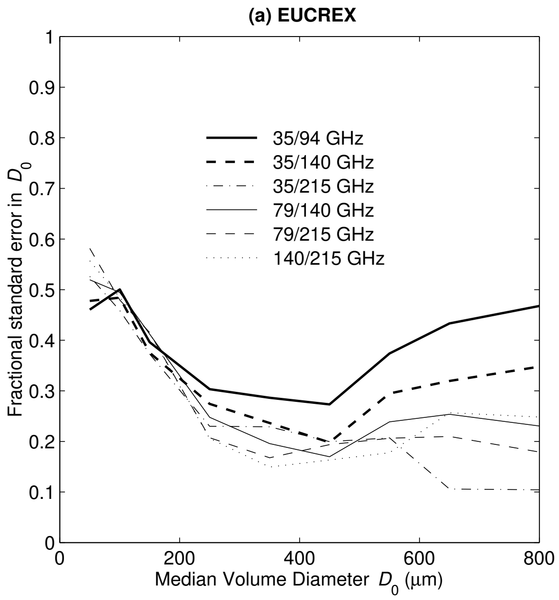

Figure 5.11: Error in D_0 estimated by dual-wavelength radar.

5.3.4 Dual-wavelength measurements with realistic radar sensitivities

The next step was to consider the effect of minimum sensitivities of −30 and −40 dBZ on the accuracy of DWR and on quantities derived from it. Normally-distributed random noise with a standard deviation calculated from (5.9) and (5.11) was added to DWR (assuming that both frequencies had the same minimum detectable reflectivity) and the errors in IWC and D_0 were recalculated. In reality of course the higher frequencies would probably be more sensitive, but for dual-wavelength radar the least sensitive radar of the two is the determining factor for the accuracy of DWR.

A retrieval algorithm for a dual-wavelength radar needs to know the accuracy to which it can measure DWR and from this define a minimum value of DWR for sizing (as a function of Z_{low} and Z_{high}) such that any values measured below this are deemed too inaccurate for size estimation and are rejected. We set this limit to be twice the standard deviation of DWR; i.e. DWR $> 2\,\Delta$DWR.

Figure 5.12 shows the error in IWC as a function of the reflectivity of the lowest frequency radar of the pair, for a minimum detectable reflectivity of −30 dBZ. The error for reflectivities of between −30 and −20 dBZ is large and only slightly better than the estimate for a single wavelength radar. Above −20 dBZ the most effective frequency combinations are clearly 35/215 and 79/215. The same for D_0 is shown in Fig. 5.13. One should be aware that in the lowest 10 dB of detectability some of the error is systematic, because by rejecting low values of DWR which fail the DWR $> 2\,\Delta$DWR criterion, we are only accepting those pixels for which the random fluctuations happened to produce a larger DWR. Hence the measured size will usually be an overes-

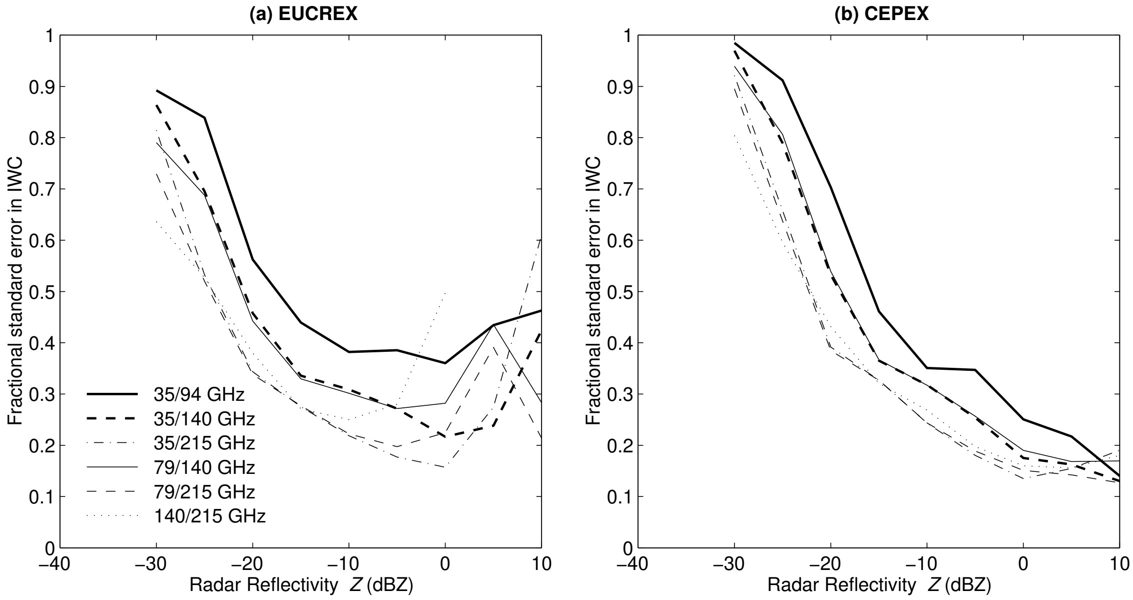

Figure 5.12: Error in IWC derived from spaceborne dual-wavelength radar as a function of the reflectivity at the lower frequency, for a minimum detectable reflectivity of $-30\,$dBZ.

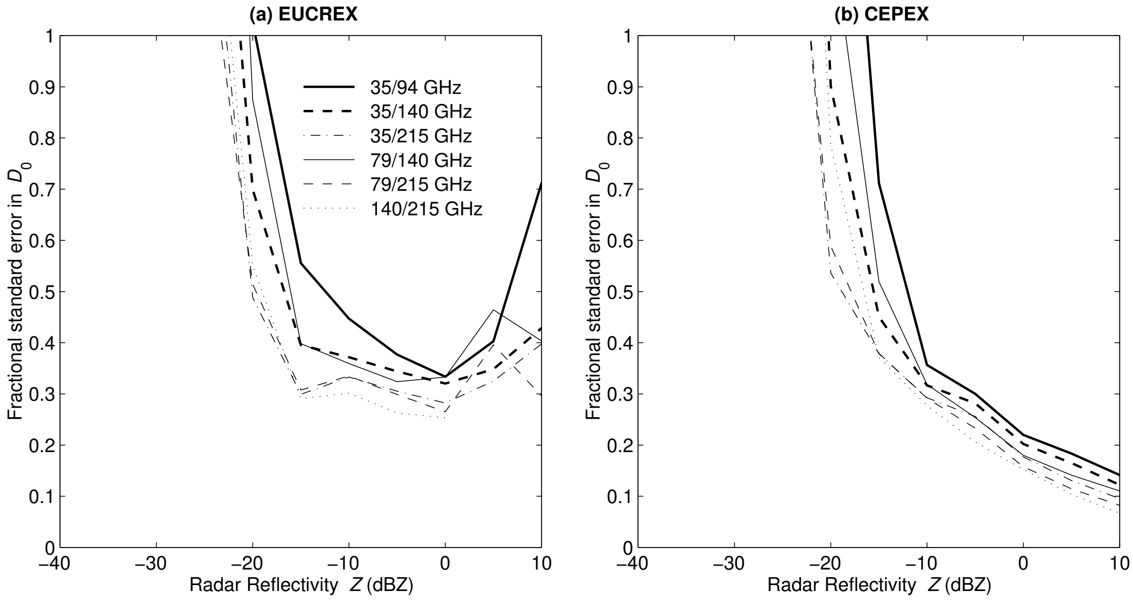

Figure 5.13: Error in D_0 as a function of the reflectivity at the lower frequency, for a minimum detectable reflectivity of $-30\,$dBZ.

timate. There is therefore a case for not estimating size when $Z_{\text{low}} < -20\,$dBZ.

Figure 5.14 shows the fraction of detected cloud at a given reflectivity that can be sized. In the EUCREX data the 140/215 combination was best, being able to make size measurements in 90% of detected clouds with a reflectivity of $-20\,$dBZ, whereas the value was only 10% for 35/94. For CEPEX the 35/215 and 79/215 combinations were able to measure size in the largest fraction

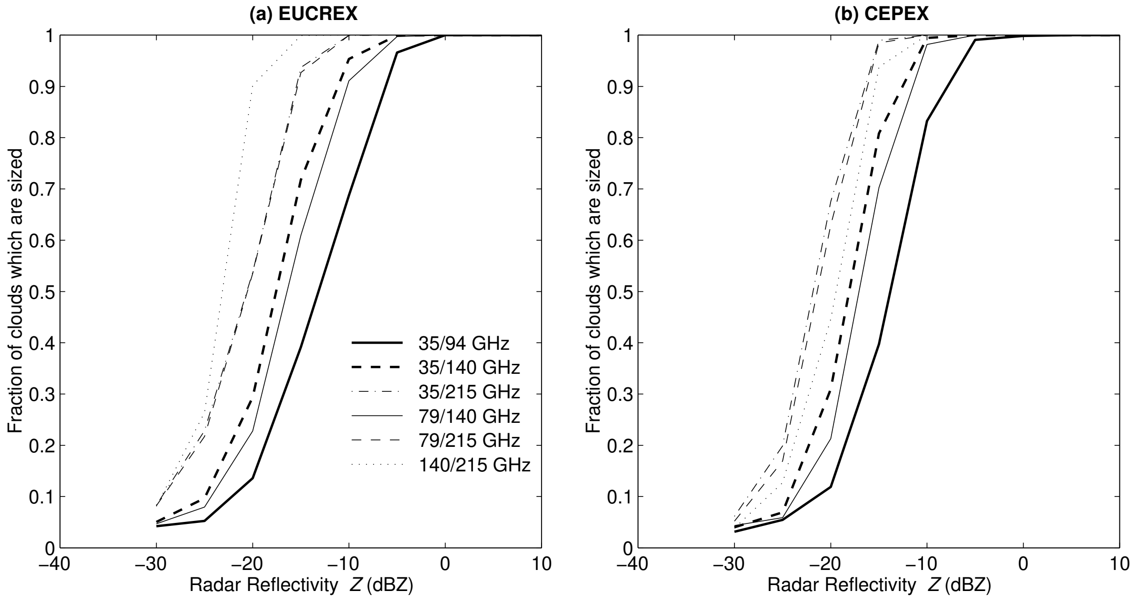

Figure 5.14: The fraction of detected cloud at a given frequency that can be sized, for a minimum detectable reflectivity of −30 dBZ.

of clouds. Dual-wavelength systems which include a 215 GHz radar are clearly the best both for accuracy and the fraction of clouds which can be sized, simply because at small sizes DWR is so much larger.

Figures 5.15–5.17 show the same as Figs. 5.12–5.14 but with a minimum detectable reflectivity of −40 dB. Again reliable size measurements are not possible in the lowest 10 to 20 dB of sensitivity, but the advantages of the higher sensitivity in faint clouds are apparent. Even if the sensitivity of the radars was somehow improved dramatically, if still only 2830 pulses were being averaged at each frequency then DWR would still have an intrinsic uncertainty of 0.12 dB and a lower limit for size measurement would remain. Meneghini and Kozu (1990) discussed a number of techniques for increasing the number of independent pulses M_{I}. A popular choice for a spaceborne radar is pulse compression, where conventional high-power, short-duration pulses are replaced by long coded pulses of low peak power. Frequency agility is also a possible means of increasing M_{I}.

5.4 Attenuation

5.4.1 Atmospheric gases

Radars at frequencies higher than 94 GHz are generally considered to be unsuitable for ground-based observations of cirrus because of the strong water-vapour and oxygen absorption in the

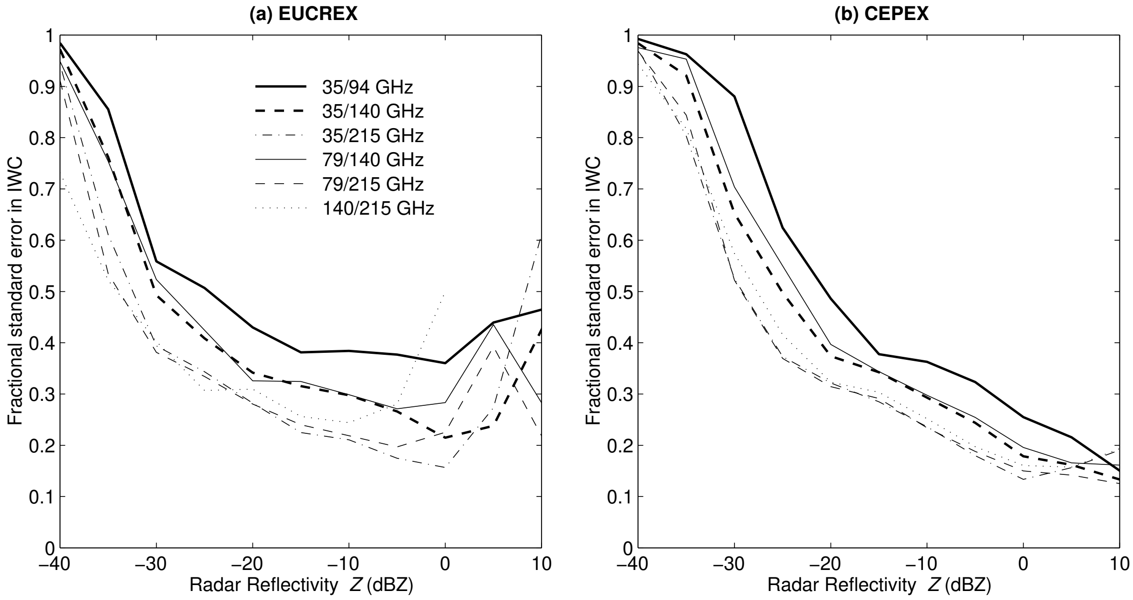

Figure 5.15: Error in IWC derived from spaceborne dual-wavelength radar as a function of the reflectivity at the lower frequency, for a minimum detectable reflectivity of $-40\,$dBZ.

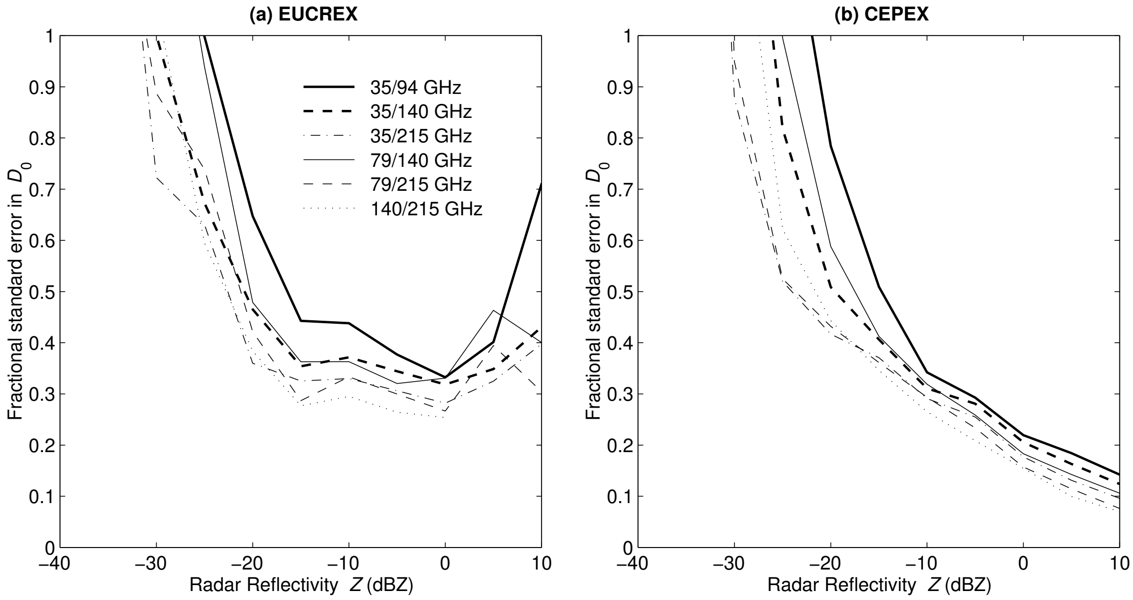

Figure 5.16: Error in D_0 as a function of the reflectivity at the lower frequency, for a minimum detectable reflectivity of $-40\,$dBZ.

boundary layer. From space attenuation is far less of a problem. The nadir two-way gaseous attenuation from space has been calculated using the line-by-line model of Liebe (1985), for a number of standard atmospheres taken from McClatchey et al. (1972), with saturated layers added at altitudes typical of cirrus. Figure 5.18 shows the profiles of temperature, relative humidity and the corresponding two-way nadir attenuation at each of the five frequencies, for the two most at-

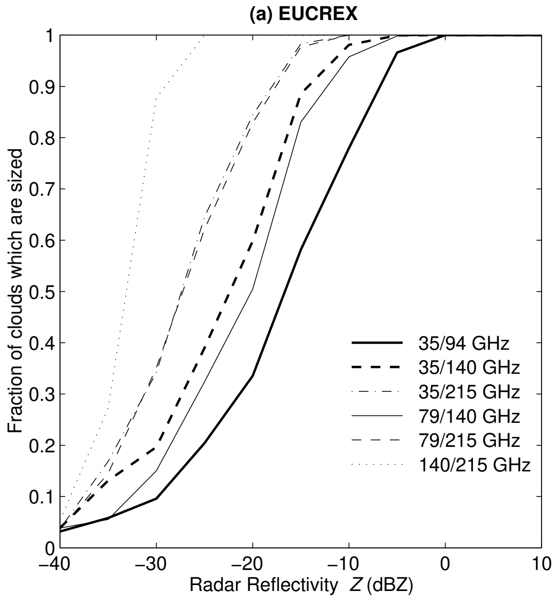

Figure 5.17: The fraction of detected cloud at a given frequency that can be sized, for a minimum detectable reflectivity of -40 dBZ.

tenuating atmospheres (mid-latitude summer and tropical). It can be seen that the attenuation at 4 km/0°C reaches at most 0.8 dB at 140 GHz and 2 dB at 215 GHz. This is not a great problem for a dual-wavelength system with one frequency above 94 GHz and one at or below 94 GHz, since the reflectivity at the higher frequency can be matched with the less-attenuated lower frequency radar in the Rayleigh-scattering cloud top. Then attenuation can be corrected through the remainder of the cloud since it is reasonable to assume that the relative humidity is 100% where there is a cloud echo, and temperature is generally diagnosed well by global forecast models. Supposing after attenuation correction a 1 dB error in DWR remained just above the melting layer, then for a 79/215 GHz system this is not disastrous, representing only a 15% error in D_0 provided $D_0 > 500\,\mu$m at this point. It is apparent that the temperature of the cloud is very important; the mid-latitude cirrus layer at around -25°C in Fig. 5.18 is much more attenuating than the tropical anvil cirrus at -70°C because the saturation vapour pressure is so much higher at higher temperatures.

As well as monitoring ice clouds, a spaceborne radar is likely to also be employed for the detection of low-level clouds. The attenuation to the surface is considerable at 140 and 215 GHz in humid atmospheres and is unlikely to be fully offset by increased sensitivity due to the higher frequency. One of the three lower frequencies (35, 79 or 94 GHz) would probably be most suitable for the detection of low-level liquid water clouds, and it is doubtful that any useful additional information could be extracted from a second radar. The possibility of errors in the correction for attenuation is not a major concern because reflectivity is not well correlated with liquid water con-

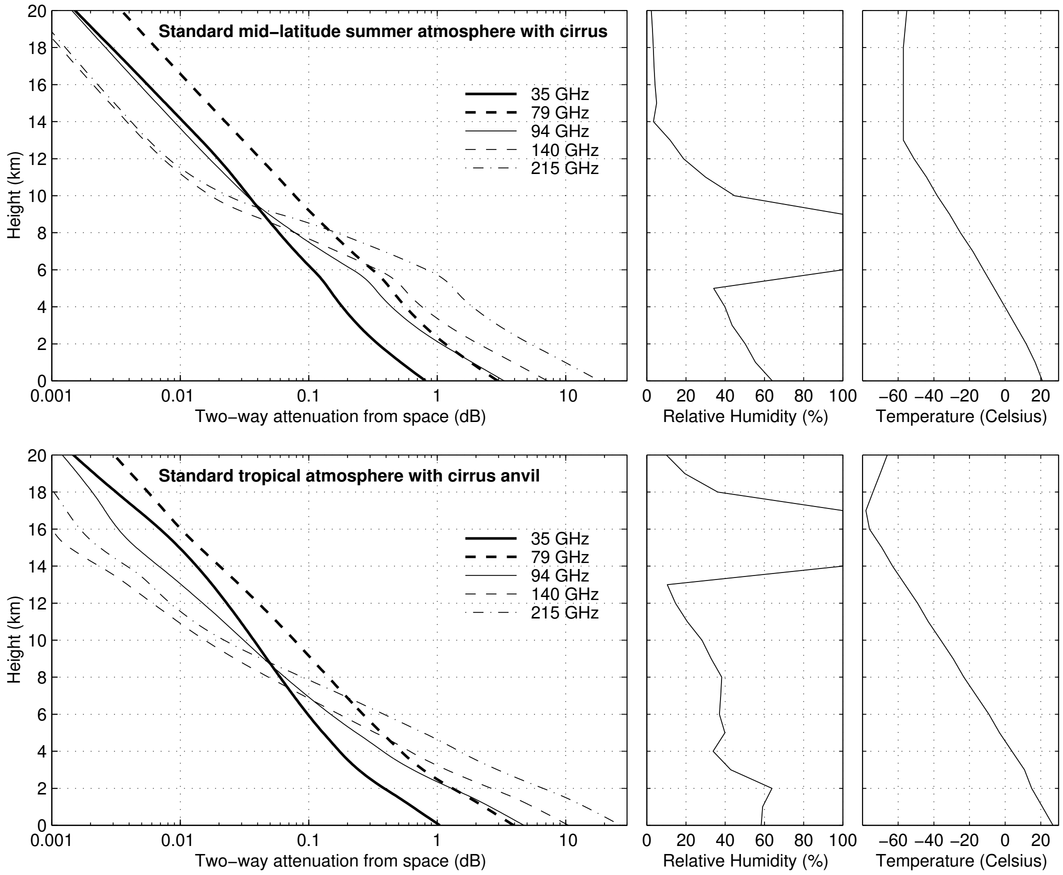

Figure 5.18: The two-way attenuation from space at the frequencies 35, 79, 94, 140 and 215 GHz for two standard atmospheres with cirrus layers added at appropriate altitudes. The temperature and relative humidity profiles are shown to the right.

tent or any property of low clouds that one might wish to measure (Fox and Illingworth 1997b).

5.4.2 Ice crystals

Attenuation by the ice crystals themselves is much smaller than that for liquid water with the same water content, but increases sharply with frequency. We have calculated the extinction of the radar beam at each frequency from Mie theory for the EUCREX and CEPEX data, and Fig. 5.19 shows scatterplots of the two-way extinction against reflectivity factor for the frequencies 79, 140 and 215 GHz. At 79 GHz it is small enough to be neglected. This is not necessarily the case at higher frequencies. At 140 GHz, 0.2% of the CEPEX and 0.07% of the EUCREX data have a two-way extinction of over 1 dB km^{-1}. The respective values are 2.1% and 0.2% at 215 GHz. One should bear in mind that these high values are likely to be at cloud base, and the magnitude of DWR due to Mie scattering is likely to be much larger than any introduced by differential attenuation in ice.

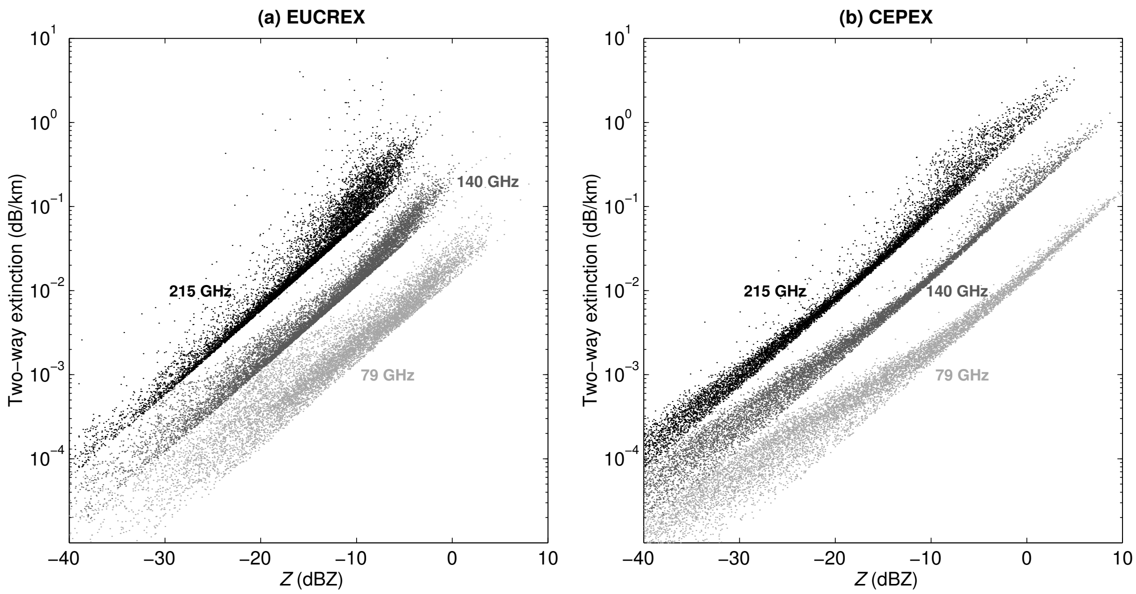

Figure 5.19: Scatterplots of two-way ice crystal attenuation versus reflectivity at 79, 140 and 215 GHz, for the EUCREX and CEPEX datasets.

5.5 The effect of antenna configuration

5.5.1 Errors in DWR due to beamwidth differences

To minimise instrumental bulk and ensure that the midpoints of the radar beams are very close it is probable that both frequencies of a spaceborne dual-wavelength system would use the same antenna. Previous work has considered a spaceborne cloud radar with an antenna diameter of around 2 m, which corresponds to a 1 km footprint from nadir at 94 GHz. The same antenna at 35, 79, 140 and 215 GHz would yield footprints of 2.69, 1.19, 0.67 and 0.44 km respectively. An important question is whether cloud inhomogeneities could cause random errors in DWR which would overwhelm those due to Mie scattering. Other alternatives exist however; the higher frequency radar could be defocussed, or constructed so that it under-illuminates the antenna. In this way the beams could be configured to match almost exactly, although at the cost of sensitivity at the higher frequency. From the radar equation we see that for a given transmit power the gain is proportional to the area of the antenna illuminated. Therefore if radars at the frequencies 79, 94, 140 and 215 GHz were to under-illuminate the antenna such that the resulting footprint matched that of a 35 GHz radar, then the losses in sensitivity would be 7.08, 8.60, 12.08 and 15.72 dB respectively. The same values would be applicable if the higher frequency radar was defocussed instead. These losses are large and so defocussing or under-illumination would only be considered if the alternative was unacceptably large errors in DWR.

It is necessary to estimate the magnitude of these errors using knowledge of the typical spatial structure of real cirrus clouds. This information has been obtained using vertically-pointing ground-based 35 and 94 GHz observations from the radar facility at Chilbolton, England taken between June and September 1996. Ten second averages of reflectivity factor were recorded with a vertical resolution of 75 m. Averaging was performed to reduce the vertical resolution to 525 m, close to the 500 m proposed for a spaceborne radar. A number of 1024-point time-series of reflectivity factor (in dBZ) in cirrus were selected, and the temporal scale converted to a spatial scale using a simple Taylor transformation and the mean wind speed over Chilbolton at that time and altitude as diagnosed by the UK Meteorological Office Unified Model. Only time-series in which all points registered cloud were considered. Information on the horizontal structure was then obtained by fitting power laws of the form

$$E = E_0\, k^{\mu} \tag{5.12}$$

to the Fourier spectra of these data, where k is wavenumber, E is power spectral density, and E_0 and μ are constants. The best fit lines were least squares fits in log-log space after 7-point averaging of the spectra to reduce scatter. The parameter μ was found to vary between -1.8 and -2.4 in cirrus, which compares with the range -1 to -2 found by Danne et al. (1996). A spectrum typical of those we analysed was obtained on 22 June 1996 and is shown in Fig. 5.20. It had the form $E = 2.03 \times 10^{-5} k^{-2.16}$ dBZ^2 m (where k is in m^{-1}), and we will use this from now on.

The next step was to determine the difference in reflectivity due to different footprints, by simulating two-dimensional cloud fields from the one-dimensional spectral information. This could have been done analytically but for the mathematical complication that useful spectra can only be calculated from reflectivity in logarithmic units, whereas averaging must be performed on reflectivity in linear units. Cloud fields were generated by calculating the inverse two-dimensional Fourier transform of synthetic matrices containing wave amplitudes consistent with the energy at the various scales indicated by the one-dimensional spectrum. The phase of each wave component of the matrix was random, so that each cloud field was different. The mathematical detail can be found in the Appendix. The domains were square and measured 15.36 km on a side with a resolution of 120 m. Fourier analysis of cross-sections through the domain confirmed that they had almost identical spectral properties to the original data. An example is shown in Fig. 5.21. Note that these cloud fields are spectrally isotropic, whereas real cirrus clouds with fallstreaks are not because the fallstreaks tend to be aligned parallel to the vertical wind-shear vector. On average this is not expected to significantly bias the results.

Following Illingworth et al. (1997), we shall consider a 1 second averaging time for the radar

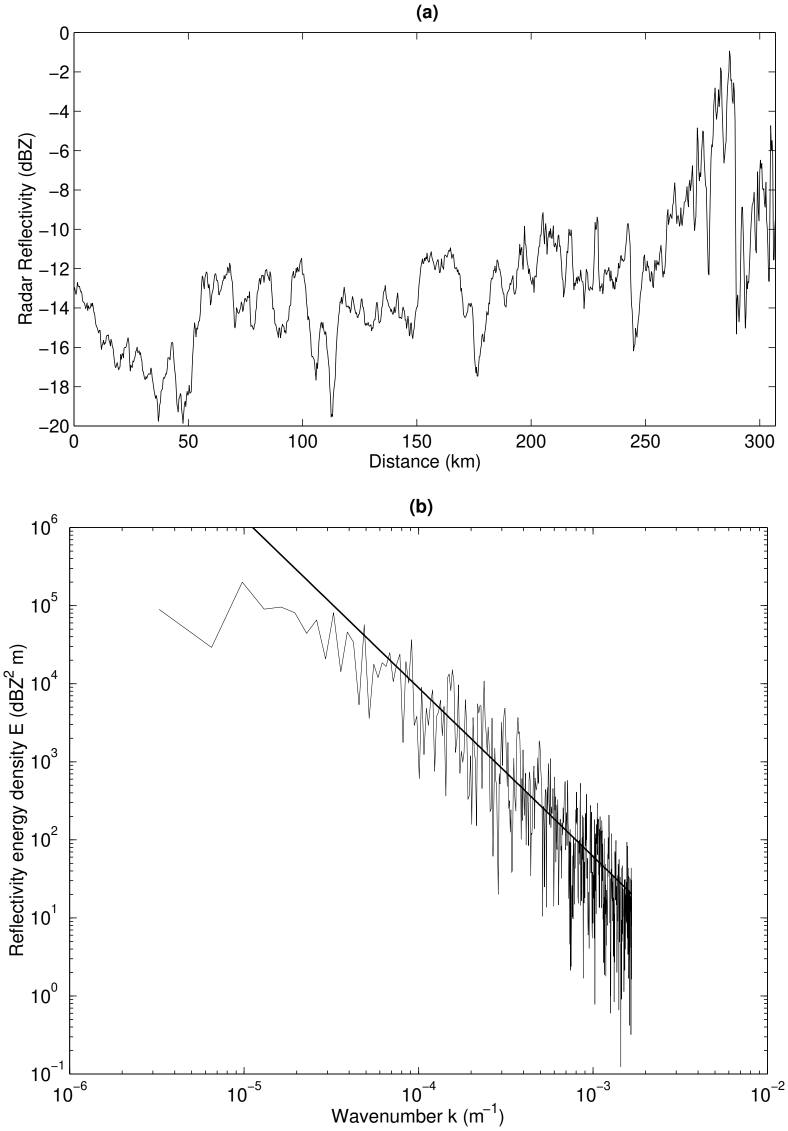

Figure 5.20: **(a)** 35 GHz reflectivity factor at an altitude of 7 km, measured from Chilbolton on 22 June 1996. The abscissa has been converted from time to space using a mean wind at this altitude of 30 m s^{-1}. **(b)** The corresponding power spectrum. The best fit line is $E = 2.03 \times 10^{-5} k^{-2.16}$.

to achieve sufficient sensitivity, which results in a pixel length of 7 km. The beam patterns are assumed to be Gaussian. The standard deviation of DWR due only to differing beamwidths has been calculated for each frequency combination from 64 simulated cloud fields; these are listed in Table 5.3. Clearly the error is reduced for the shorter wavelength pairings because cloud reflectivity fluctuates less at smaller scales. These values need to be put into perspective by comparing with the typical magnitudes of DWR which occur in cirrus, as shown in Fig. 5.2. For the three frequency combinations which do not include 35 GHz, the error in DWR is less than 0.1 dB which is less than the minimum error in DWR due to averaging over only 2830 pulses (0.12 dB). For combinations which include 35 GHz, it is over 0.2 dB and so could reduce the accuracy of size measurements at

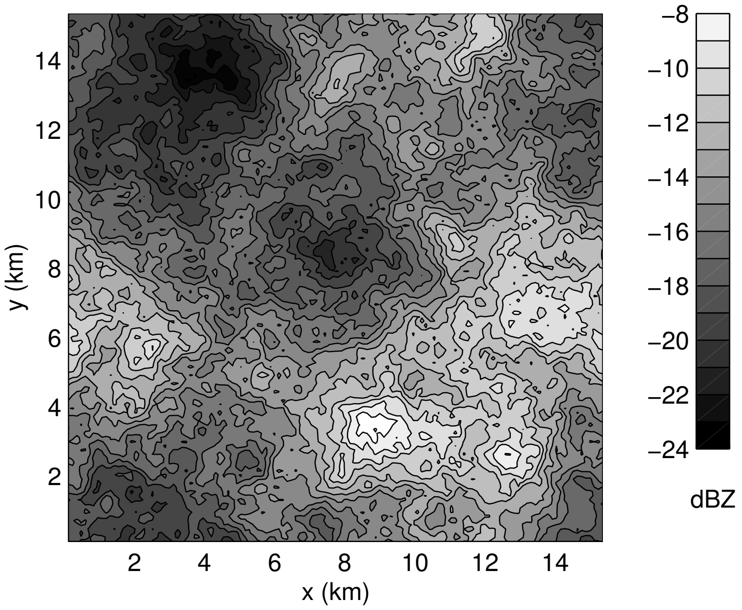

Figure 5.21: Example of a simulated two-dimensional cloud field.

Dual-wavelength frequencies	Error in DWR (dB)
35/94	0.21
35/140	0.25
35/215	0.27
79/140	0.067
79/215	0.097
140/215	0.031

Table 5.3: The error in DWR due to different beamwidths.

small sizes. In any case these errors are not really large enough to consider defocussing or under-illumination as a worthwhile option for the higher frequency radar. This is in contrast to the use of dual-wavelength radar for hail detection (first proposed by Atlas and Ludlam 1961); it was found by Rinehart and Tuttle (1982) that reflectivity gradients of the order of 20 dB km^{-1} at the edge of convective storms could produce anomalous values of DWR due to differences in the side-lobe level, even if the main lobes were well matched. However, gradients of this magnitude are never observed in cirrus.

A further problem with using the same parabolic antenna for two frequencies is that both sources cannot be placed precisely on the focal line, so the beam pattern is somewhat degraded and there is an increase in the level of the first few sidelobes (Meneghini and Kozu 1990).

5.5.2 Errors in DWR caused by non-coincident footprints

It has been suggested that financial constraints may exclude the possibility of a payload of two active instruments on a cloud profiling satellite, and that work should be carried out to determine whether or not dividing the instruments between two satellites in very close orbits would severely reduce the accuracy of size retrievals (Raschke et al. 1997). It has been shown that a second satellite could at best trail the first by 5 minutes, with the footprints drifting towards and away from each other by as much as 5 km. The effect of this has been simulated using cloud fields with a resolution of 500 m and measuring 64 $\times$ 64 km. The swaths of two spaceborne radars, each with a footprint of 1 km and a 7 km pixel length, were offset by up to 10 km in the directions both parallel and perpendicular to the satellite motion. Figure 5.22 shows the error in DWR as a function of separation distance in both directions. A 5 km offset of the footprints perpendicular to the direction of motion of the satellite results in an error in DWR of between 2 and 2.5 dB. For a wind speed of 30 m s^{-1}, 5 minutes corresponds to 9 km, so the reflectivity measured by two satellites in the same orbit but 5 minutes apart could differ by as much as 3.5 dB. It has been assumed that advection is much more important than cloud evolution over these timescales, but cloud development could in theory introduce even more error.

We conclude that for dual-wavelength radar at least, there little point in even attempting to derive size with errors of this magnitude, and the same is probably true of radar/lidar synergy (Liu and Illingworth 1997). It would in fact be better for two separate satellite-borne radars to be in completely different orbits to obtain a better global coverage.

5.6 Other considerations

5.6.1 Crystal habit

So far we have considered only a nadir pointing radar viewing spherical ice crystals. A problem arises however because non-spherical crystals tend to fall with their longest axis aligned horizontally (although the azimuthal orientation is random), and the magnitude of DWR in fact depends on the dimension of the crystals in the direction parallel to the direction of propagation of the incident radiation. In consequence the median *equivolumetric* diameter D_0, which we need to measure, is underestimated by nadir or zenith pointing dual-wavelength radars if the reflectivity of the cloud is dominated by the contribution from non-spherical crystals.

A straightforward solution is to view at an angle of 45° from nadir, which results in DWR

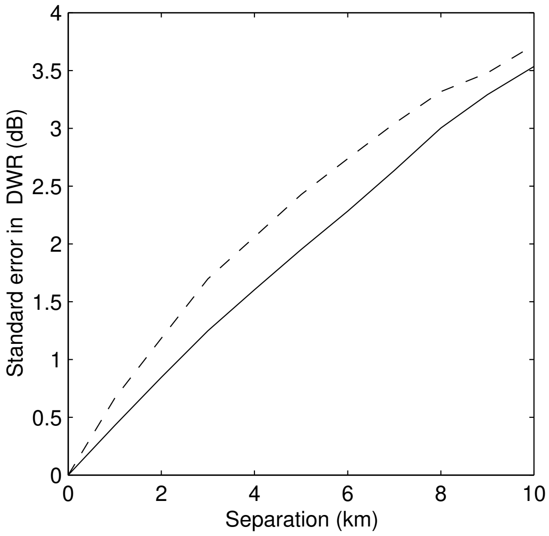

Figure 5.22: The standard error in DWR as a function of swath separation for radars mounted separately on two satellites. The solid line is for swaths separated in the direction parallel to the direction of motion of the satellites (satellites in the same orbit but one lagging the other), and the dashed line is for swaths separated in the direction perpendicular to the direction of motion (satellites in adjacent orbits).

being much more closely related to equivolumetric diameter, and the spherical approximation can be used much more confidently. Figure 5.23 shows DWR versus D_0 for horizontally-aligned oblate crystals with various aspect ratios, as viewed by each of the six wavelength-combinations both from nadir and at 45° from nadir. These were calculated using the T-matrix method (Waterman 1969)[3] for an exponential size distribution. It would appear that if the crystals which dominate the reflectivity are significantly aspherical then viewing from nadir could result in a serious underestimate of crystal size; to a first approximation when the aspect ratio is 0.5, say, then for a given D_0 the dual-wavelength ratio will be 0.5 of its value for a sphere. This problem is found to be almost eliminated by viewing at 45°, and calculations for prolate crystals produce similar results. The presence of canting crystals should not really be a problem since on average the dimension of the crystal measured by the radars should still be close to D_0. The obvious drawback of the alternative viewing angle is that attenuation is increased by a factor of $\sqrt{2}$, and the greater distance from the satellite to the cloud would further reduce the sensitivity by 3 dB.

5.6.2 Calibration

Any gains in the accuracy of IWC by the use of two radars are lost if the absolute calibration of the radars cannot be determined better than the intrinsic accuracy of the technique itself. The minimum

[3]T-matrix code written and provided by S. Vivekanandan.

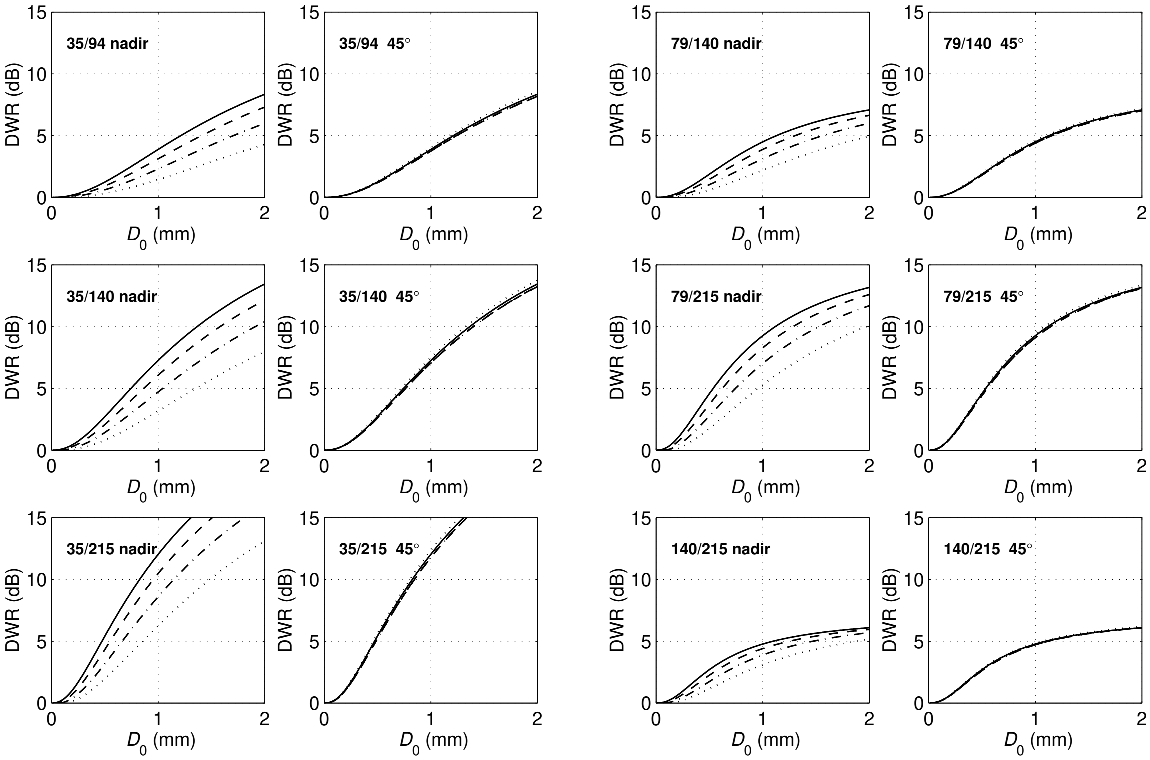

Figure 5.23: Dual-wavelength ratio DWR as a function of median volume diameter D_0 for six frequency combinations. The crystals are horizontally aligned and oblate, with four different aspect ratios: 1 (solid line), 0.8 (dashed line), 0.6 (dot-dashed line) and 0.4 (dotted line). The results for both nadir and 45° from nadir are shown, and the size distributions are exponential.

error in IWC is around 15% with the dual-wavelength method (see Figs. 5.12 and 5.15), so the radars need be calibrated to within 0.5 dB. In theory the return from the ocean could provide a useful high-reflectivity means of regular calibration. However the backscatter from the sea depends on the amplitude of surface waves with a wavelength of the order of the wavelength of the radar, and errors in determining this may exceed 0.5 dB. Water vapour attenuation at the higher frequencies may also be difficult to account for exactly. Calibration campaigns with aircraft and ground based radars would almost certainly prove necessary.

The relative calibration of the radars is less of a problem; Hogan et al. (1998) were able to match the reflectivities measured by the two radars in the Rayleigh-scattering cloud top. Unfortunately this is generally the region of the cloud with lowest reflectivity, so the radars must be sufficiently sensitive that the precision of Z here is still high. This is especially true when one of the radars is at 215 GHz, since for the reflectivities to be matched to within 0.1 dB, D_0 must be less than around 70 µm, compared with 150 µm for the 35/94 combination.

5.7 Conclusions

We have explored the feasibility of spaceborne single and dual-wavelength radar, at a range of frequencies, for the global measurement of ice water content, visible extinction coefficient and crystal size in cirrus.

Firstly the accuracy of single wavelength estimates of IWC and β_{vis} were calculated from EUCREX and CEPEX data for the wavelengths 35, 79, 94, 140 and 215 GHz. Results for 94 GHz were in agreement with those of Brown et al. (1995), but because of increased Mie scattering at higher frequencies, at 140 GHz the errors were reduced by up to 5% compared with 94 GHz, and at 215 GHz by between 10 and 20%. Two-way gaseous attenuation is shown to be unlikely to significantly bias the results, since even at 215 GHz it would typically reach only 2 dB at the melting level for a nadir-viewing radar, which could be corrected for with reasonable accuracy. Attenuation by ice crystals was found to exceed 1 dB km^{-1} at 215 GHz in 2.1% of the CEPEX and 0.8% of the EUCREX data, which is less easy to correct for but does not represent a significant bias given the inherent errors in the Z–IWC and Z–β_{vis} relationships. We conclude that if only cirrus clouds are of interest then a 215 GHz radar would be the preferred choice, but if the detection of low level clouds was also a requirement then to minimise attenuation, 79 or 94 GHz should be used.

The next step was to consider a spaceborne dual-wavelength radar that could measure DWR exactly. In this case the errors in IWC and β_{vis} were mostly in the range 25–35% and varied little depending on which frequency combination was used. These errors are due to variations in the shape of the distribution and represent the greatest achievable accuracy of the dual-wavelength technique. For $D_0 > 250\,\mu$m, the error in D_0 ranged between 15 and 25% when the higher frequency of the two radars was 215 GHz, and between 20 and 40% otherwise. Diameter measurements at smaller sizes were less accurate, especially in the EUCREX data.

We then considered the accuracy achievable by radars with minimum sensitivities of -30 and -40 dBZ, and a dwell time of 1 second. At reflectivities over 20 dB more than the minimum reflectivity, errors in IWC and D_0 were nearly always less than 30% when the highest frequency was 215 GHz, and less than 40% when the highest frequency was 140 GHz. In the lowest 15–20 dB of sensitivity, random errors in DWR were large enough and average crystal size small enough that dual-wavelength measurements were little better than those from a single wavelength radar. Frequency combinations which included 215 GHz were able to measure size in a much greater fraction of clouds at low signal-to-noise ratio.

The weakness of this technique is clearly in low reflectivity clouds containing only small crystals, where a lidar and radar or multiple wavelength lidar would probably be more accurate. In thicker more radiatively significant cloud the dual-wavelength radar method is relatively accurate, while lidar would begin to experience appreciable attenuation and multiple scattering.

The possibility of errors in DWR from a number of other sources was considered. These should be compared with the intrinsic minimum error of 0.12 dB due to a dwell time of 1 second, and the magnitudes of DWR that we wish to measure, indicated in Fig. 5.2. The error due to beam-width differences was found to be typically between 0.2 and 0.3 dB for frequency combinations which included 35 GHz, and between 0.03 and 0.1 dB otherwise. Mounting the two radars on different satellites was found to introduce an error of at least several decibels, which is far too great for such a scenario to ever be considered seriously. Dual-wavelength ratio measured by nadir pointing radars would be sensitive to the aspect of horizontally-aligned crystals, but evidence has been presented from scattering calculations to suggest that viewing at an angle of 45° from nadir should virtually eliminate the problem. However it is not yet clear whether the natural variation in aspect ratio is sufficient to warrant the loss of 3 dB of sensitivity that would result from viewing at 45° from nadir.

All things considered, it appears that the best wavelength combination for observing cirrus clouds is 79 and 215 GHz.

CHAPTER SIX

Measuring crystal size in cirrus using 35 and 94 GHz radars

6.1 Introduction

It was shown in the previous chapter that dual-wavelength radar has the potential to measure crystal size in cirrus from a spaceborne platform, and therefore be a valuable tool to obtain a global climatology of ice water content. There is a clear need for this concept to be tested from the ground. Unfortunately the most promising frequency combination for a spaceborne system, 79 and 215 GHz, is not possible from the surface because attenuation by water vapour in the boundary-layer is very strong at 215 GHz, so we shall use 35 and 94 GHz radars. There are a number of advantages that ground-based radar observations have over those from satellite which in theory should largely counteract the fact that lower frequencies must be used:

1. Higher sensitivity: a ground-based radar viewing cirrus at an altitude of 10 km is around 34 dB more sensitive than the same instrument viewing at nadir from an altitude of 500 km;

2. Higher vertical resolution: a ground based cloud radar typically has a resolution of 75 m, whereas that proposed for a spaceborne system is 500 m;

3. Much longer dwell times: for a swath length of 7 km, a spaceborne radar dwells for only 1 second, while a vertically pointing ground-based instrument can dwell for several minutes to get the same resolution, given the typical wind-speeds that occur at cirrus altitudes.

In this chapter results are presented from a case study in which thick cirrus was observed by the vertically-pointing 35 and 94 GHz radars at Chilbolton, England. Microphysical parameters are derived and compared with those diagnosed by the Mesoscale Version of the UK Meteorological Office (UKMO) Unified Model[1]. In addition we investigate the evolution of the microphysical properties of cloud parcels by tracing the variation of ice water content (IWC) and median volume diameter (D_0) along individual fallstreaks.

The use of two ground-based radars at different wavelengths to estimate hydrometeor size was first proposed by Atlas and Ludlam (1961) as a means of hail detection using, for instance, a Rayleigh-scattering S-band radar (3 GHz) and an X-band radar (10 GHz) which Mie-scatters only in the presence of large hail. Such schemes have always had to contend with differences in reflectivity due to attenuation by rain at the shorter wavelength (Tuttle and Rinehart 1983), and it was found that even with well matched beams of very similar beamwidth, differences in the side-lobe level were able to cause large reflectivity differences in the vicinity of strongly reflective cores where a significant fraction of the signal is returned from the side-lobes (Rinehart and Tuttle 1982). However, it was the ambiguity caused by the very different scattering properties of wet and dry hail which made this technique unworkable.

Dual-wavelength observations in cirrus suffer none of these problems; attenuation by ice is generally small enough to be neglected, attenuation by atmospheric gases is a minor correction, and reflectivity gradients comparable in magnitude to those at the edge of the cores of convective storms are never observed in cirrus. In mixed-phase clouds the technique could produce erroneous results, since although super-cooled water droplets would probably make a negligible contribution to the reflectivity, they could cause appreciable attenuation (Gosset and Sauvageot 1992). The cirrus observed in this case study had a temperature ranging between -50 and -20°C, so was almost certainly entirely in the ice-phase.

The same concept was used successfully by Illingworth et al. (1995) to measure the size of snowflakes using 3 and 35 GHz radars, but the use of dual-wavelength radar for sizing in cirrus was first proposed by Matrosov (1993). He carried out scattering calculations for a first-order gamma distribution of solid ice spheroids with a variety of different wavelength combinations and aspect ratios, and in each case dual-wavelength ratio (DWR) was calculated as a function of D_0, the median diameter of the volume-weighted size distribution. In fact he concluded that 94 GHz was too low a frequency to be used as the non-Rayleigh scattering component of a dual-wavelength system, because in the range of D_0 he considered (up to 0.6 mm), at most DWR attained a value of

[1]Model data provided by Peter Panagi and Ed Dicks.

only 3 dB. However, in this chapter observations shall be presented of DWR up to 7.5 dB, which we interpret as $D_0 \sim 0.6$ mm. The reason for the difference is that (as in the previous chapter) we use real size spectra measured by aircraft to derive empirical relationships between DWR and the required meteorological parameters, and it turns out that for the calculation of radar reflectivity and particularly DWR, cirrus size distributions are not well represented by gamma distributions because they tend to under-represent the number of millimetre-sized crystals. The sensitivity of derived quantities to assumed density and to crystal alignment is also investigated.

The work in this chapter has been written up as a paper (Hogan et al. 1998), and is also the subject of two conference papers (Hogan et al. 1997a,b).

6.2 Interpretation of dual-wavelength data

Relationships need to be established between DWR and some measure of crystal size, such as median volume diameter (D_0) or effective radius (r_e). For the intensive variables ice water content (IWC) and visible extinction coefficient (β_{vis}) we require relationships between DWR and the ratios $R_f = Z_f/\mathrm{IWC}$ and $S_f = Z_f/\beta_{vis}$, where f denotes frequency. Then in real data the procedure is simply to use a look-up table to estimate R_{35} from DWR, and then to calculate IWC using $\mathrm{IWC} = Z_{35}/R_{35}$. The same method is used for β_{vis}.

Firstly in this section we use idealised size spectra to examine the sensitivity of derived quantities to the various assumptions that it is necessary to make. Then real size spectra from the European Cloud Radiation Experiment (EUCREX) are used to derive empirical relationships which will be used in Section 6.3 to interpret real observations.

6.2.1 Sensitivity studies

In Chapter 5 it was assumed that for scattering purposes, crystals can be approximated as homogeneous spheres with a density which is a simple function of diameter. There is a need to test the sensitivity of retrievals to density, the shape of the size distribution and the presence of non-spherical crystals.

In the first instance we shall assume that the size spectra of ice crystals can be well approximated by the gamma distribution (Kosarev and Mazin 1989):

$$n(D) = N_0 D^{\mu} \exp\left(-[3.67 + \mu] D/D_0\right), \tag{6.1}$$

where μ is the shape parameter, and D is the equivolumetric diameter. In this case R_f is given by

$$R_f(D_0) = \frac{Z_f}{\mathrm{IWC}} = \frac{\displaystyle\int_0^{D_{\max}} \frac{|K(\rho)|^2}{0.93} D^{6+\mu} \exp(-[3.67+\mu]D/D_0)\gamma_f(D)\,dD}{\displaystyle\frac{\pi}{6}\int_0^{D_{\max}} \rho D^{3+\mu} \exp(-[3.67+\mu]D/D_0)\,dD} \tag{6.2}$$

where $\gamma_f(D)$ is the Mie/Rayleigh backscatter ratio. Note that (6.1) is not normalised, but that the number concentration parameter N_0 has been cancelled from (6.2). The dielectric parameter $|K|^2$ is calculated as a function of density using the expressions of Maxwell-Garnet (1904) and Liebe et al. (1989), and is almost identical at 35 and 94 GHz. It should also be noted that both $|K|^2$ and $\gamma_f(D)$ are virtually independent of temperature. The value 0.93 is present in (6.2) to make reflectivity factor relative to liquid water at centimetre wavelengths.

We shall also initially assume the Brown and Francis (1995) density function

$$\rho = 0.07 D^{-1.1}\ \ \mathrm{g\,cm^{-3}}, \tag{6.3}$$

(where D is in millimetres), although the findings of Chapter 4 regarding density will also be considered.

Scattering calculations have been carried out using the T-matrix method[2] which is applicable for homogeneous spheres and spheroids (Waterman 1969). Calculations using more advanced methods to compare realistic shapes, such as hexagonal columns and plates (Schneider and Stephens 1995) and dendritic snowflakes (O'Brien and Goedecke 1988), with equivalent spheroids show that the errors associated with the spheroidal approximation are in general less than 15% (0.6 dB), provided maximum dimension, aspect ratio and total ice mass are maintained.

The ice crystal distributions given by (6.1) have been discretised into 500 sizes ranging from 10 µm to $D_{\max} = 5$ mm in 10 µm intervals. In the following sensitivity studies, D_0 and R_{35} are plotted as functions of DWR for various values of μ, ρ and aspect ratio.

Sensitivity to distribution shape

To test the sensitivity of retrieved parameters to the shape of the distribution, four values for the shape parameter μ (-1, 0, 2 and 8) were considered. The plots in Fig. 6.1 show that if a gamma distribution is appropriate, then derived quantities should be fairly insensitive to the typical range

[2] T-matrix code written and provided by S. Vivekanandan.

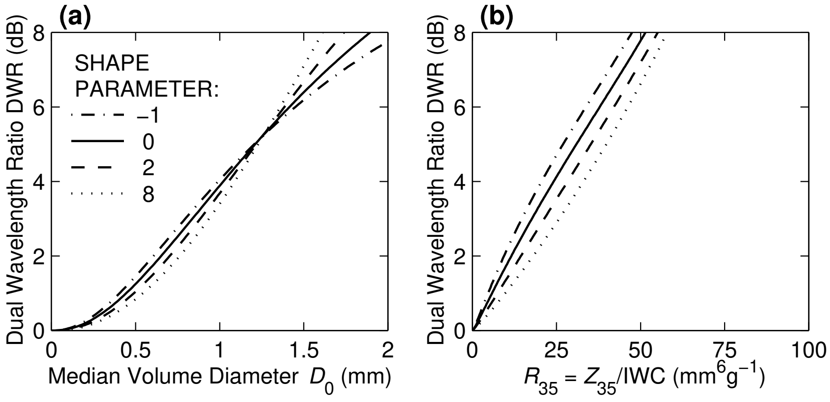

Figure 6.1: DWR as a function of D_0 and R_{35} for four values of shape parameter μ.

of μ that one would expect, varying by perhaps 10%. This finding is somewhat meaningless if there exist a large number of very large or very small crystals that are not represented well by a gamma distribution. For instance, it has been suggested (e.g. Arnott et al. 1994) that high concentrations of crystals smaller than 50 µm are ubiquitous in cirrus, but are not represented in monomodal size distributions, or detected by the standard airborne imaging probes which typically have a minimum detectable size of around 25 µm. If present these crystals could dominate the radiative properties of cirrus clouds while being effectively undetected by radar, therefore invalidating the use of radars to infer radiative properties. However some recent studies have measured down to 5–10 µm using replicators (Mitchell et al. 1996), balloonborne videosondes (Kinne et al. 1997), and a video ice particle sampler (McFarquhar and Heymsfield 1997), and all suggest that small crystals make a minor contribution to IWC and optical depth, implying that (6.1) is valid at least for small to medium sized crystals, and also that airborne imaging probes can be used to determine cloud radiative properties. Similarly Heymsfield et al. (1998) showed that an excess of small crystals in the tops of thick tropical cirrus clouds was not necessary to explain the high albedos of these clouds, as has been suggested. Large crystals really only have the potential to be a problem for radar, but have not really been considered before. In Section 6.2.2 we determine their importance using aircraft-measured size spectra spanning diameters from 25 to 6400 µm.

Sensitivity to crystal habit

Until now we have assumed that crystals can be approximated as spheres, but in reality they occur in a multitude of different shapes and tend to fall with their longest axis parallel to the ground (see Liou 1986 and references therein). This could prove to be a problem for vertically-pointing dual-wavelength radar, because the extent of the deviation of Z_{94} from the Rayleigh approximation is

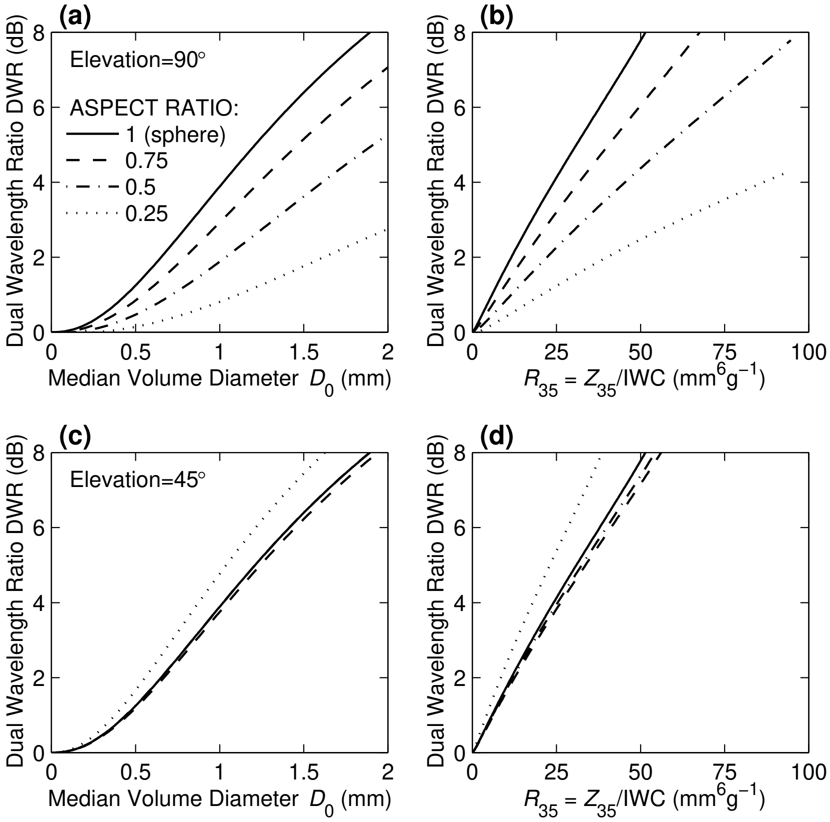

Figure 6.2: DWR as a function of D_0 and R_{35} at vertical incidence (top row) and at an elevation of 45° (bottom row), for oblate crystals of four different aspect ratios. The radiation is vertically polarised at both wavelengths.

not so much a function of D_0, as of the dimension of the crystals in the direction parallel to the direction of propagation of the incident radiation. At vertical incidence this dimension is in fact the shortest axis of the crystal, so the effect of assuming that non-spherical crystals are spherical is to underestimate D_0. This is illustrated in the top row of Fig. 6.2, where it can be seen that oblate crystals with aspect ratios of 1, 0.75, 0.5 and 0.25 produce a large range of D_0 and R_{35}; for example the presence of crystals with an axial ratio of 0.5 results in D_0 being underestimated by a factor of two and IWC overestimated by a similar amount. Calculations for prolate crystals (not shown) produce similar results.

The problem was also highlighted in Section 5.6.1 where it was shown that a straightforward solution is to dwell at an elevation of 45°, so that the dimension on which DWR depends is much closer to the equivalent spherical diameter, and for any wavelength combination in this retrieval scenario the error in retrieved size or IWC is less than 5% down to a crystal aspect ratio of 0.4. It can be seen in the bottom row of Fig. 6.2 that for lower aspect ratios the errors begin to increase, and for an aspect ratio of 0.25, the error reaches around 25%. However in Fig. 4.15 we see that very few crystals have an aspect ratio of less than 0.4 (or greater than 2.5), especially at the sizes

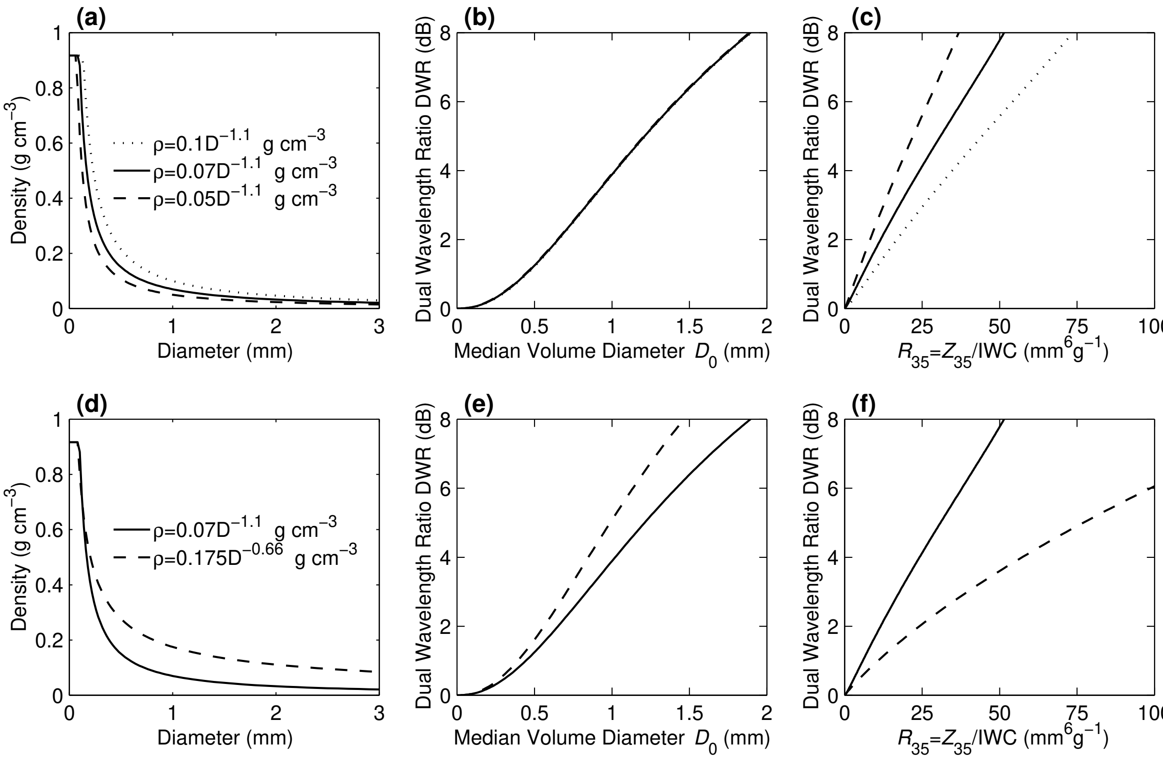

Figure 6.3: The sensitivity of dual-wavelength retrieved quantities to density. The density functions described in the text are plotted in (a) and (d), with DWR as a function of D_0 and R_{35} to their right.

the radar is sensitive to. These findings are very encouraging, and should also be applicable to canting crystals which are on average horizontally aligned, and to randomly oriented crystals. It is important however that DWR is calculated using the same polarisation at both frequencies. In this study the radars were vertically-pointing, but in future the strategy of dwelling at an elevation of 45° will be adopted.

Sensitivity to density

So far we have used the density function given by (6.3), which was found by Brown and Francis (1995) to give the best agreement between IWC calculated from 2D probe size spectra and that measured by the Total Water Probe aboard the UKMO C-130 aircraft. However, Fig. 4 of Brown and Francis (1995) indicated that while a simple density function provided an unbiased estimate of IWC, the 2D cloud probe and the TWP differed with a root-mean-squared difference of around 40%. Much of this disagreement may be attributable to instrumental error, but the possibility exists that the density of crystals varies naturally from cloud to cloud by this amount.

The effect of a 40% error in density is explored by considering the density functions

$\rho = 0.05D^{-1.1}$ and $\rho = 0.1D^{-1.1}$ $\mathrm{g\,cm^{-3}}$, in addition to that given by (6.3). The top row of Fig. 6.3 shows the variation of D_0 and R_{35} with DWR for these three densities, assuming an exponential size distribution ($\mu = 0$). Because DWR is independent of density for a single crystal, under- or over-estimating the density of all crystals in the distribution by the same factor has *no effect* on the size derived from DWR. There is a direct effect on the derived IWC however (indicated by the value of R_{35}). Reflectivity factor is approximately proportional to ρ^2, so for a given measured Z and DWR, the inferred IWC is approximately inversely proportional to ρ. Note that single wavelength estimates of IWC are susceptible to random variations in density from cloud to cloud in exactly the same way, and the errors quoted by Brown et al. (1995) for the accuracy of such measurements took no account of this.

It was seen in Chapter 4 that a newer expression derived from the findings of Francis et al. (1998) is likely to be closer to the truth than (6.3):

$$\rho = 0.175D^{-0.66}\ \mathrm{g\,cm^{-3}}. \tag{6.4}$$

The bottom row of Fig. 6.3 shows the effect of density functions (6.3) and (6.4) on size and IWC retrievals, and it can be seen that derived IWC differs by more than a factor of two when DWR is greater than around 1 dB. This illustrates the vital importance to this technique that the issue of density is resolved. The evidence presented in Chapter 4 supported the use of (6.4) because it applies to a measure of diameter which is closer to the equivolumetric diameter, so we shall use it for the analysis of real radar data in this chapter.

It should be noted that the largest crystals which the radar is sensitive to may well be growing by aggregation, in which case their density would not be expected to decrease with increasing size. The relationships of Brown and Francis (1995) and Francis et al. (1998) were derived to get the most accurate estimate of IWC, so it is quite conceivable that they do not represent the density of millimetre-sized crystals very well.

6.2.2 Empirical relationships from the EUCREX dataset

As in the previous chapter, we use aircraft data to determine the best relationship between DWR and the required meteorological parameters. The EUCREX data has been used, which is applicable to mid-latitude cirrus, but this time, following the recommendations in Chapter 4, the crystal size spectra have been binned by area and accordingly the new density function given by (6.4) is used. Figure 6.4 shows scatterplots of DWR versus median volume diameter, effective radius, R_{35} (the

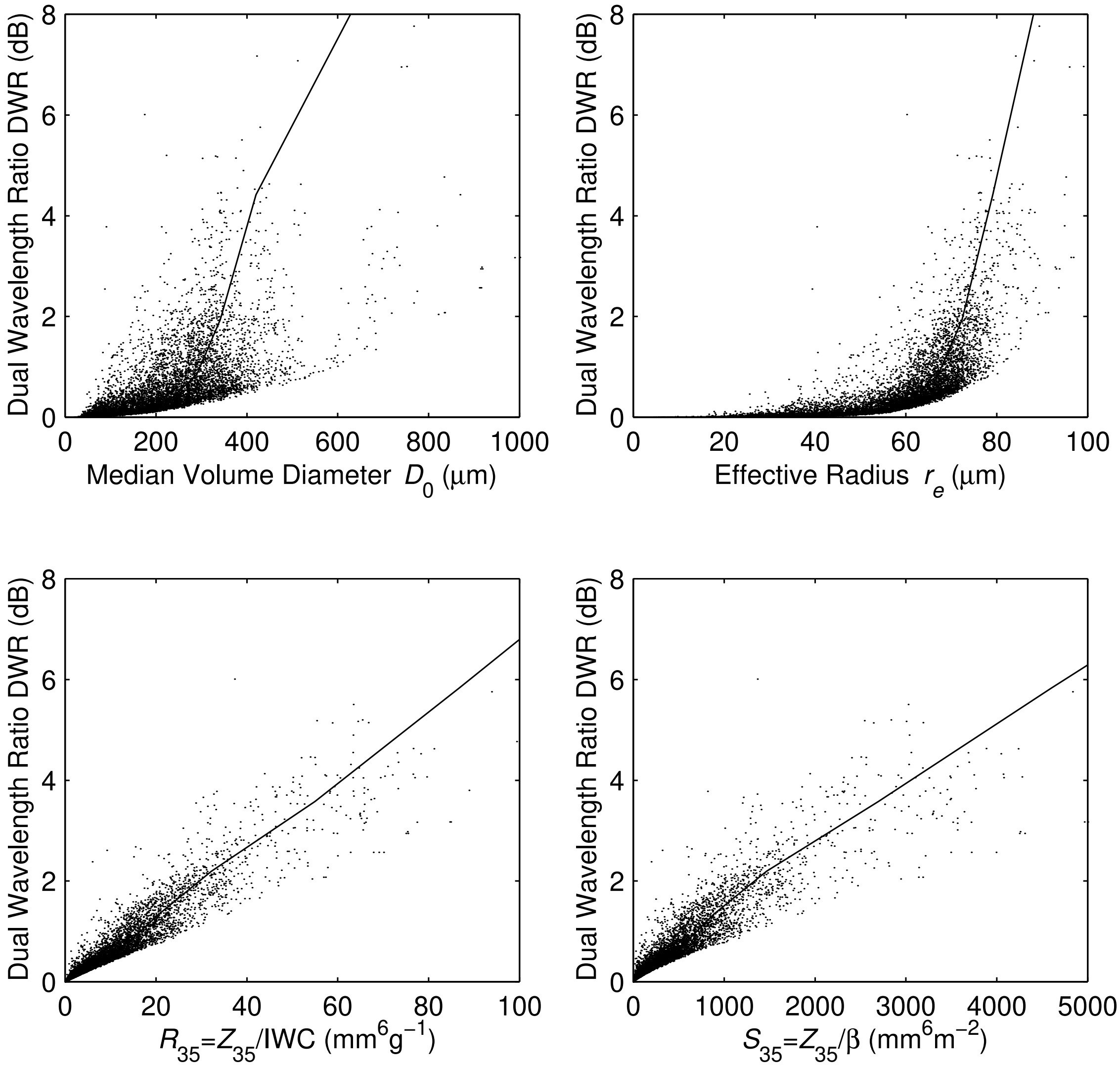

Figure 6.4: Scatterplots of 35 and 94 GHz dual-wavelength ratio as a function of D_0, r_e, R_{35} and S_{35}, from over 10 000 points in the EUCREX dataset. The data were binned by area, and the density given by (6.4) was used. Overlayed are best fit lines which will be used for the interpretation of the observations in Section 6.3.

ratio of 35 GHz reflectivity to ice water content) and S_{35} (the ratio of 35 GHz reflectivity to visible extinction coefficient). Best fit lines have been derived in the same way as described in Chapter 5, and are shown as solid lines superimposed on Fig. 6.4. It can be seen that D_0 is not particularly well correlated with DWR, although one should remember that D_0 is not in itself an important parameter for radiation, it merely gives an indication of the size of particles present.

It is very important to note that D_0 derived from DWR using this empirical relationship is very different from that assuming an exponential or gamma distribution (indicated in plot (e) of Fig. 6.3); for instance a measured DWR of 6 dB would be interpreted as a D_0 of 1.4 mm if an exponential distribution was assumed, while the real spectra indicate a value closer to 0.5 mm. The reason

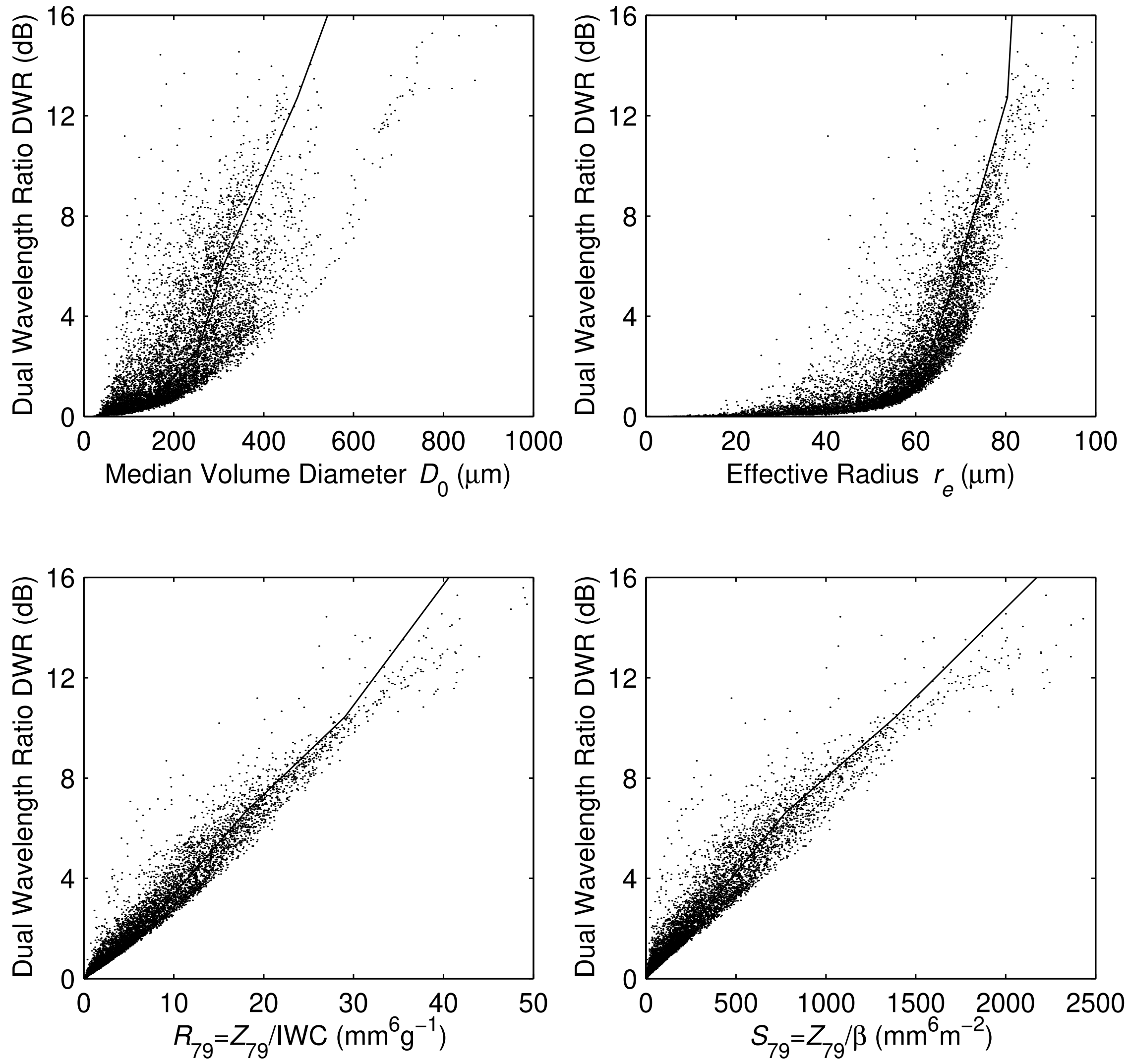

Figure 6.5: As for Fig. 6.4, but for a dual-wavelength radar at 79 and 215 GHz.

for the difference is that real clouds contain significantly more larger crystals than indicated by a simple gamma distribution (an indication that aggregation is occurring), which when weighted by the sixth power of diameter contribute much to Z (and therefore DWR) but little to D_0. This finding is applicable to many cirrus retrievals techniques which use radar, and explains why Matrosov (1993) found that DWR did not exceed 3 dB for realistic values of D_0. As a general rule it would be advisable for new techniques to be tested using aircraft data, which *must* contain the contributions from precipitation-sized particles; the EUCREX data consisted of a composite of 2D cloud and 2D precipitation probe size spectra, but when DWR was calculated from the 2D cloud probe spectra alone (i.e. crystals smaller than 800 μm in diameter), it was found to always be less than 2 dB. The maximum DWR with the full spectra was 8.6 dB.

The correlations between DWR and both R_{35} and S_{35} are better than for size, indicating that it should be possible to derive the important parameters of IWC and β_{vis} fairly accurately (see Figs. 5.9 and 5.11 in the previous chapter). It is interesting to note that the best fit line between DWR and R_{35} in Fig. 6.4 is very similar to that for an exponential distribution indicated by the dashed line in plot (f) of Fig. 6.3, which implies that for deriving IWC and β_{vis} (although not D_0), idealised distributions *are* applicable.

For comparison, Fig. 6.5 shows the same as Fig. 6.4 but for the frequency combination 79 and 215 GHz, which was recommended in Chapter 5 as the most suitable for a spaceborne dual-wavelength radar. It can be seen that the main advantage is that DWR is around three times larger, but in addition the correlations with r_e, R_{35} and S_{35} are better. This is probably because the very large crystals are Mie scattering at *both* wavelengths, and thus their relative importance for reflectivity is reduced.

6.2.3 Calibration

Naturally any gains in the accuracy of IWC derived from dual- rather than single-wavelength radar are lost if the radars are not accurately calibrated, both relative to each other and in an absolute sense. The approach used here has been to calibrate the 35 GHz radar by comparison with the 3 GHz radar at Chilbolton in light, Rayleigh-scattering rain. This radar in turn has been calibrated in moderate rain to better than 0.5 dB from the consistency of differential reflectivity and differential phase measurements (Goddard et al. 1994b). The 94 GHz radar is then calibrated on a case study basis by matching with the reflectivity at 35 GHz in the Rayleigh-scattering cirrus cloud tops. The small correction for attenuation by atmospheric gases is made using the line-by-line model for millimetre-wave propagation of Liebe (1985) coupled with the thermodynamic variables diagnosed by the UKMO Unified Model. Attenuation by the ice crystals themselves is negligible at these frequencies (see Section 5.4.2).

6.3 22 June 1996 Case Study

On 22 June 1996, vertically-pointing 35 and 94 GHz radar reflectivity measurements were taken at Chilbolton through a thick cirrus cloud. The cloud was associated with a strong jet stream which peaked at 40 m s^{-1} at 9 km over the site. Gaseous attenuation was corrected for using the methodology outlined in the previous section, and the two-way differential attenuation through the depth of the cloud (5 to 10 km) was found to amount to only 0.1 dB, although the total two-way gaseous attenuation to 10 km at 94 GHz was 2 dB. Liquid water in the stratocumulus layer beneath would also

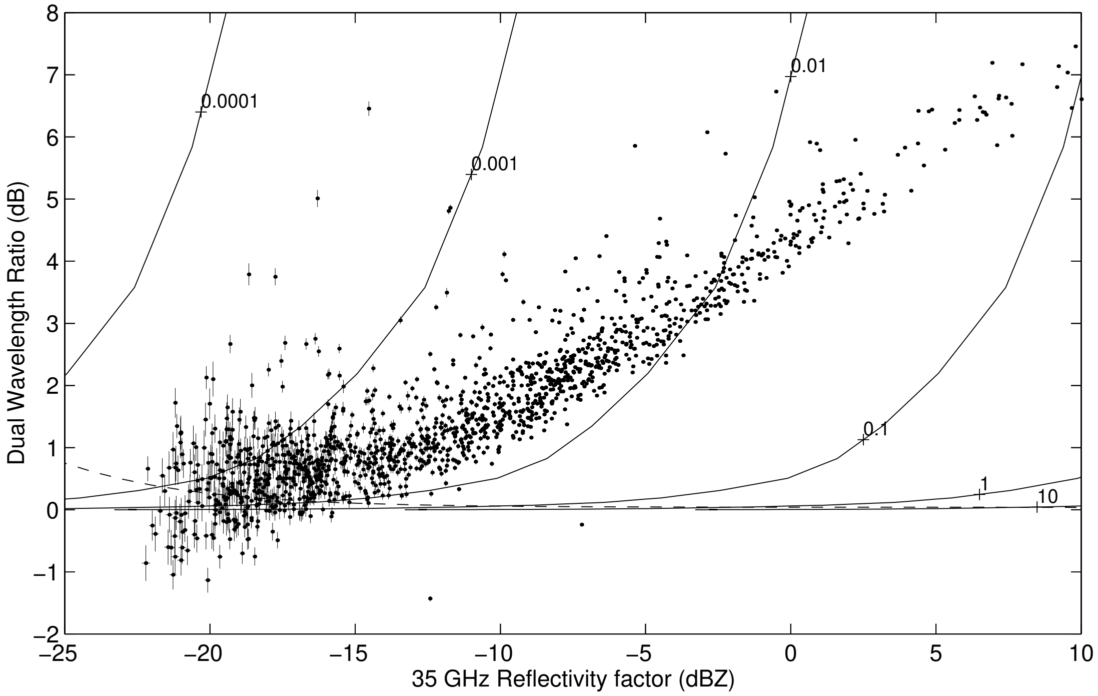

Figure 6.8: Scatterplot of Z_{35} versus DWR for the data presented in Fig. 6.7 with lines of constant IWC (labelled in g m^{-3}) overlayed. The error bars have been calculated assuming all pulses were independent, and the dashed line indicates the threshold for the rejection of data for the purposes of size retrieval, at an altitude of 7 km.

need to know the errors in reflectivity and hence in DWR. It was shown in Chapter 2 that for a radar with a noise-equivalent reflectivity (for a single pulse) N, the standard error of a reflectivity measurement averaged over M_{I} independent pulses is given by

$$\Delta Z \simeq \frac{4.343}{\sqrt{M_{\mathrm{I}}}} \left(1 + 10^{0.1(N[\mathrm{dBZ}]-Z[\mathrm{dBZ}])}\right) \ \mathrm{dB} \tag{6.5}$$

At a range of 1 km, $N = -34$ dBZ at 35 GHz and $N = -23$ dBZ at 94 GHz. The pulse repetition frequencies were 3125 and 5000 Hz at 35 and 94 GHz respectively, although only every fifth pulse at 94 GHz and every tenth pulse at 35 GHz were actually used in the real-time averaging. The observations in Fig. 6.7 are presented in Fig. 6.8 as a scatterplot of Z_{35} against DWR, with lines of constant IWC superimposed. The error bars represent the accuracy achievable assuming all pulses were independent. The scatter of the data at low reflectivity (where mean DWR should be close to 0 dB) appears to be somewhat more than that indicated by the length of the error bars, indicating that not all pulses were in fact independent. However, exact calculation of the number of independent pulses requires knowledge of the spectrum of fall velocities within the radar pulse volume, which was unavailable in this data.

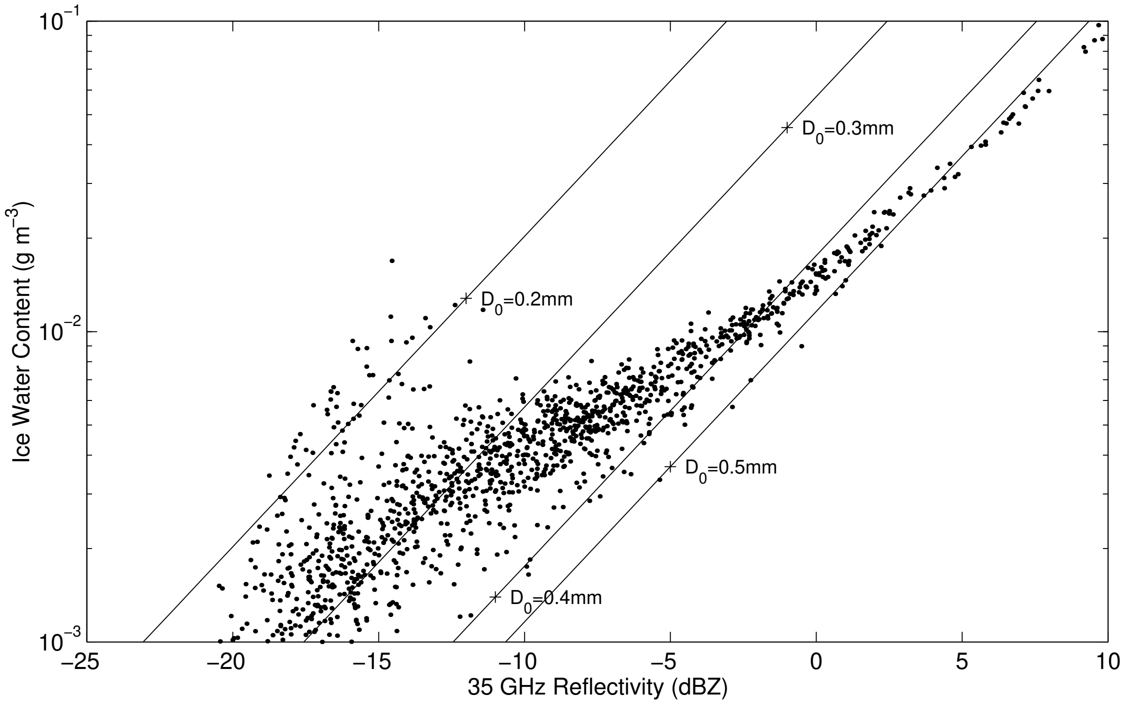

Figure 6.9: Scatterplot of IWC versus Z_{35} for the data presented in Fig. 6.7 with lines of constant D_0 overlayed. Only those points satisfying the criterion for sizing given in the text have been included (which is approximately equivalent to accepting only those points lying above the dashed line in Fig. 6.8).

We follow the suggestion of Matrosov (1993) and calibrate DWR by matching Z_{35} and Z_{94} at cloud top, but it is clear that the scatter of the data at low reflectivity is such that this cannot be done to a high degree of accuracy. The problem stems from the fact that the 94 GHz radar was around 10 dB less sensitive than the 35 GHz when these data were taken. We have imposed the condition that for an observation to be used, DWR must be larger than twice its standard error. This threshold at an altitude of 7 km is illustrated by the dashed line in Fig. 6.8 and all points below this are rejected for the purposes of size and IWC measurement.

Those data which have been accepted for size retrieval are plotted in Fig. 6.9 as a scatterplot of IWC against Z_{35}, with lines of constant D_0 superimposed. An increased spread of the data at low reflectivities is clearly apparent, probably due to the larger errors in DWR.

Figure 6.10 shows IWC and D_0 calculated from the observations using the empirical relationships derived in Section 6.2.2. Also shown is IWC as diagnosed by the model, with model datapoints indicated by black dots, and a comparison between the ice water path (IWP) measured by the model and the radars. Optical depth has been calculated as the simple vertical integral of the radar-derived visible extinction coefficient, and is shown in the lowest plot together with that of the model (which has been calculated from model IWP using the Unified Model parameterisasmaller than that from the lower half.

Effective radius is not plotted since it was observed to be fairly constant at around 75 µm. This is considerably larger than the value used by the Unified Model, although the value in the upper half of the cloud is likely to be smaller.

The cloud-free layer in the model at around 8 km was not observed in the radar data, and is due to the workings of the large-scale cloud and precipitation schemes (see Smith et al. 1994, 1995), in which IWC is calculated every timestep simply as the total water content (a prognostic variable) minus the saturation vapour density, with an allowance for humidity fluctuations over the gridbox. The timestep for the Mesoscale Version of the model is 5 minutes. An excess of ice is precipitated out instantaneously, so that ice water cannot persist in regions where the relative humidity is below a certain critical value, even if it is falling from a saturated layer above. In this case the model relative humidity fell to around 85%. In fact between 9 and 9.5 km the horizontally-averaged reflectivity exhibited an increase with height of about 2 dB in an otherwise monotonically decreasing profile, indicating that a little evaporation was occurring. This illustrates a shortcoming in the model which may have an impact on radiative properties.

We next examined the profile of radar and microphysical properties along individual fall-streaks. Figure 6.11 shows part of the 35 GHz reflectivity data at the highest available resolution of 75 metres and 10 seconds, together with the trajectories of three fallstreaks. These were derived by first finding the times corresponding to the maxima in Z_{35} at each rangegate. A point near cloud top was selected, and then the nearest maximum at the next height down was chosen. This process was repeated through the depth of the cloud, and finally a fifth-order polynomial was fitted through the selected points. In Fig. 6.12 the corresponding plots of DWR against Z_{35}, and D_0 against IWC have been plotted. It can be seen that in the evaporating region at cloud base the crystals tend to be larger for a given IWC compared with those in the bulk of the cloud. This is consistent with the idea that the smallest crystals evaporate first.

6.4 Conclusions

In this chapter the potential of dual-wavelength radar for remote measurement of crystal size, and hence of ice water content, has been demonstrated from real observations.

Firstly scattering calculations were performed to test the sensitivity of the retrieved meteorological parameters to our initial assumptions. The problem of establishing a generally applicable density function from aircraft data was discussed in Chapter 4, and it was shown here that the two given IWC was observed, consistent with the idea that the small crystals are the first to evaporate at cloud base. Effective radius was calculated to be around 75 μm in the lower half of the cloud where size measurements were possible, which is considerably larger than the value of 30 μm used by the UKMO Unified Model.

In this very limited study the model was found to perform reasonably well in locating the cirrus cloud, although the nature of the large-scale cloud scheme is such that there is a direct dependence of IWC on relative humidity. This meant that layers of cirrus were formed in coincidence with saturated and sub-saturated layers when in reality crystals fall an appreciable distance through sub-saturated air, with only a slightly detectable decrease in reflectivity due to evapouration.

It is evident that for useful, quantitative radar measurements in cirrus clouds, the instruments themselves must be both well calibrated and very sensitive. In this study DWR was observed to approach 0 dB for reflectivity factors below around -18 dBZ. Even with considerable averaging the 94 GHz radar had a minimum detectable reflectivity of only around -20 dBZ at cirrus altitudes, so random scatter of the data at these low signal-to-noise ratios made precise matching of the two radars in the Rayleigh-scattering cloud top very difficult. It was shown by Brown et al. (1995) that a minimum detectable reflectivity of -30 dBZ is required to detect the bulk of radiatively significant cloud, so at the very least both radars really need to be this sensitive for any meaningful comparison of radiative properties either with a model or with some other remote sensing technique.

This study shows that cloud radar clearly has a role to play in model validation, although for an objective assessment of model performance at least a month-long dataset of radar observations would be required. Such observations should be carried out at an elevation angle of 45°, as in theory this should minimise the errors which are introduced when horizontally aligned crystals are present. Simultaneous radar and aircraft measurements are seen as essential to validate the technique; it is unfortunate that the 94 GHz radar was not operational during the CIRRAD flight which would have made this possible, although of course the aircraft precipitation probe would also have had to have been functioning also, since it has been found that millimetre-sized crystals can contribute significantly to DWR.

Other comparisons would be interesting, such as with Meteosat infrared radiances. By using the radar to simply locate cloud these could be used to estimate optical depth, which could then be compared with that retrieved using the dual-wavelength method.

CHAPTER SEVEN

Conclusions and future work

Clouds play a fundamental role in the earth's radiation budget, and in order to determine their effects on the climate system there is an urgent need for vertically-resolved remote measurements of cloud radiative properties. In this thesis the potential of dual-wavelength radar to measure cloud properties has been investigated.

7.1 Summary of results and comparison with user requirements

In the introduction the accuracy and sensitivity requirements for remote cloud measurements were estimated. Here we outline the main results and compare the likely accuracy of the proposed algorithms with that required to provide a useful constraint on climate models.

7.1.1 Stratocumulus

In Chapter 3 two complementary ground-based techniques for the measurement of liquid water content (LWC) in stratocumulus were described, both of which circumvented the problem of drizzle. Their likely accuracy was assessed using aircraft data from ASTEX. The first used dual-wavelength radar at 35 and 94 GHz and should be able to be able to measure LWC with an error of ± 0.05 g m^{-3} at a spatial resolution of 150 m and a temporal resolution of 1 minute. The technique is inapplicable in the presence of light rain, which Mie scatters at 94 GHz and means that differences in reflectivity are no longer entirely attributable to attenuation, although reflectivity itself could be used as an indicator of where this is likely to be the case.

The second method used Doppler spectra to determine Z_c, the reflectivity of the small 'cloud' droplet component of the spectrum, which is well correlated with LWC. It should be able to measure LWC to within 30% for clouds with an LWC of greater than 0.01 g m^{-3}, and to within 10% for clouds with an LWC of greater than 0.1 g m^{-3}. The limitation of the technique is air turbulence which can act to broaden the spectrum and smear out the important cloud mode. The turbulence standard deviations necessary to do this were calculated for a large number of ASTEX size spectra, but the range of values that really occur in stratocumulus to compare with are not widely reported in the literature.

It was shown in Chapter 1 that the requirement is for instruments to be able to detect a cloud with an LWC of 0.01 g m^{-3}, and both retrieved LWC and effective radius (r_e) should be accurate to 10%. It can be seen from Figs. 3.10 and 3.13 that to satisfy the first of these requires a radar with a sensitivity of -50 dBZ at worst. This should be achievable for a ground-based radar at a range of 1 km with a 10 second dwell. To minimise errors associated with low signal-to-noise ratios it would be advantageous for the radar to be sensitive down to -60 dBZ. The required accuracy of 10% can just about be achieved for LWC by both techniques when LWC is large, but is unattainable when LWC is less than 0.1 g m^{-3}.

No method for deriving r_e was discussed, but it was shown by Fox and Illingworth (1997a) that r_e is well correlated with the reflectivity of the droplets smaller than 50 μm (which is very similar to Z_c), and should be derivable to within 10% using Doppler spectra (although not independently of LWC). It should be noted that r_e varies over a much smaller dynamic range than LWC.

Clearly the next step is to test the two techniques in the field using real data, in particular to establish how serious the potential problems of precipitation-sized drops (for the dual-wavelength method) and turbulence (for the Doppler spectrum method) really are.

In summary, the properties of stratocumulus clouds are very difficult to extract using active instruments. For radar, their intrinsically low reflectivity and the frequent contamination of the data by insects and ground clutter present considerable practical difficulties. Lidars suffer extreme attenuation in liquid water clouds so are virtually impossible to use quantitatively. Given their huge importance in the earth's radiation budget, it is vital that remote sensing algorithms are developed to measure vertical profiles of r_e and LWC, ideally from space, but there is clearly a long way to go.

7.1.2 Cirrus

A number of important findings have emerged from analysis of aircraft data in this thesis which could have repercussions for the quantitative interpretation of all radar measurements in cirrus:

- It has been shown from reanalysis of work presented in the literature that the popular expression for average crystal density given by $\rho = 0.07D^{-1.1}$ g m^{-3} (where D is the equivolumetric diameter in millimetres) is almost certainly an underestimate, and that the new expression $\rho = 0.175D^{-0.66}$ g m^{-3} is likely to be much more accurate.

- This also makes much more sense when we consider the effective radius (r_e), a parameter which is closely linked to density. Most radar techniques for the retrieval of crystal size are formulated in terms of the median volume diameter (D_0), which has physical meaning but is not used in radiative transfer calculations, and a potentially valuable by-product of this new density is an expression relating r_e to D_0, given by (4.8).

- The CIRRAD flight served to confirm that the method of calculating reflectivity factor from aircraft size spectra is robust, lending support to the approach of using aircraft data to verify the potential of dual-wavelength radar.

- It was shown that representing cirrus size distributions as exponential or gamma can be inappropriate for radar retrieval algorithms because a significant contribution to reflectivity factor can be from crystals larger than 800 µm, the numbers of which are often greatly underestimated by simple monomodal distributions. It is far better to derive empirical relationships from large aircraft datasets, which *must* contain the contributions from precipitation sized particles.

Chapters 5 and 6 examined the potential of dual-wavelength radar to measure crystal size in cirrus, and hence provide a more accurate estimate of ice water content than would be possible using a single radar. In Chapter 5 the feasibility of a spaceborne dual-wavelength was explored, and it was shown that attenuation from space to cirrus altitudes is small enough that the great advantages of using higher frequencies can be exploited. Aircraft size spectra from the EUCREX and CEPEX campaigns were analysed to show that the all-round best frequency combination is 79 and 215 GHz, which for a minimum sensitivity of −30 dBZ should be able to measure ice water content (IWC) with an accuracy of between 15% and 30% provided the reflectivity is greater than −20 dBZ (corresponding to an IWC of around 0.01 g m^{-3}). At lower signal-to-noise ratios the random fluctuations in the signal were enough to make measurements of IWC no more accurate than with a single radar. Evidence was presented to show that viewing at an angle of 45° from nadir should virtually eliminate the ambiguity in the interpretation of measurements caused by the possible presence of horizontally-aligned, non-spherical crystals.

Application of the technique was demonstrated from the ground in Chapter 6 using observations of a thick cirrus cloud by the 35 and 94 GHz radars at Chilbolton. The observed cloud location and ice water path compared compared well with the analyses of the UKMO Unified Model, although an effective radius of around 75 μm was derived from the radar measurements, which is 2.5 times larger than the constant value used in the radiation scheme of the model. The new density function was used in the analysis, although sensitivity studies indicated that using the older formula would have resulted in approximately twice as much ice water being diagnosed by the technique, which highlights the need to verify that the new expression is correct. The main problem with the study was that the 94 GHz radar could only detect down to a reflectivity of -20 dBZ, which is around 10 dB less sensitive than the 35 GHz radar, and meant that size measurements were not possible in the upper half of the cloud. It is hoped that this was a temporary fault which will be be cured when the radar is Dopplerised.

Hence we conclude that the accuracy and sensitivity requirements for retrievals in cirrus set out in Chapter 1 are satisfied very well by a dual-wavelength radar. From space, frequencies up to 215 GHz are feasible, so size and IWC measurements are generally more accurate than from the ground in thick clouds, and satisfy the most stringent requirement that in tropical cirrus, IWC and r_e should be measurable to within $+40\%$ and -30%. In clouds with a reflectivity less than 10 dB greater than the minimum reflectivity detectable, this requirement is not met because sizing of crystals is virtually impossible.

The opinion was expressed by Atlas et al. (1995), although disputed by Brown et al. (1995), that a minimum detectable reflectivity of -30 dBZ was insufficient to detect the bulk of radiatively significant cirrus. It should be noted therefore that a 215 GHz radar is likely to be more sensitive that the 94 GHz radar originally considered for a spaceborne radar (Mead et al. 1989), and also that if only a single radar were affordable from space, then a 215 GHz radar would be 10–20% more accurate than a 94 GHz radar for estimating IWC.

It has been shown that the idea of mounting two active instruments on separate satellites, the so-called ‘Split Mission Scenario’ (see Raschke et al. 1997), would introduce a random error of 2–3.5 dB into the dual-wavelength ratio, thereby making size retrieval impossible. The same conclusion was reached by Liu and Illingworth (1997) for crystal sizing using a radar and a lidar. This highlights the need for a concerted effort to convince funding bodies that the scientific requirement is for two active instruments to be located on the same platform.

7.2 Further points

On a more personal note, I would like to take the liberty of describing some of what I regard as the 'pitfalls' of cloud radar research, which have become abundantly clear to me through the course of doing the work for this thesis.

It was stated in Chapter 2 and we shall restate it again here that the most crucial requisite of a cloud radar is that it is highly sensitive. The situation at Chilbolton during the recording campaign of 1996 was therefore somewhat odd in that the two 'cloud' radars were considerably *less* sensitive than the 3 GHz rain radar (by 17 dB in the case of the 94 GHz radar), despite their specifications to have roughly the same sensitivity. The reason always cited for the the use of millimetre wavelengths is that Rayleigh scattering efficiency increases as the fourth power of frequency, but in practice this benefit is often lost because the transmitters have an intrinsically lower power output and the antennae are invariably built with a much smaller diameter. Hence the real advantages (which should not themselves be understated) are that ground clutter is much reduced and the far field approximation is valid at a much shorter range. Nonetheless it was seen in Chapter 6 that in cirrus the 35 GHz radar at Chilbolton had a minimum detectable reflectivity of -30 dBZ, the same as that proposed for a spaceborne radar, despite the theoretical 34 dB sensitivity advantage that is present because of the much shorter range. At the very least a ground-based cloud radar should be sensitive to -40 dBZ at cirrus altitudes ($\sim$10 km) and to -60 dBZ at stratocumulus altitudes ($\sim$1 km), so it is absolutely vital if radars are to have any future in measuring the radiative properties of clouds, and increasing our understanding of cloud processes, that sensitivity is the top priority in radar design.

The second point relates to the need to be quantitative. A number of vertically-pointing 35 GHz radars are being installed at various locations around the world (Moran et al. 1998, Mather et al. 1998), as part of the US Department of Energy's Atmospheric Radiation Measurement (ARM) program. These would be left to operate unattended for a number of years together with an array of other active and passive sensors, and by the use of techniques pioneered by (for instance) Matrosov et al. (1998) and Intrieri et al. (1993), should be able to obtain local climatologies of important cloud parameters. This should be seen as a very welcome development, although there is a danger in other circles that too little effort is being spent on making quantitative deductions from such data; it is relatively easy to produce and propagate impressive-looking high-resolution colour plots of uncalibrated reflectivity through cloud (often from which the noise has not been subtracted), and give the impression that such detail *must* be useful. However, on their own they contain *no information* *whatsoever* on water content or particle size, and in fact it is dangerous to use even the cloud boundaries reported by an uncalibrated radar to validate models since radiatively significant clouds with a low radar reflectivity can be easily lost in the noise, in which case the full extent of the cloud is not reported. If the radar is uncalibrated then there is no way of knowing the minimum detectable reflectivity and therefore how likely this is. The problem is demonstrated clearly from the observations presented in Chapter 6 in which the 94 GHz radar measured cloud top to be around 1.5 km lower than the 35 GHz radar because of its lower sensitivity.

It should be mentioned that one of the most difficult problems is that of calibration; simply calculating the 'RF budget', by considering all the coefficients in the Radar Equation and the properties of each constituent part of the hardware, can be in error by as much as 3 dB. The use of calibration spheres with a known backscatter cross-section is cumbersome and one must ensure that the target is at the exact peak of the antenna gain pattern. Even then the beam is not filled (as it would be in clouds), so accurate calibration is not guaranteed. At Chilbolton we are fortunate in that the 3 GHz weather radar can be calibrated accurately using the method of Goddard et al. (1994b), which can then be used to calibrate the millimetre-wave radars. If an analogous technique to calibrate a cloud radar using the clouds themselves could be developed, it would be extremely valuable, as most cloud radar sites do not have a rain radar at the same location.

Even with a calibrated and very sensitive radar it is far from easy to make quantitative deductions about cloud properties, given the perennial problem that the radar measures the sixth moment of the size distribution, so there is still much work to be done to exploit all the ways in which all the parameters from an array of active and passive instruments can be used to routinely measure size and water content in clouds of all types.

7.3 Future work

The problem of crystal density, and the way it affects radar, merits further investigation. It was shown that the equivalent area diameter (D_{a}) measured by airborne 2D probes is closer to the equivolumetric diameter (D_{v}) than the mean of the two orthogonal dimensions of the crystal image (D_{m}), and therefore that the density should be reformulated. This finding was then applied to the interpretation of dual-wavelength measurements, with the assumption that the extent of non-Rayleigh scattering is dependent simply on D_{v}. This is not necessarily true; it may the case that the diameter of a sphere which gives the same dual-wavelength ratio as that of an arbitrarily shaped crystal is closer to the diameter of some kind of envelope which encloses the entire crystal, in which case

D_m may be a more suitable parameter after all. There is clearly a need for scattering calculations to be performed to clarify the issue.

However the main area of future work which follows from the work presented in this thesis is to validate the ground-based retrieval techniques proposed in Chapters 3 and 6 with aircraft intercomparison flights. The CIRRAD flight was a very useful experience and highlighted a number of logistical priorities which should maximise the chances of future flights being a success.

The ideas in this thesis represent only a small subset of the possible ways in which cloud parameters can be retrieved remotely, and the key to the future success of remote measurements will undoubtedly lie in the synergy of many instruments, both active and passive. Much use could be made of the parameters that are routinely measured by satellites, particularly infrared radiances, and there is also a role for specialised radiosondes. Once we have confidence that cloud parameters can be measured with sufficient accuracy then there are a myriad of possible avenues of research to be pursued for a ground-based cloud observing facility such as Chilbolton, with the focus clearly on meteorological applications rather than on algorithm development (which has necessarily been the preoccupation of this thesis). The retrieval scenario originally envisaged for the implementation of these techniques was an unattended dual-wavelength radar operating for at least a month, from which a dataset of cloud parameters at high temporal and vertical resolution could be obtained and used to judge the performance of the UKMO forecast model. In addition to providing valuable data the exercise would act as a testing ground for a spaceborne radar.

Measurements of cloud parameters on a global scale are required to provide a true validation for climate models, so attention recently has focussed on the feasibility of active instruments in space which over a period of several years would build up a global cloud climatology with which model climatologies could be compared. Proposals have usually involved a 94 GHz radar, a visible lidar and an array of advanced radiometers on a low-altitude polar orbiting satellite. For instance, the 'CloudSat' mission is being developed for the NASA Earth System Science Pathfinder mission series (Walter 1997), and the 'Earth Radiation Mission' is being actively considered by the European Space Agency as part of its Earth Explorer Program (Ingmann 1997). There is thus an urgent need for retrieval algorithms to be developed which would be able to measure cloud parameters from space to the specifications stated by modellers, and to determine which instruments should be considered most important for such a mission, given that the satellite will naturally have both a limited payload and a limited budget.

APPENDIX

Simulation of two-dimensional cloud fields

Here we describe how two-dimensional cloud fields can be simulated given a one-dimensional energy spectrum, derived from observations, of the form

$$E_1 = \hat{E}_1 \, k^{\mu} \tag{A.1}$$

where k is the wavenumber, E_1 is the 1D spectral energy density, and $\hat{E}_1$ and μ are constants (see Chapter 5). From this we can define a 2D spectral energy density E_2 which is a function of the components of wavenumber in the x and y directions, k_x and k_y, or alternatively in terms of the absolute wavenumber k and the orientation angle θ. We have the constraint that E_1 at a particular wavenumber is equal to the integral over all E_2 with the same absolute wavenumber:

$$E_1(k) = \int_0^{2\pi} E_2(k,\theta)\, k d\theta. \tag{A.2}$$

Since we require the cloud field to be spectrally isotropic, E_2 is not a function of θ, and hence

$$E_2 = \frac{E_1(k)}{2\pi k} = \frac{\hat{E}_1 \, k^{\mu-1}}{2\pi} = \frac{\hat{E}_1 \, (k_x^2 + k_y^2)^{\frac{\mu-1}{2}}}{2\pi}. \tag{A.3}$$

We require a square reflectivity field Z_{n_x,n_y} consisting of $N \times N$ points, with a grid spacing of Δx, and a mean reflectivity of $\bar{Z}$. The indices n_x and n_y each range from 0 to $N-1$ and correspond to horizontal distances between 0 and $(N-1)\Delta x$. Z_{n_x,n_y} can be computed as the discrete inverse two-dimensional Fourier transform of the complex matrix z_{j_x,j_y}, which represents the amplitude and phase of each wave component of the field:

$$Z_{n_x,n_y} = \frac{1}{N^2} \sum_{j_y=0}^{N-1} \sum_{j_x=0}^{N-1} \exp(-2\pi i\, j_x n_x/N) \exp(-2\pi i\, j_y n_y/N)\, z_{j_x,j_y}. \tag{A.4}$$

The indices j_x and j_y also each range from 0 to $N-1$ and, following the convention of most FFT algorithms, translate to wavenumber as follows:

$$k_x = \begin{cases} j_x \Delta k, & j_x < N/2 \\ \pm N\Delta k/2, & j_x = N/2 \\ -(N-j_x)\Delta k, & j_x > N/2 \end{cases} \tag{A.5}$$

and similarly for k_y, where the smallest element of wavenumber is given by

$$\Delta k = \frac{2}{N\,\Delta x}. \tag{A.6}$$

We need to derive z_{j_x,j_y} from the continuous energy spectrum given by (A.3). Firstly a discrete energy, E_{j_x,j_y}, is derived from E_2 on the same grid as z. To a first approximation, E_{j_x,j_y}, the energy in the wavenumber range $k_x - \frac{1}{2}\Delta k$ to $k_x + \frac{1}{2}\Delta k$ and $k_y - \frac{1}{2}\Delta k$ to $k_y + \frac{1}{2}\Delta k$ is equal to $E_2(k_x,k_y)\,\Delta k^2$. However it is necessary to take account of aliasing, especially when μ is greater than around -1.5.

Then

$$z_{j_x,j_y} = N^2 (2E_{j_x,j_y})^{\frac{1}{2}} \exp(i\phi_{j_x,j_y}) \tag{A.7}$$

where ϕ is a matrix containing the phases of each wave component of z_{j_x,j_y}. For a random cloud field the elements of ϕ should be random numbers between 0 and 2π. However for the final reflectivity field to be real it is necessary to impose the condition

$$z(-k_x,-k_y) = z(k_x,k_y)^* \tag{A.8}$$

where the asterisk denotes complex conjugate. We also prescribe the mean value of the final reflectivity field $\bar{Z}$ by assigning

$$z(0,0) = N^2\,\bar{Z}. \tag{A.9}$$

Finally Z is obtained from z using (A.4). Note that even with the condition in (A.8), round-off error in most FFT algorithms is likely to produce very small imaginary parts in Z which should be ignored.

References

Ackerman, S. A., W. M. Smith, J. D. Spinhirne and H. E. Revercomb, 1990: The 27–28 October 1996 FIRE IFO cirrus case study: Spectral properties of cirrus clouds in the 8–12 µm window. *Mon. Weather Rev.,* **118**, 2377-2388.

Arking, A., 1991: The radiative effects of clouds and their impact on climate. *Bull. Am. Met. Soc.,* **71**(6), 795–813.

Arnott, W. P., Y. Y. Dong and J. Hallett, 1994: Role of small ice-crystals in radiative properties of cirrus: A case study, Fire II 22 Nov 1991. *J. Geophys. Res.,* **99**, 1371–1381.

Atlas, D., 1954: The estimation of cloud parameters by radar. *J. Meteor.,* **11**, 309–317.

Atlas, D., and F. H. Ludlam, 1961: Multi-wavelength radar reflectivity of hailstorms. *Quart. J. Roy. Met. Soc.,* **87**, 523–534.

Atlas, D., S. Y. Matrosov, A. J. Heymsfield, M.-D. Chou and D. B. Wolff, 1995: Radar and radiation properties of ice clouds. *J. Appl. Met.,* **34**(11), 2329–2345.

Auer, A. H., and D. L. Veal, 1970: The dimension of ice crystals in natural clouds. *J. Atmos. Sci.,* **27**, 919–926.

Aydin, K., and C. X. Tang, 1997: Relationships between IWC and polarimetric radar measurands at 94 and 220 GHz for hexagonal columns and plates. *J. Atmos. Oceanic Tech.,* **14**(5), 1055–1063.

Bader, M. J., S. A. Clough and G. P. Cox, 1987: Aircraft and dual polarization radar observations of hydrometeors in light stratiform precipitation. *Quart. J. Roy. Met. Soc.,* **113**, 491–515.

Baker, B. A., R. G. Corbin and J. Latham, 1980: The influence of entrainment on the the evolution of cloud droplet spectra: I. A model of inhomogeneous mixing. *Quart. J. Roy. Met. Soc.,* **106**, 581–598.

Baran, A. J., P. D. Watts and J. S. Foot, 1998: Potential retrieval of dominating crystal habit and size using radiance data from a dual view and multiwavelength instrument: A tropical cirrus anvil case. *J. Geophys. Res.,* **103**(D6), 6075–6082.

Barker, H. W., 1996: A parameterization for computing grid-averaged solar fluxes for inhomogeneous marine boundary-layer clouds. 1. Methodology and homogeneous biases. *J. Atmos. Sci.,* **53**(16), 2289–2303.

Barkstrom, B. R., E. Harrison, G. Smith, J. Kibler, R. Cess and the ERBE Science Team, 1989: Earth Radiation Budget Experiment (ERBE) archival and April 1985 results. *Bull. Am. Met. Soc.,* **70**, 1254–1262.

Beard, K. V., 1976: Terminal velocity of cloud and precipitation drops aloft. *J. Atmos. Sci.,* **33**, 851–864.

Blackman, T. M., 1996: *Observations and interpretations of differential phase shift in precipitation using S- and K_a band radars.* PhD Thesis, University of Manchester, UK.

Bringi, V. N., T. A. Seliga and W. A. Cooper, 1984: Analysis of aircraft hydrometeor spectra and differential reflectivity (Z_{DR}) measurements during the co-operative convective precipitation experiment. *Radio Science,* **19**, 157–167.

Brown, P. R. A., 1993: Measurement of the ice water content of cirrus using an evaporative technique. *J. Atmos. Oceanic Tech.,* **10**, 579–590.

Brown, P. R. A., and P. N. Francis, 1995: Improved measurements of the ice water content in cirrus using a total-water probe. *J. Atmos. Oceanic Tech.,* **12**(2), 410–414.

Brown, P. R. A., and H. A. Swann, 1997: Evaluation of key microphysical parameters in three-dimensional cloud-model simulations using aircraft and multiparameter radar data. *Quart. J. Roy. Met. Soc.,* **544B**, 2245–2275.

Brown, P. R. A., A. J. Illingworth, A. J. Heymsfield, G. M. McFarquhar, K. A. Browning and M. Gosset, 1995: The role of spaceborne millimeter-wave radar in the global monitoring of ice-cloud. *J. Appl. Met.,* **34**(11), 2346–2366.

Browning, K. A., 1994: Survey of perceived priority issues in the parametrizations of cloud related properties in GCMs. *Quart. J. Roy. Met. Soc.,* **120**(516B), 483–487.

Cess, R. D., et al., 1990: Intercomparison and interpretation of climate feedback processes in 19 atmospheric general circulation models. *J. Geophys. Res.,* **95**, 16 601–16 615.

Cess, R. D., et al., 1995: Absorption of solar-radiation by clouds—Observations versus models. *Science,* **267**(5197), 496–499.

Cess, R. D., et al., 1996: Cloud feedback in atmospheric general circulation models: An update. *J. Geophys. Res.,* **101**, 12 761–12 795.

Cherry, S. M., J. W. G. Goddard and M. Ouldridge, 1984: Simultaneous measurements of rain by airborne distrometer and dual polarization radar. *Radio Science,* **19**, 169–176.

Clothiaux, E. E., M. A. Miller, B. A. Albrecht, T. P. Ackerman, J. Verlinde, D. M. Babb, R. M. Peters and W. J. Syrett, 1995: An evaluation of a 94 GHz radar for remote sensing of cloud properties. *J. Atmos. Oceanic Tech.,* **12**(2), 201–229.

Cunnningham, R. M., 1978: Analysis of particle spectral data from optical array (PMS) 1D and 2D sensors. *Fourth Symposium on Met. Obs. Instruments, Denver, Col., April 10–14, 1978,* 345–350.

Danne, O., G. G. Mace, E. E. Clothiaux, X. Dong, T. P. Ackerman and M. Quante, 1996: Observing structures and vertical motions within stratiform clouds using a vertical pointing 94-GHz cloud radar. *Beitr. Phys. Atmosph.,* **69**(1), 229–237.

Doviak, R. J., and D. S. Zrnić, 1993: *Doppler radar and weather observations.* 2nd Ed. Academic Press.

Eccles, P. J., and E. A. Mueller, 1971: X-band attenuation and liquid water content estimation by dual-wavelength radar. *J. Appl. Met.,* **10**, 1252–1259.

Evans, W. F. J., C. Reinhart, E. Puckrin, 1995: A ground-based measurement of the anomalous cloud absorption effect. *Geophys. Res. Letters,* **22**(16), 2135–2138.

Foot, J. S., 1988: Some observations of the optical properties of clouds. II: Cirrus. *Quart. J. Roy. Met. Soc.,* **114**, 145–164.

Fox, N. I., and A. J. Illingworth, 1997a: The retrieval of stratocumulus cloud properties by ground-based cloud radar. *J. Appl. Met.,* **36**(5), 485–492.

Fox, N. I., and A. J. Illingworth, 1997b: The potential of a spaceborne radar for the detection of stratocumulus clouds. *J. Appl. Met.,* **36**(6), 676–687.

Francis, P. N., A. Jones, R. W. Saunders, K. P. Shine, A. Slingo and Z. Sun, 1994: An observational and theoretical study of the radiative properties of cirrus: Some results from ICE '89. *Quart. J. Roy. Met. Soc.,* **120**, 809–848.

Francis, P. N., P. Hignett and A. Macke, 1998: The retrieval of cirrus cloud properties from aircraft multi-spectral reflectance measurements during EUCREX '93. *Quart. J. Roy. Met. Soc.,* **124**, 1273–1291.

Frish, A. S., D. H. Lenschow, C. W. Fairall, W. H. Schubert and J. S. Gibson, 1995: Doppler radar measurements of turbulence in marine stratiform clouds during ASTEX. *J. Atmos. Sci.,* **52**(16), 2800–2808.

Frish, A. S., G. Feingold, T. Uttal, C. W. Fairall and J. B. Snider, 1997: Stratus cloud properties with a cloud radar and microwave radiometer. *Proc. 28th AMS Conference on Radar Meteorology,* Austin, Texas, 440–441.

Frost, I. R., 1991: *Comparison of dual-polarization meteorological radar and aircraft data using image processing techniques.* PhD Thesis, University of Manchester, UK.

Gans, R., 1912: Über die form ultramikroskipischer goldteilchen (On the shape of ultra-microscopic gold particles). *Ann. Phys.,* **37**, 881–900.

Goddard, J. W. F., J. D. Eastment and M. Thurai, 1994a: The Chilbolton Advanced Meteorological Radar: a tool for multi-disciplinary atmospheric research. *Electron. & Commun. Eng. J.,* **6**(2), 77–86.

Goddard, J. W. F., J. Tan and M. Thurai, 1994b: Technique for calibration of meteorological radars using differential phase. *Electronics Letters,* **30**(2), 166–167.

Gossard, E. E., 1994: Measurement of cloud droplet size spectra by Doppler radar. *J. Atmos. Oceanic Tech.,* **11**, 712–726.

Gossard, E. E., R. G. Strauch and R. R. Rogers, 1990: Evolution of dropsize distributions in liquid precipitation observed by ground-based Doppler radar. *J. Atmos. Oceanic Tech.,* **7**, 815–828.

Gossard, E. E., J. B. Snider, E. E. Clothiaux, B. Martner, J. S. Gibson, R. A. Kropfli and A. S. Frisch, 1997: The potential of 8-mm radars for remotely sensing cloud drop size distributions. *J. Atmos. Oceanic Tech.,* **14**(1), 76–87.

Gosset, M., and H. Sauvageot, 1992: A dual-wavelength radar method for ice-water characterization in mixed-phase clouds. *J. Atmos. Oceanic Tech.,* **9**, 538–547.

Grant, A. L. M., and P. Hignett, 1998: Aircraft observations of the surface energy balance in TOGA-COARE. *Quart. J. Roy. Met. Soc.,* **124**, 101–122.

Greenwald, T. J., G. L. Stephens, T. H. Vonder Haar and D. L. Jackson, 1993: A physical retrieval of cloud liquid water over the global oceans using Special Sensor Microwave/Imager (SSM/I) observations. *J. Geophys. Res.,* **98**(D10), 18 471–18 488.

Gregory, D., and D. Morris, 1996: The sensitivity of climate simulations to the specification of mixed phase clouds. *Climate Dynamics,* **12**, 641–651.

Guyot, A., and J. Testud, 1998: The dual beam technique applied to aircraft cloud radar. *Submitted to J. Atmos. Oceanic Tech.*.

Hadley Centre, 1994: *Hadley Centre climate data requirements.* UK Meteorological Office, Bracknell, Berkshire.

Han, Q., W. B. Rossow and A. A. Lacis, 1994: Near-global survey of the effective droplet radii in liquid water clouds using ISCCP data. *J. Climate,* **7**, 465–497.

Hartmann, D. L., 1993: Radiative effects of clouds on Earth's climate. In *Aerosol-cloud-climate interactions.* P. V. Hobbs (Ed.), Academic Press.

Hayasaka, T., N. Kikuchi and M. Tanaka, 1995: Absorption of solar-radiation by stratocumulus clouds—aircraft measurements and theoretical calculations. *J. Appl. Met.,* **34**(5), 1047–1055.

Hendry, A., Y. M. M. Antar and G. C. McCormick, 1987: On the relationship between the degree of preferred orientation in precipitation and dual-polarization radar echo characteristics. *Radio Science,* **22**, 37–50.

Heymsfield, A. J., 1972: Ice crystal terminal velocities. *J. Atmos. Sci.,* **29**, 1251–1261.

Heymsfield, A. J., 1993: Microphysical structures of stratiform and cirrus clouds. In *Aerosol-cloud-climate interactions.* P. V. Hobbs (Ed.), Academic Press.

Heymsfield, A. J., and D. Baumagardner, 1985: Summary of workshop on processing 2-D probe data. *Bull. Am. Met. Soc.,* **66**, 437–440.

Heymsfield, A. J., G. M. McFarquhar, W. D. Collins, J. A. Goldstein, F. P. J. Valero, J. Spinhirne, W. Hart and P. Pilewskie, 1998: Cloud properties leading to highly reflective tropical cirrus: Interpretations from CEPEX, TOGA COARE and Kwajalein, Marshall Islands. *J. Geophys. Res.,* **103**(D8), 8805–8812.

Hogan, R. J., and A. J. Illingworth, 1998: The potential of spaceborne dual-wavelength radar to make global measurements of cirrus clouds. *J. Atmos. Oceanic Tech.*, in press.

Hogan, R. J., A. J. Illingworth and H. Sauvageot, 1997a: Dual wavelength determination of cirrus microphysical properties. *Proc. 28th AMS Conference on Radar Meteorology,* Austin, Texas, 364–365.

Hogan, R. J., A. J. Illingworth and H. Sauvageot, 1997b: Determination of cirrus microphysical properties using 35 and 94 GHz radars. *Workshop on 'Synergy of active instruments in the Earth Radiation Mission', 12-14 November 1997,* GKSS, Geestacht, Germany.

Hogan, R. J., A. J. Illingworth and H. Sauvageot, 1998: Measuring crystal size in cirrus using 35 and 94 GHz radars. *Submitted to J. Atmos. Oceanic Tech.*

Hoyt, D. V., and K. H. Shatten, 1997: *The role of the sun in climate change.* Oxford University Press, Inc.

IGPO, 1994: *Utility and feasibility of a cloud profiling radar.* IGPO Publication series No. 10. International GEWEX Program Office. 140 pp.

Illingworth, A. J., J. W. G. Thomason, J. W. F. Goddard, H. Sauvageot and P. M. Simpson, 1995: Sizing of ice aggregates and snowflakes using coincident 3 and 35 GHz reflectivity observations. *Proc. 27th AMS Conference on Radar Meteorology,* Vail, Colorado.

Illingworth, A. J., C. Liu, I. Astin and B. Richards, 1997: *Study of the critical requirements for a cloud radar.* Final report, ESTEC Contract 11346/95/NL/CN.

Ingmann, P., 1997: The Earth Radiation Mission. *Workshop on 'Synergy of active instruments in the Earth Radiation Mission', 12-14 November 1997,* GKSS, Geestacht, Germany.

Intrieri, J. M., G. L. Stephens, W. L. Eberhart and T. Uttal, 1993: A method for determining cirrus cloud particle sizes using lidar and radar backscatter techniques. *J. Appl. Met.,* **32**(6), 1074–1082.

Jayaweera, D. O., and B. J. Mason, 1965: The behavior of freely falling cylinders and cones in a viscous fluid. *J. Fluid Mech.,* **22**, 709-720.

Joss, J., K. Schram, J. C. Thams and A. Waldvogel, 1970: *On the quantitave determination of precipitation by radar.* Scientific Communication No. 63, Research Dept. of the Federal Commission on the Study of Hail Formation, Ticinese Observatory of the Swiss Central Meteorological Institute, Federal Institute of Technology, Zürich, 33 pp.

Kinne, S., T. P. Ackerman, M. Shiobara, A. Uchiyama, A. J. Heymsfield, L. Miloshevich, J. Wendell, E. W. Eloranta, C. Purgold and R. W. Bergstrom, 1997: Cirrus cloud radiative and microphysical properties from ground observations and in situ measurements during FIRE 1991 and their application to exhibit problems in cirrus solar radiative transfer modeling. *J. Atmos. Sci.,* **54**, 2320–2344.

Knollenberg, R. G., 1970: The optical array: An alternative to scattering for airborne particle size determination. *J. Appl. Met.,* **9**, 86–103.

Kosarev, A. L., and I. P. Mazin, 1989: Empirical model of physical structure of the upper level clouds of the middle latitudes. *Radiation Properties of Cirrus Clouds.* Nauka, 29–52.

Lhermitte, R. M., 1987: A 94 GHz Doppler radar for cloud observations. *J. Atmos. Oceanic Tech.,* **4**, 36–48.

Lhermitte, R. M., 1988: Observation of rain at vertical incidence with a 94 GHz Doppler radar—and insight on Mie scattering. *Geophys. Res. Let.,* **15**(10), 1125–1128.

Li, H., A. J. Illingworth and J. Eastment, 1994: A simple method of Dopplerizing a pulsed magnetron radar. *Microwave J.,* **37**(4), 226.

Liebe, H. J., 1985: An updated model for millimeter-wave propagation in moist air. *Radio Science,* **20**(5), 1069–1089.

Liebe, H. J., T. Manabe and G. A. Hufford, 1989: Millimeter-wave attenuation and delay rates due to fog/cloud conditions. *IEEE AP,* **37**, 1617–1623.

Liou, K.-N., 1980: *An introduction to atmospheric radiation.* Academic Press.

Liou, K.-N., 1986: Influence of cirrus clouds on weather and climate processes: A global perspective. *Monthly Weather Rev.,* **114**, 1167–1199.

Liou, K.-N., and G. D. Wittman, 1979: Parameterization of the radiative properties of clouds. *J. Atmos. Sci.,* **36**, 1261–1273.

Liu, C. and A. J. Illingworth, 1997: Retrieving cirrus cloud microphysical properties using a future radar/lidar system. *Workshop on 'Synergy of active instruments in the Earth Radiation Mission', 12-14 November 1997,* GKSS, Geestacht, Germany.

Locatelli, J. D., and P. V. Hobbs, 1974: Fall speeds and masses of solid precipitation particles. *J. Geophys. Res.,* **79**, 2185–2197.

Lohmeier, S. P., S. M. Sekelsky, J. M. Firda, G. A. Sadowy and R. E. McIntosh, 1997: Classification of particles in stratiform clouds using the 33 and 95 GHz polarimetric cloud profiling radar system (CPRS). *IEEE Trans. Geosci. Remote Sensing,* **35**(2), 256–270.

London, J., 1957: A study of the atmospheric heat balance. Final report, AFC-TR-57-287, OTSPB129551, 99 pp., Coll. of Eng., New York University.

Magono, C., and C. V. Lee, 1966: Meteorological classification of natural snow crystals. *J. Fac. Sci. Hokkaido Univ.,* **7**(2), 321–362.

Manabe, S., and R. F. Strickler, 1964: Thermal equilibrium of the atmosphere with a convective adjustment. *J. Atmos. Sci.,* **21**(4), 361–385.

Marshall, J. S., and W. McK. Palmer, 1948: The distribution of raindrops with size. *J. Meteor.,* **5**, 165–166.

Martin, G. M., D. W. Johnson and A. Spice, 1994: The measurement and parameterization of effective radius of droplets in warm stratocumulus clouds. *J. Atmos. Sci.,* **51**(13), 1823–1842.

Martin, G. M., D. W. Johnson, P. R. Jonas, D. P. Rogers, I. M. Brooks and R. W. Barlow, 1997: Effects of airmass type on the interaction between warm stratocumulus and underlying cumulus clouds in the marine boundary layer. *Quart. J. Roy. Met. Soc.,* **123**, 849–882.

Martner, B. E., R. A. Kropfli, L. E. Ash and J. B. Snider, 1993: Dual-wavelength differential attenuation radar measurements of cloud liquid water content. *Proc. 26th AMS Conference on Radar Meteorology,* Norman, Oklahoma.

Mather, J. H., T. P. Ackerman, W. E. Clements, F. J. Barnes, M. D. Ivey, L. D. Hatfield and R. M. Reynolds, 1998: An atmospheric radiation and cloud station in the tropical western pacific. *Bull. Am. Met. Soc.,* **79**(4), 627–642.

Matrosov, S. Y., 1993: Possibilities of cirrus particle sizing from dual-frequency radar measurements. *J. Geophys. Res.,* **98**(D11), 20 675–20 683.

Matrosov, S. Y., 1997: Variability of microphysical parameters in high-altitude ice clouds: Results of the remote sensing method. *J. Appl. Met.,* **36**(6), 633–648.

Matrosov, S. Y., R. F. Reinking, R. A. Kropfli and B. W. Bartram, 1996: Estimation of ice hydrometeor types and shapes from radar polarization measurements. *J. Atmos. Oceanic Tech.,* **13**, 85–96.

Matrosov, S. Y., A. J. Heymsfield, R. A. Kropfli, B. E. Martner, R. F. Reinking, J. B. Snider, P. Piironen and E. W. Eloranta, 1998: Comparisons of ice cloud parameters obtained by combined remote sensor retrievals and direct methods. *J. Atmos. Oceanic Tech.,* **15**(1), 184–196.

Maxwell-Garnet, J. C., 1904: Colours in metal glasses and metallic films. *Philos. Trans. Roy. Soc.,* **A203**, 385–420.

McClatchey, R. A., R. W. Fenn, J. E. A. Selby, F. E. Volz and J. S. Garing, 1972: Optical properties of the atmosphere (3rd. ed.), Air Force Cambridge Research Laboratories, Rep. No. AFCRL72-0497, L. G. Hanscom Field.

McFarquhar, G. M., and A. J. Heymsfield, 1997: Parameterization of tropical cirrus ice crystal size distributions and implications for radiative transfer: Results from CEPEX. *J. Atmos. Sci.,* **54**, 2187–2200.

McFarquhar, G. M., and A. J. Heymsfield, 1998: The definition and significance of an effective radius for ice clouds. *J. Atmos. Sci.,* **55**, 2039–2052.

Mead, J. B., R. E. McIntosh, D. Vandemark and C. T. Swift, 1989: Remote sensing of clouds and fog with a 1.4-mm radar. *J. Atmos. Oceanic Tech.,* **6**, 1090–1097.

Meneghini, R., and T. Kozu, 1990: *Spaceborne weather radar.* Artech House.

Meneghini, R., and L. Liao, 1996: Comparisons of cross-sections for melting hydrometeors as derived from dielectric mixing formulas and a numerical-method. *J. Appl. Met.,* **35**(10), 1658–1670.

Mitchell, J. F. B., C. A. Senior and W. J. Ingram, 1989: CO_2 and climate: A missing feedback? *Nature,* **341,** 132–134..

Mitchell, D. L., S. K. Chai, Y. Liu, A. J. Heymsfield and Y. Dong, 1996: Modeling cirrus clouds. Part I: Treatment of bimodal size spectra and case study analysis. *J. Atmos. Sci.,* **53**(20), 2952–2966.

Moran, K. P., B. E. Martner, M. J. Post, R. A. Kropfli, D. C. Welsh and K. B. Widener, 1998: An unattended cloud-profiling radar for use in climate research. *Bull. Am. Met. Soc.,* **79**(3), 443–455.

Nakaya, U., and T. Terada, 1935: Simultaneous observations of the mass, falling velocity and form of snow crystals. *J. Fac. Sci. Hokkaido Univ.,* **2**(1), 191–201.

Nicholls, S., 1984: The dynamics of stratocumulus: Aircraft observations and comparisons with a mixed layer model. *Quart. J. Roy. Met. Soc.,* **110**, 783–820.

O'Brien, S. G., and G. H. Goedecke, 1988: Scattering of millimeter waves by snow crystals and equivalent homogeneous symmetric particles. *Appl. Optics,* **27**(12), 2439–2444.

Ono, A., 1969: On the shape and riming properties of ice crystals in natural clouds. *J. Atmos. Sci.,* **26**, 138–147.

Paluch, I. R., and D. G. Baumgardner, 1989: Entrainment and fine-scale mixing in a continental convective cloud. *J. Atmos. Sci.,* **46**, 261–278.

Paluch, I. R., C. A. Knight and L. J. Miller, 1996: Cloud liquid water content and radar reflectivity of non-precipitating cumulus clouds. *J. Atmos. Sci.,* **53**(11), 1587–1603.

Papoulis, A., 1965: *Probability, random variables, and stochastic processes.* McGraw-Hill, New York.

Parol, K., J. C. Buriez, G. Brogniez and Y. Foquart, 1991: Information content of the AVHRR channels 4 and 5 with resect to the effective radius of cirrus cloud particles. *J. Appl. Met.,* **30**, 973–984.

Passarelli, R. E., P. Romanik, S. G. Geotis and A. D. Siggia, 1981: Ground clutter rejection in the frequency domain. *Proc. 20th AMS Conference on Radar Meteorology,* Boston, Massachusetts.

Platt, C., N. Abshire and G. McNice, 1978: Some microphysical properties of an ice cloud from lidar observation of horizontally aligned crystals. *J. Appl. Met.,* **17**, 1220–1224.

Randall, D. A., J. A. Coakley Jr., C. W. Fairall, R. A. Kropfli and D. H. Lenshow, 1984: Outlook for research on sub-tropical marine stratiform clouds. *Bull. Am. Met. Soc.,* **65**, 1290–1301.

Randall, D. A., Harshvardhan, D. A. Dazlich and T. G. Corsetti, 1989: Interactions among radiation, convection and large-scale dynamics in a general-circulation model. *J. Atmos. Sci.,* **46**(13), 1943–1970.

Raschke, E., P. Ingmann, T. P. Ackerman, E. Attema, A. Culoma, A. J. Illingworth, J. P. V. Poiares Baptista and H. Russchenberg, 1997: Summary and Recommendations. *Workshop on 'Synergy of active instruments in the Earth Radiation Mission', 12-14 November 1997,* GKSS, Geestacht, Germany.

Rinehart, R. E., and J. D. Tuttle, 1982: Antenna beam patterns and dual-wavelength processing. *J. Appl. Met.,* **21**, 1865–1880.

Rossow, W. B., and R. A. Schiffer, 1991: ISCCP cloud data products. *Bull. Am. Met. Soc.,* **72**, 2–20.

Ryzhkov, A. V., D. S. Zrnić and B. A. Gordon, 1998: Polarimetric method for ice water content determination. *J. Appl. Met.,* **37**, 125–134.

Sachidananda, M., and D. S. Zrnić, 1985: Z_{DR} measurement considerations for a fast scan capability radar. *Radio Science,* **20**(4), 907–922.

Sauvageot, H., and J. Omar, 1987: Radar reflectivity of warm cumulus clouds. *J. Atmos. Oceanic Tech.,* **4**, 264–272.

Schneider, T. L., and G. L. Stephens, 1995: Theoretical aspects of modeling backscattering by cirrus ice particles at millimeter wavelengths. *J. Atmos. Sci.,* **52**(23), 4367–4385.

Seliga, T. A., and V. N. Bringi, 1976: Potential use of radar differential reflectivity measurements at orthogonal polarizations for measuring precipitation. *J. Appl. Met.,* **15**, 69–76.

Slingo, A., 1990: Sensitivity of the earth's radiation budget to changes in low clouds. *Nature,* **343**, 49–51.

Slingo, A. S., S. Nicholls and J. Schnetz, 1982: Aircraft observations of marine stratocumulus during JASIN. *Quart. J. Roy. Met. Soc.,* **108**, 833–856.

Smith, R. N. B., 1990: A scheme for predicting layer clouds and their water content in a general circulation model. *Quart. J. Roy. Met. Soc.,* **116**, 435–460.

Smith, R. N. B., D. Gregory and C. Wilson, 1994: Calculation of saturated specific humidity and large-scale cloud. Unified Model Documentation paper No. 29 (Version 2), UK Meteorological Office.

Smith, R. N. B., D. Gregory, J. F. B. Mitchell and A. C. Bushell, 1995: Large-scale precipitation. Unified Model Documentation paper No. 26 (Version 3), UK Meteorological Office.

Stephens, G. L., S. C. Tsay, P. W. Stackhouse Jr. and P. J. Flatau, 1990: The relevance of the microphysical and radiative properties of cirrus clouds to climate and climatic feedback. *J. Atmos. Sci.,* **47**, 1742–1752.

Taylor, J. P., J. M. Edwards, M. D. Glew, P. Hignett and A. Slingo, 1996: Studies with a flexible new radiation code. 2. Comparisons with aircraft short-wave observations. *Quart. J. Roy. Met. Soc.,* **122**(532B), 839–

861.

Testud, J., and P. Amayenc, 1989: Stereoradar meteorology: a promising technique for observation of precipitation from a mobile platform. *J. Atmos. Oceanic Tech.,* **6**(1), 89–108.

Thomas, L., J. C. Cartwright and D. P. Wareing, 1990: Lidar observations of the horizontal orientation of ice crystals in cirrus clouds. *Tellus,* **42B**, 211–216.

Thomason, J. W. G., A. J. Illingworth and V. Marécal, 1995: Density and size distribution of aggregating snow particles inferred from coincident aircraft and radar observations. *Proc. 27th AMS Conference on Radar Meteorology,* Vail, Colorado.

Tiedtke, M., 1993: Representation of clouds in large-scale models. *Quart. J. Roy. Met. Soc.,* **104**, 677–690.

Tiedtke, M., E. Klinker, N. G. Kvamsto, J.-J. Morcrette, R. Rizzi and M. Vesperini, 1993: Cloud and radiation modelling at ECMWF. *IAMAP Int. Workshop on Cloud-Radiation Interactions.* Camp Springs, MD, IAMAP.

Tinsley, B. A., and G. W. Deen, 1991: Apparent tropospheric response to MeV-GeV particle-flux variations—a connection via electrofreezing of supercooled water in high-level clouds. *J. Geophys. Res.,* **96**(D12), 22 283–22 296.

Tuttle, J. D., and R. E. Rinehart, 1983: Attenuation correction in dual-wavelength analyses. *J. Climate Appl. Met.,* **22**, 1914–1921.

Twomey, W., 1974: Pollution and the planetary albedo. *Atmos. Environ.,* **8**, 1251–1256.

van de Hulst, H. D., 1957: *Light scattering by small particles.* Wiley and sons, 470 pp.

Vowinckel, E., and S. Orvig, 1970: The climate of the north polar basin. In *World Survey of Climatology,* **14**, *Climates of Polar Regions,* S. Orvig (Ed.), Elsevier, Amsterdam, 129–252.

Walter, S. J., 1997: CLOUDSAT: Profiling clouds from space. *Workshop on 'Synergy of active instruments in the Earth Radiation Mission', 12-14 November 1997,* GKSS, Geestacht, Germany.

Waterman, P., 1969: Scattering by dielectric obstacles. *Alta Freq.,* **38**, 348–352.

White, A. B., C. W. Fairall and J. B. Snider, 1995: Surface-based remote-sensing of marine boundary-layer cloud properties. *J. Atmos. Sci.,* **52**(16), 2827–2838.

Wielicki, B. A., J. T. Suttles, A. J. Heymsfield, R. M. Welch, J. D. Spinhirne, M.-L. Wu, D. O'C. Starr, L. Parker and R. F. Arduini, 1990: The 27–28 October 1986 FIRE IFO cirrus case study: Comparison of radiative transfer theory with observations by satellite and aircraft. *Mon. Weather Rev.,* **118**, 2356–2376.

Winker, D. M., R. H. Couch and M. P. McCormick, 1996: An overview of LITE—NASA Lidar In-space Technology Experiment. *Proc. IEEE,* **84**(2), 164–180.

Young, S. A., 1995: Analysis of lidar backscatter profiles in optically thin clouds. *Appl. Optics,* **34**, 7019–7031.